Freie Universität Berlin

Functionalized Graphene Sheets as Multivalent 2D Platforms and Their Antitumor Applications

DISSERTATION

zur Erlangung des akademischen Grades des Doktors der

Naturwissenschaften (Dr. rer. nat.)

eingereicht im Fachbereich Biologie, Chemie, Pharmazie der Freien

Universität Berlin

vorgelegt von

Zhaoxu Tu

aus Anhui, China

Berlin, May 2018

The work presented in this thesis was conducted in the research group of Prof. Dr. Rainer Haag from September 2014 until May 2018 at the Institut für Chemie und Biochemie of the Freie Universität Berlin.

1st Reviewer: Prof. Dr. Rainer Haag, Freie Universität Berlin
2nd Reviewer: Prof. Dr. Mohsen Adeli, Freie Universität Berlin

Location of Defense: 34.16/17, Takustr. 3, 14195 Berlin
Date of Defense: 09.07.2018

Acknowledgements

My deepest gratitude goes first and foremost to Prof. Dr. Rainer Haag, my supervisor, for the opportunity he gave me to study in his group. He has walked me through all the stages from experiments, academic papers to the Doctoral thesis with a lot of encouragement and guidance. Without his consistent and illuminating instruction, this thesis could not have reached its present form. And I also appreciate his help in planning my future development and in the search for a postdoc position.

Second, I would like to express my heartfelt gratitude to Prof. Dr. Mohsen Adeli, who is my co-supervisor and also the second referee. He taught me a lot of things, especially about graphene derivatives, from almost the first day I came to this lab. And he spent a lot of time and effort in correcting my papers and thesis. Meanwhile, he provided me with plenty of scientific suggestions, which was a great help for accomplishing my projects and for my future career.

I especially want to thank Prof. Dr. Wei Chen at the China Pharmaceutical University for providing me the opportunity to perform *in vivo* tests for my projects. From Sep. 2017 to Nov. 2017, I went to his group for a short-term internship. During that time, I learned a lot of techniques and skills about animal experiments and many nice results were obtained before I came back to Berlin.

I thank Daniel Stoebener, Felix Reisbeck, Anja Stöshel, and Cathleen Schlesener for providing me the hyperbranched polyglycerol (hPG) and functionalized hPG. I would like to thank Prof. Dr. Rolf Mülhaupt for providing me the thermally reduced graphene oxide (TRGO). I acknowledge Dr. Virginia Wycisk for providing me the pH-sensitive dye. I also appreciate that Guy Guday and Ievgen Donskyi developed the protocol that could produce graphene nanosheets with high quality, which is quite helpful for my projects.

I would like to acknowledge Dr. Katharina Achazi for introducing me the basic principles and experimental techniques in the biolab. I thank Dr. Stefanie Wedepohl, Paul Hillmann, Elisa Quaas, and all the other members in the biolab for their patient explanations and great help during my experiments. I appreciate that Prof. Dr. Christoph Böttcher, Dr. Boris Schade, Andrea Schulz, Dr. Kai Ludwig taught and helped me with TEM operation. I would like to acknowledge Prof. Dr. Eckart Rühl and Steffen Thierbach for the measurement of Raman microscopy. I appreciate Dr. Chong Cheng and Guy Guday for the measurement and analysis of AFM. I would like to thank Dr. Haishi Qiao, Yuting Yan, and Zhonglin Zhu for performing and analyzing the *in vivo* experiments.

I would like to especially thank Dr. Pamela Winchester for language polishing the manuscripts. I appreciate very much that Dr. Olaf Wagner translated the summary part of

my Doctoral thesis into German. I would like to thank Jutta Hass, Eike Ziegler, Dr. Wiebke Fischer, Christiana Halsdorfer, Achim Wiedekind, and Gaby Hertel for the great support in chemical ordering, lab techniques, as well as all the other issues.

All former and current colleagues in Haag group are appreciated for their great assistance during my Doctoral study. In particular, I would like to acknowledge the members in the "carbon subgroup" and my partners from the labs and the offices for every discussion and useful suggestion.

I thank the China Scholarship Council (CSC) for providing me the financial support during my whole Doctoral period.

Last but not the least, I am very thankful to my parents, sisters and girlfriend for their endless love throughout all these years. Without their support and encouragement, I could not have finished my studies in Germany. I hope to go back home soon after the defense and celebrate with them together.

Table of Contents

1 Introduction

1.1 Properties and functionalization of graphene derivatives

1.1.1 Biophysicochemical properties

2D nanomaterials have received great interest for biomedical applications in recent years, as this family of nanomaterials has shown many unprecedented properties.[1,2] Among 2D materials, graphene is without doubt the most widely investigated, and currently is closest to real-world applications and market.[3,4] Due to such properties and bioactivity, graphene-based nanomaterials have been proposed for different biomedical applications.[3,4] Commonly used graphene derivatives including graphene, graphene oxide (GO), reduced graphene oxide (rGO), nanographene, graphite oxide differ in their functionality, lateral and height profiles, as well as the integrity of their π-conjugated system (Figure 1).[5] This structural versatility differentiates their physicochemical features and consequently their interactions with the biological systems.[6,7]

Graphite oxide is a highly oxidized form of graphene consisting layers of GO with defected structure and many functional groups.[5] Graphite oxide was first prepared by oxidation of graphite using a mixture of sulfuric and nitric acid, and then potassium permanganate.[8] The graphite oxide can be subsequently exfoliated into monolayer GO by sonication. Monolayer GO is an amphiphilic single layer graphene sheet with many carboxyl, epoxide, and hydroxyl functional groups generated during the oxidation process.[8] GO exhibits colloidal stability and pH-dependent negative surface charge, attributable to the carboxyl groups. In addition, the abundant surface functionalities endow GO with excellent water solubility and can easily be further functionalized. The basal sheet of GO still consists of numerous unmodified hydrophobic aromatic domains, which allows GO to be applied as a surfactant, stabilizing aromatic rings and hydrophobic molecules through π-π stacking and hydrophobic forces. However, the intensive oxidation during the preparation of GO results in a highly defective density, reducing its electrical, mechanical, and thermal properties.

rGO can be obtained by thermal, chemical, or UV reduction of GO.[9] The number of functional groups and oxygen content of GO can be greatly reduced upon reduction and its electrical, mechanical, and thermal features to some extent recovered.[9] Due to the elimination of oxygen, rGO is much more hydrophobic than GO.[9] Additionally, reductive agents, such as hydrazine are toxic, which limits the bio-applications of rGO.[9] Therefore, low toxic reducing agents are urgently required to produce biocompatible rGO.

Guo et al.[10] developed a method by which GO could be efficiently reduced to biocompatible rGO via L-ascorbic acid.

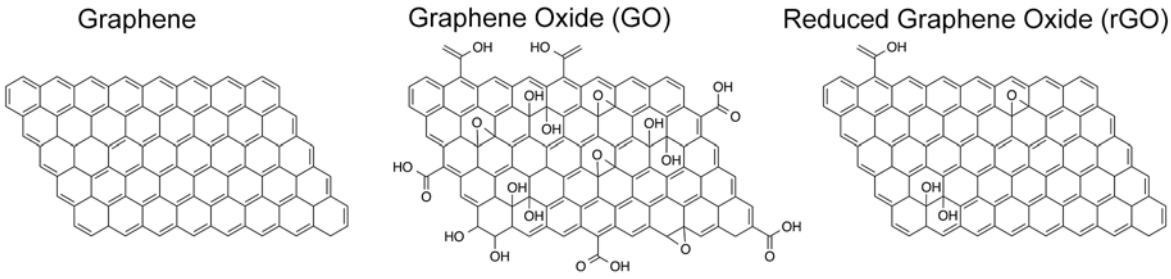

Figure 1. The chemical structure of Graphene, GO and rGO.

1.1.2 Functionalization

1.1.2.1 Covalent functionalization

Although graphene sheets displayed many amazing features, functionalization is essential to achieve better performances.[11] Because for many applications graphene derivatives should be dispersible in organic or aqueous solvents [3-5]. High dispensability improve the prossesibility of graphene derivatives and open a way to construct many systems out of these 2D nanomaterials [5-7]. Pristine graphene consists entirely of aromatic rings.[3,4] In contrast, GO has many carboxyl groups on the edges and at defect sites, with many epoxide and hydroxyl groups on the basal plane.[8] Although these functional groups can be largely eliminated by reduction to rGO, some will remain, particularly hydroxyl groups.[9,10] Many methods for covalent functionalization of graphene leverage these oxygen-containing groups rather than trying to modify the less reactive aromatic rings.[12] However, both pristine graphene and GO can be modified by a range of reactions including cycloaddition and radical reactions that occur on defect-free aromatic rings.[12,13]

Macromolecules, particularly polymers, bearing amino groups and hydroxyl groups can be conjugated to GO via condensation and ring-opening reactions.[14-21] The resulting GO derivatives possess properties of both graphene sheets and the attached macromolecules. It has been revealed that various amino acids affect the structure and morphology of graphene sheets differently and aliphatic amino acids increase the interlayer spacing of graphene, while tyrosine-modified graphene presents a scrolled structure.[14] GO can be modified via facile amidation reactions with polymers such as chitosan (CS).[15] High concentrations of hydrophilic polymers can significantly improve the aqueous dispersibility of the GO derivatives.[15,16] Compared with natural macromolecules, synthetic polymers are often cheaper and easier to synthesize in bulk.

Polyethylene glycol (PEG)[17] and polyvinyl alcohol (PVA)[18] have proven to be biocompatible and are widely employed to modify biomedical materials. PVA-grafted GO nanocomposites have similarly been prepared via carbodiimide-activated esterification reactions.[19] PNIPAM can be conjugated to GO sheets via “grafting to”[20] and “grafting from”[21] methods, creating stimuli-responsive materials.

It has been widely reported that the epoxy groups found on the GO basal plane are susceptible to nucleophilic ring-opening reactions with amino-terminated polymers.[22-27] Niu et al. developed an approach to covalently functionalize GO with poly-L-lysine (PLL) through such a reaction.[22] GO nanosheets have also been functionalized with 3-aminopropyltriethoxysilane (APTS) through this type of ring-opening reaction.[23] The hydroxyl groups on GO can also be modified by different (macro)molecules in a process termed post-functionalization or post-modification. 2-ureido-4[1H]-pyrimidinone was conjugated to GO by reaction between its hydroxyl groups and isocyanate linker from the pyrimidinone.[24] Hydroxyls can also be converted to other functional groups including amines,[25] carboxyls,[26] or thiols[27] to facilitate further modification. GO sheets rich with amine groups have been successfully prepared by Pumera et al. via a Bucherer-type reaction.[25] Carboxylic or thiol groups can also be attained, as demonstrated by Yu et al. and Pumera et al, respectively.[26,27] These can then be further modified through a wide range of conventional organic reactions, providing a large catalog of possible products.

Direct functionalization of graphene aromatic rings is nontrivial but can be a very powerful route to produce graphene derivatives.[11-13] More importantly, these reactions can be used to modify both GO and pristine graphene. The degree of functionalization can also be more flexible, as it is not determined or limited by the presence of existing functionalities such as the carboxyl and hydroxyl groups of GO.

Cycloaddition reactions occur when two or more molecules with unsaturated bonds combine and form a cyclic adduct.[28-34] Many papers have reported successful cycloaddition reactions with fullerene or carbon nanotubes,[28] and in recent years these successes have been repeated with graphene and GO, as well (Scheme 1).[29-34] Nitrene intermediates generated by the thermal decomposition of azides can combine with the unsaturated carbons in graphene in [2+1] cycloaddition reactions.[29] Nitrene reactions can be used to attach many polymers with various functionalities to the basal plane of graphene. Recently, our group developed a novel functionalization route which is suitable for both carbon nanotubes (CNT) and graphene, based on [2+1] cycloaddition with commercially available 2,4,6-trichloro-1,3,5-triazine and sodium azide.[32] 1,3-dipoles can

combine with dipolarophiles in graphene to form five-membered rings via a six-electron [3+2] cycloaddition.[34]

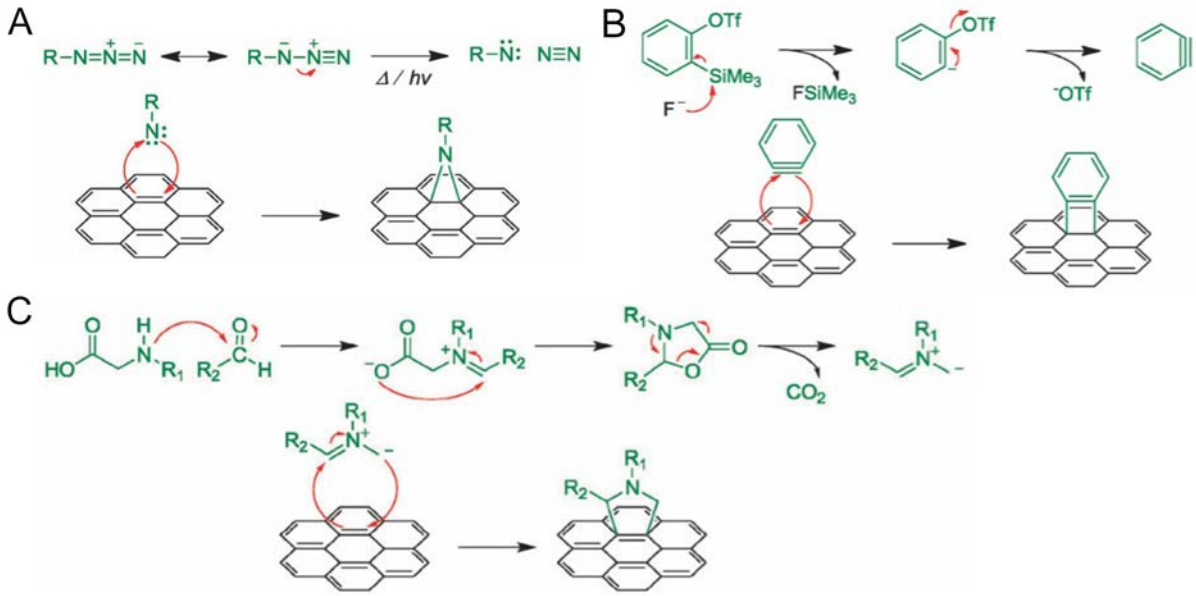

Scheme 1. Mechanism of the functionalization of graphene via cycloaddition. (A) [2+1] cycloaddition; (B) [2+2] cycloaddition and (C) [3+2] cycloaddition. Reproduced with permission.[13] Copyright 2013, Royal Society of Chemistry.

Self-initiated photografting and photopolymerization (SIPGP) was recently demonstrated as a facile polymerization method to functionalize graphene sheets via UV illumination without the use of initiator.[35-37] One significant benefit of SIPGP is that it does not introduce further defects to the graphene basal plane. UV irradiation can abstract hydrogen atoms from sp^3 carbon defects in graphene, generating free radicals.[35] SIPGP has been demonstrated with many vinyl monomers, and generates well-defined, homogeneous, stable polymer brushes on graphene.[36] SIPGP can be used to produce complex controlled graphene derivatives, especially in combination with other techniques. For instance, GO-chitosan composites assembled through electrostatic interactions have been subsequently modified by SIPGP to graft PS and PDMAEMA brushes from photoactive sites on different surfaces, producing Janus structures. The polymer brushes can be tuned by selection of vinyl monomers, and the thickness of the coating layer could be tuned by the UV irradiation time.[37]

1.1.2.2 Noncovalent functionalization

Covalent functionalization of graphene sheets is very valuable, making a range of simple and complex graphene-based composites accessible. However, covalent chemical

modifications of the graphene basal plane, including both oxidation during the preparation of GO and covalent conjugation of molecules onto graphene or GO sheets in the post-modification step, disrupts the continuous aromatic structure of pristine graphene sheets.[11-13] Therefore, noncovalent modification of graphene is of great interest for applications where the aromaticity and a preserved π system are crucial.[38] Noncovalent functionalization is typically due to π–π stacking, hydrophobic interactions, or electrostatic forces. It is well-known that π–π stacking can adhere molecules to each other.[39-42] Given the very large π system of graphene, similar interactions could attach functionalities onto its surface. In fact, graphite powder can be exfoliated into graphene sheets with aromatic amphiphiles containing aromatic segments and hydrophilic dendrons.[39] Similar results have been shown with the successful modification of RGO sheets with chiral mesogenic molecules,[40] as well as with a range of pyrene moieties,[41] again via π- π interactions. Several attempts have been made to use π–π functionalized graphene sheets for biological applications.[41,42]

Amphiphilic copolymers have been widely investigated as a means to enhance the solubility and stability of hydrophobic molecules and particles in aqueous solution.[43-45] This concept works well with hydrophobic graphene sheets to stabilize them under physiological conditions. Hydrophobic interactions allow the formation of RGO/heparin conjugates, where the hydrophobic portion of heparin binds to rGO, while the hydrophilic, negatively charged segment helps stabilization of the complexes in aqueous environments.[43] The resulting dispersion does not precipitate or aggregate even after 6 months, due to the charge repulsion.

GO sheets have a negative surface charge due to the carboxyl groups introduced during preparation, making it possible to use electrostatic forces to bind positively charged macromolecules onto its surface noncovalently.[46-48] Chitosan/GO complexes, formed by these type of electrostatic interactions, can be crosslinked using genipin to produce composite structures (GCS/GO) that can be transformed into films using solution-casting methods.[47] The strong interaction between GO and chitosan allowed for well-dispersed, homogeneous mixtures, which are strong candidates for biomedical applications, given that chitosan is a biological polymer. Similar films have also been created using GO and poly-L-lysine (PLL) to use as coatings.[48] These GO/PLL films have shown positive results in supporting the growth of mesenchymal stem cells (MSC) and can accelerate osteogenic differentiation.

1.2 Graphene derivatives and mammalian cells

Graphene-based nanomaterials have caused great interest for biomedical applications including cancer therapy.[3,6,7] However, it is quite important to understand the interaction between graphene derivatives and mammalian cells before practical administrations.[49] Fortunately, many studies have been performed and a great deal of knowledge about the cellular uptake, plasma membrane interaction, and organelle interaction of graphene-based nanomaterials is already known.

1.2.1 Cellular uptake

The cellular internalization pathways of nanoparticles have been intensively investigated and it is found that their uptake characteristics is dominated by several parameters such as size, surface charge, and geometry (Figure 2).[50,51] Phagocytosis (particles larger than 1000 nm) and pinocytosis (soluble materials) are two main pathways and both are energy-dependent routes. Furthermore, pinocytosis could be subdivided into four classes: macropinocytosis (large solute macromolecules), clathrin-mediated endocytosis (particles around 120 nm), caveolae-mediated endocytosis (particles around 60 nm), and clathrin/caveolae-independent endocytosis (particles around 90 nm).

It was reported protein-coated graphene nanosheets (PCGO) almost followed the same cellular uptake properties.[52] PCGO with small size (0.42 ± 0.26 μm) in diameter was mainly internalized by C2C12 cells via clathrin-mediated endocytosis (CME) while the large sheets (0.86 ± 0.37 μm) preferred to enter cells by phagocytosis. Raman microscopy was also employed to investigated the cellular uptake of GO with attached gold NPs to enhance the intrinsic Raman signal of GO nanosheets inside cells.[53] The results confirmed the GO sheets with small size was taken up by Ca Ski cells through energy-dependent CME.

In addition to size, surface charge plays also a pivotal role in the cellular internalization of NPs.[54] Attributed to their stronger affinity to the plasma membrane, NPs with positive charge usually have higher uptake efficacy than the negatively charged or neutral analogues. GO was also decorated with several kinds of moieties, including PEG, BSA, and PEI to obtain graphene derivatives with different surface charges and their corresponding cellular uptake characteristics were studied and compared.[55,56] The results demonstrated the endocytosis efficacy of PEG- and BSA-covered GO was retarded while huge enhancement was observed for positively charged PEI-modified GO sheets.

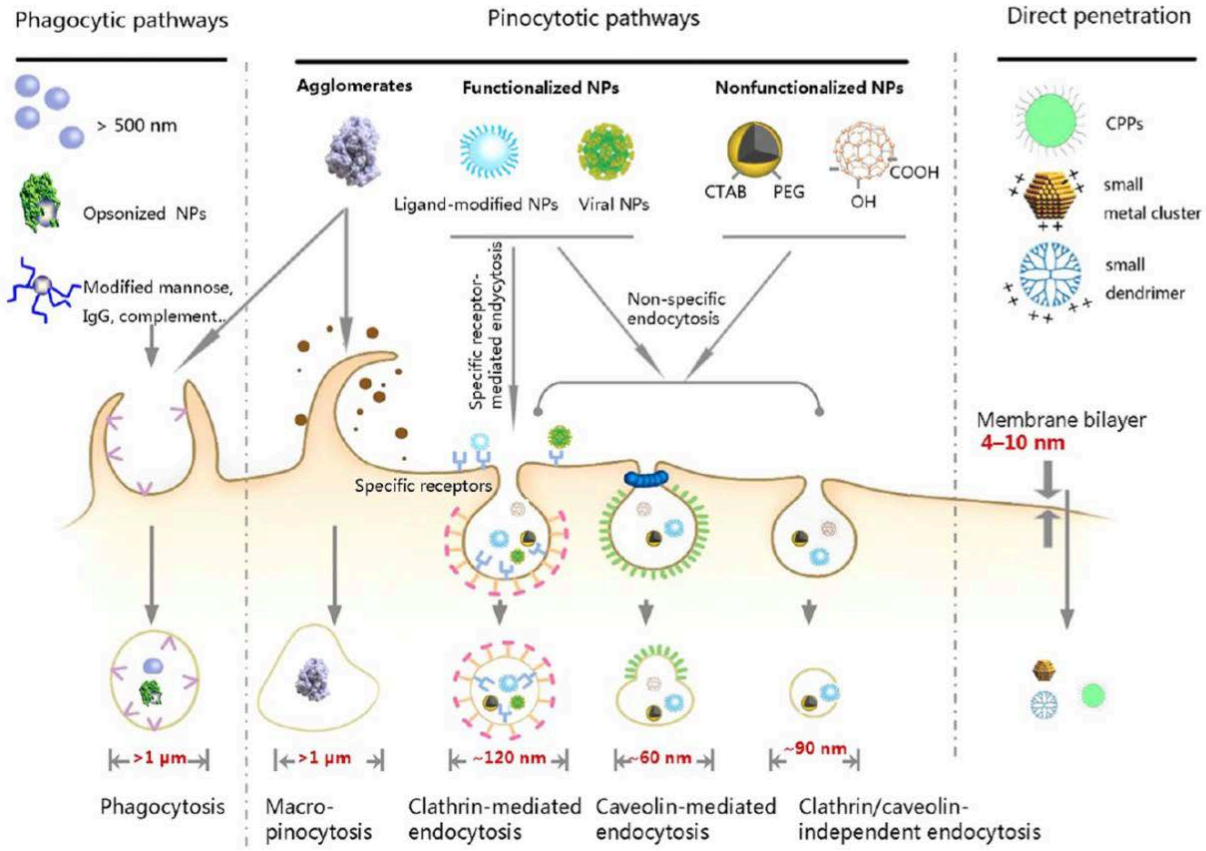

Figure 2. The cellular uptake pathways of nanoparticles with different characteristics. CPPs, cell-penetrating peptides; IgG, immunoglobulin G. Reproduced with permission.[50] Copyright 2012, American Chemical Society.

Besides size and surface charge, it is also acknowledged that the biological behaviors of graphene derivatives changes greatly with different cell types.[57] The cellular internalization mechanism of PEG-covered GO nanosheets was studied with eight inhibitors and three different cell lines (human Saos-2 osteoblasts, human HepG2 hepatocytes, and murine RAW-264.7 macrophages).[57] Their results showed micropinocytosis was a general entry pathway for all three different cell lines. Furthermore, microtubule-dependent pathway was another significant route for Saos-2 osteoblasts while CME played an important role in the uptake activities of HepG2 hepatocytes and RAW-264.7 macrophages.

Many reports displayed that targeting groups including folic acid, galactose, RGD peptide, and others effectively enhance the internalization of NPs into tumor cells with overexpressed specific acceptors on their membrane.[58-61] These ligands could also be employed to modify graphene sheets to improve their accumulation in tumor cells. GO decorated with aminopeptidase N (APN or CD13)-targeting ligands showed high cellular uptake and cytotoxicity towards certain cancer cells, especially those with overexpressed

CD13 receptors.[58] Recently, some interesting studies displayed that the permeability of plasma membrane increased a lot with the generated mild heat under near-infrared (NIR) laser irradiation, which make it easier for the sheets to cross.[62-64]

1.2.2 Plasma membrane interaction

The cytotoxicity of graphene-based materials is a significant topic and should be taken into consideration for further biomedical applications.[65,66] Some reports demonstrate that functional graphene sheets exhibited low toxicity both *in vitro* and *in vivo*.[67,68] However, others argued that graphene sheets with high concentrations would destroy the dynamics and integrity of the plasma membrane,[69-73] which led to the death of cells with leakage of lactate dehydrogenase (LDH).[69,70] Enthrallingly, one finding revealed the impair of plasma membrane by GO sheets could also improve the sensitivity of cancer cells to chemotherapeutic agents.[71-73] The interaction of graphene sheets and mammalian cells not only damaged their membrane but also generated excessive reactive oxygen species (ROS) and the combination of these factors resulted in a considerable toxicity for graphene-based nanomaterials. In another study, the cytotoxicity of graphene sheets was related with their size and shape, adding yet another wrinkle to this complex topic.[74]

Hemocompatibility is a crucial issue and should be taken into consideration where graphene-based nanomedicine are administrated via intravenous injection. In one work, both pristine graphene and GO exhibited low hemolysis up to 75 μg/mL.[75] However, a contradictory conclusion was obtained by another research group, showing concentration-dependent hemolysis ability for GO and rGO. And the hemolysis effect was highly affected by the sizes and oxidation degree of graphene derivatives.[76]

It is widely accepted that graphene nanomaterials exhibit plasma membrane impairment, which affords substantial cytotoxicity especially in high concentrations. Many researchers tried to reduce the cytotoxicity of graphene sheets via protein or polymer coverage.[77-79] The formation of protein corona could effectively mitigate the cytotoxicity of GO by decreasing its physical interaction with plasma membrane.[77,78] In addition to protein, biocompatible polymers, such as PEG, PVA, and PAA could also obviously improve the biocompatibility of graphene derivatives both *in vitro* and *in vivo* (Figure 3).[79]

It was reported that graphene sheets with larger lateral sizes (bigger than 1 μm) tend to attach onto the plasma membrane instead of penetration.[80,81] Min et al.[80] discovered attached GO could protect cells from taking up exogenous compounds,

including nanoparticles, nucleic acids, and toxic molecules. These cytoprotective effects of GO were confirmed by another work from Kim et al.[81] With GO pretreatment, mesenchymal stem cell (MSC) could be protected from ROS-mediated death, thereby improved the engraftment and therapeutic efficacy of MSCs.

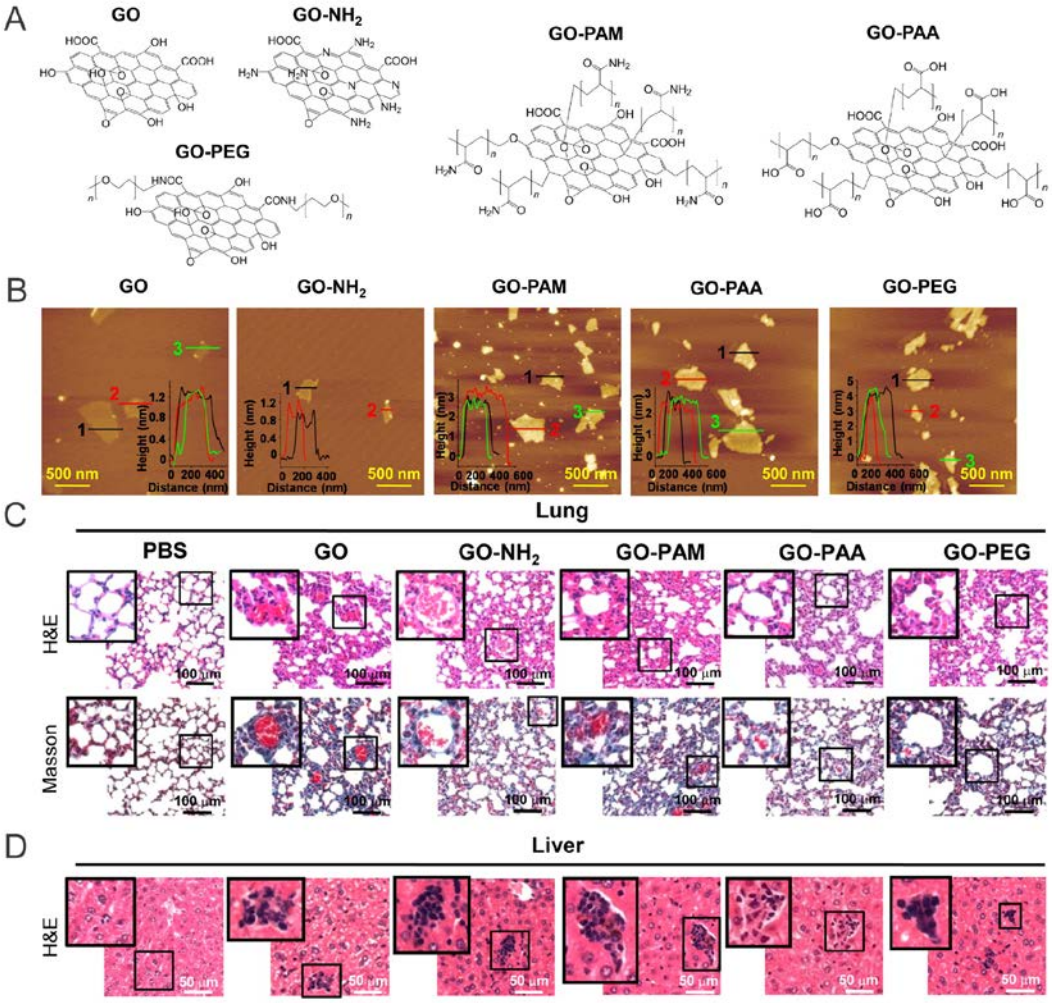

Figure 3. (a) Chemical structures of GO and its derivatives, including GO-NH_2, GO-PAM, GO-PAA and GO-PEG; (b) Representative AFM images with height profiles embedded. (c) Histological examination of lungs with H&E and Masson's trichrome staining; (d) Histological examination of livers with H&E staining. The mice in (c) and (d) was treated with 1 mg/kg GO materials for 14 days before tests. Dark spots represent GO-cell complexes in livers. Blue color indicates collagen in lung for Masson's trichrome staining. Reproduced with permission.[79] Copyright 2016, American Chemical Society.

1.2.3 Organelles interaction

In most studies, the graphene nanomaterials are entrapped within endosome and subsequently lysosome after their internalization. Some studies revealed that graphene

sheets with specific modifications could escape from the endosome/lysosomes and accumulate in other organelles. However, the characteristics (i.e., functionalities, surface charge, size, and others) of graphene derivatives to a large extent define their accumulation and interplay with a specific cellular compartment.

It has been discussed that graphene derivatives are taken up into cells mainly via endocytotic pathways. Therefore, endosome/lysosome played a pivotal role in the intracellular entrapment and transportation of functionalized graphene sheets.[82-84] Guo and his coworkers[82] observed both carbon nanotubes and graphene oxides entered in macrophage lysosomes, and this accumulation could potentially lead to the destabilization of lysosome membrane. It is known that the microenvironment in lysosome is acidic and the pH is less than 5.6, while the pH of the physiological conditions is around 7.4.[85,86] This is a fascinating characteristic and could be employed to design smart nanocarriers for targeting drug delivery. Many therapeutic agents including doxorubicin (DOX), Chlorin e6 (Ce6), dihydroartemisinin (DH), and transferrin (Tf) could be loaded onto the basal plane of graphene sheets.[85-91] The loading capacity is high and the systems are quite stable under physiological conditions, while a fast release was observed in acidic surroundings, which always resulted in efficient and targeting theranostic against tumor cells.

Mitochondria, which are called “energy factory” of the cells, play a significant role in the metabolism and functioning of the cells. Mitochondria are strongly related with many important cell activities including ATP synthesis, ROS generation, and initiation of apoptotic pathways. It was found that the internalized graphene derivatives localized in both endosomes/lysosomes and mitochondria.[72,92] The mitochondria membrane is negatively charged, therefore, positively charged graphene derivatives with PEI coverage could even target and accumulate in them.[56,93] Xing and his coworkers[94] showed that graphene sheets conjugated with pyropheophorbide-a (PPa) and integrin αvβ3 monoclonal antibody (mAb) could also escape from the endosomes and accumulate in mitochondria. The graphene sheets accumulated in mitochondria could cause the time-dependent depolarization of its membrane.[92,95] The decrease in mitochondria membrane potential could induce the decline of ATP production and thus cause the damage of F-actin cytoskeleton assembly and inhibit the migration and invasion of metastatic tumor cells.[92] Furthermore, graphene sheets could also enhance the production of ROS,[96,97] and this characteristic is dominated by the oxidation degree[98,99] and size[100] of these sheets. Other studies revealed the cytotoxicity of graphene nanomaterials came from the

combination of decrease in mitochondria membrane potential and over-production of ROS.[93,101-104]

The localization of graphene derivatives in other organelles besides lysosomes and mitochondria was also observed. Portolés et al.[105] found GO nanosheets could accumulate on F-actin filaments after uptake, inducing oxidative stress, cell-cycle alterations, and apoptosis. However, Cui et al.[106] reported that GO could enter several organelles including lysosome, mitochondria, endoplasm, and cell nucleus, while, some other researchers argued the graphene sheets with superb small size, especially graphene quantum dots, had the ability to target and localize in cell nucleus.[107-109] The conclusions here are quite diverse and even disputable, which may be attributed to the different size, oxidation, and other properties of these graphene sheets.

1.3 Functionalized graphene nanosheets for cancer therapy

Graphene-based materials have been widely applied in cancer therapy, and many exciting therapeutic concepts have been realized. However, bare graphene sheets can cause serious hemolysis and interact with blood components through hydrophobic or electrostatic interactions, leading to early exclusion from the body. Therefore, functionalization of graphene sheets is necessary before their further applications for cancer therapy. Functionalization can be summed up to be polyethylene glycol (PEG), hyaluronic acid (HA), polyethylenimine (PEI), other polymers, protein, DNA, and inorganic NPs. And in some cases, two or more above-mentioned modifications were employed to obtain graphene derivatives with excellent behavior for tumor theranostic.

1.3.1 Functionalization with polyethylene glycol

Among all of the polymers for biomedical applications, PEG is no doubt the most widely adopted candidate and has been approved for clinical trials by US Food and Drug Administration. Similar to other NPs, PEG coverage could protect the graphene sheets against being capture by the reticuloendothelial system (RES) cells and therefore prolonged their blood circulation.[110] Liu and his coworkers[111] provided a detailed protocol to functionalize rGO and nano rGO with PEG through both covalent and noncovalent routes.

Photothermal effect is one of the significant properties of graphene derivatives and has been employed for photothermal therapy (PTT).[62] Graphene derivatives have been

shown to generate heat through plasmonic photothermal conversion when irradiated with infrared low-frequency photons. GO showed obviously higher and more stable PTT than gold nanorods (AuNRs).[18] PEG-coated graphene sheets demonstrated highly efficient tumor passive targeting and relatively low retention in RES and efficient PTT. More importantly, no obvious side effects were observed for the injected mice by histology, blood chemistry, and a complete blood panel analysis. Application of PEGylated graphene for photothermal tumor therapy was also confirmed by different groups.[112-119] One finding showed the sizes and surface chemistry have unassailable effects on the biological behavior of functionalized graphene sheets including antitumor therapy *in vivo*.[113] The combination of radiotherapy and photothermal cancer therapy was also achieved by labeling PEGylated rGO sheets with 131I.[114] One way to enhance the NIR absorbance of PEGylated GO was developed by loading a NIR fluorescence dye (CySCOOH) and the resulting graphene-based nanocomposite could serve as an effective nanoplatform for PTT with quite low power laser irradiation.

Due to their high surface area, the loading capacity of graphene sheets toward hydrophobic molecules is much higher than other delivery systems such as polymeric nanocarriers.[2,6,7] Dai et al.[17] did the first attempt to adopt PEGylated GO as drug delivery nanocarriers for water-insoluble cancer drugs SN38. Several groups have reported successful loading and controlled release of DOX by PEGylated graphene sheets.[87,120-123] A redox-responsive PEG detachment was introduced to enhance the release of therapeutic agents at tumor-relevant glutathione (GSH) levels. [121] In another report, tumor necrosis factor (TNF)-related, apoptosis-inducing ligand (TRAIL) and DOX was co-loaded into a GO-based nanoplatform.[87] This sequentially functionalized GO nanostructure could release its cargos, TRAIL and DOX, to their targeted sites and consequently achieved a combination cancer treatment. As the anticancer effect of DOX is attributed to its intercalation with DNA thus suppressing the macromolecular biosynthesis,[87,121] the direct delivery of DOX to the DNA-enriched cellular nucleus would hugely enhance its cytotoxicity. For this purpose, TAT peptide-conjugated PEGylated graphene quantum dots (GQDs) were developed based on this hypothesis and the expected outcome was observed.[122] Tumor vasculature targeting was also applied to enhance the tumor site accumulation and drug delivery efficacy of graphene derivatives.[123]

In addition to chemotherapy, chemo-photothermal therapy was confirmed to be more efficient.[124-130] And the DOX-loaded PEGylated nanoGO exhibited a remarkable

improvement of the cell killing ability for drug-resistant cancer cells.[125] Recently, a novel strategy was developed to facilitate the penetration of a size-changeable GQDs nanoaircraft (SCNA).[126] The nanoaircraft was stable at physiological pH while disintegrated in the weakly acidic surroundings of the tumor's microenvironment, enhancing its penetration into the deep tumor tissue. Such a SCNA-based combinational therapy strongly inhibited xenograft tumors in 18 d without serious side effects.

In addition to DOX, some other anticancer drugs also attracted the attention of researchers, including resveratrol,[84,131] Pt(IV),[132] dihydroartemisinin,[91] paclitaxel,[133] and artesunate.[134] Resveratrol (RV) is an anticancer drug obtained from natural plants that has been used to induce apoptosis in several cancer cell lines.[135] It was reported the RV-loaded PEGylated GO could efficiently suppress tumor growth both *in vitro* and *in vivo*.[84] RV-loaded PEG-phospholipid-coated graphene sheets for cancer therapy could also be prepared through sonication of RV and rGO in FA-PEG-based liposome suspensions.[131] Dihydroartemisinin (DHA) was reported as an effective anti-malarial drug in 1970s, and DHA is able to produce ROS when interacting with ferrous ions (Fe^{2+}), making it as an alternative tumor therapeutic agent.[91] A therapeutic nanoplatform based on DHA and Tf-decorated nanoGO was fabricated.[91] After internalization, ferric ions (Fe^{3+}) are released and subsequently reduced to Fe^{2+}, which could interact with DHA. The antitumor experiments demonstrated this nanodrug led to significantly improved tumor suppression with minimal side effects *in vivo*.

Photodynamic therapy (PDT) is a form of phototherapy including a photosensitizing chemical substance and irradiation, which has been proven as a powerful tumor therapy method.[136] PEGylated-nanosized GO could cause the formation of singlet oxygen to combine PDT and PTT for the inhibition of melanoma tumors in mice.[137] Graphene sheets could also be employed as nanocarriers for loading of photosensitizer molecules, including Ce6,[138-142] porphyrin derivatives,[94,143-144] and ruthenium nitrosyl.[145-147] Ce6 which is a photosensitizer was first loaded on PEGylated GO by Liu and his coworkers.[138] They showed that PTT effect of graphene sheets could be used for the promoted release of Ce6 molecules, enhancing the PDT efficacy for tumors. In another work, a redox-triggered cleavable PEG shell was introduced to accelerate the release of Ce6 with recovered photoactivity.[139] The combination of chemotherapy and PDT was also performed with DOX and Ce6 on PEGylated GO, and the anticancer theranostics was quite promising.[141] Porphyrin derivatives are another kind of photodynamic agent for cancer therapy and its tumor accumulation and the PDT efficacy could be obviously

improved after being loaded on PEGylated GO.[143] Porphyrin derivatives can also be covalently conjugated to the PEGylated GQDs, and the resulting theranostic nanocomposites could be used for a combinational PTT/PDT for cancer treatment.[144] In another interesting work, the integrin $\alpha_v\beta_3$ monoclonal antibody (mAb) was linked on PEG-covered GO nanosheets and the functionalized graphene sheets could not only target $\alpha_v\beta_3$-positive tumor cells but also translocate into mitochondria after endocytosis.[94] In the mitochondria, loaded pyropheophorbide-a was discharged and thus the PDT result was remarkably improved. Ruthenium nitrosyl (Ru) was recently found to be an effective photodynamic molecule under the irradiation (450 nm) for tumor theranostic.[145-147] Ru could be loaded on the graphene sheets via π−π stacking and hydrophobic interactions[145] or through covalent conjugation.[146,147] Mitochondria-targeting groups, such as triphenylphosphonium (TPP), could be jointly employed with Ru, and the PDT therapeutic efficacy of the resulting nanoplatform was obviously enhanced.[147]

1.3.2 Functionalization with polyethylenimine

Polyethylenimine (PEI) is a positively charged polymer with a large number of amine groups on the periphery and has been widely used for biomedical applications.[148] The PEI-functionalized graphene sheets has also been prepared and employed for antitumor therapy.[58,59,149-153] It was reported that PEI-covered GQD accumulate in the nucleus region.[149] Combretastatin A4,[58] indocyanine green,[150] and DOX[59,151] were loaded on the PEI-coating graphene sheets and remarkable tumor suppression results were observed. A gene delivery nanoplatform based on PEG and PEI dual-functionalized GO was developed and the diameter could be controlled by the PEI content.[152] The nanodevice exhibited lower cytotoxicity and higher transfection efficacy, which is promising as a novel nanomedicine for cancer gene therapy. The attempt for combination of chemo-therapy and gene-therapy was tried with DOX and p53 plasmid.[153] DOX was loaded onto the basal plane of PEI-covered GO and p53 was condensed by electrostatic interactions. Although DOX and p53 were simultaneously discharged from the nanoplatform, their synergistic therapy on tumor cells was found to be in a consecutive mode, which is fascinating and of great significance for further investigations.

1.3.3 Functionalization with hyaluronic acid

Hyaluronic acid (HA) is a linear carbohydrate polymer and has the specific targeting ability for cluster determinant 44 (CD44) which is overexpressed on the plasma membrane of many cancer cells.[154] HA has been widely employed as corona to improve the biocompatibility and solubility of NPs including graphene sheets and simultaneously enhances their active targeting capability.[85,155-163] Photochromic dye spiropyran (SP) could be conjugated to HA and then GO was decorated by this modified HA to obtain light-sentitive nanohybrids.[156] Upon irradiation with UV light (365 nm), SP was converted to merocyanine form which a fluorescent signal could be detected by confocal laser scanning microscope (CLSM), which made it easier to study their intracellular localization and *in vivo* behaviors. In another work, a redox sensitive-linker was introduced to develop a redox-dependent response for accelerated intracellular drug release.[157] A dual-receptor targeting drug delivery system was developed by conjugating Arg-Gly-Asp peptide (RGD) onto the HA-coating GO.[158] The dual targeting nanoplatform has proven to be a promising candidate for targeted tumor therapeutics. Some other kinds of therapeutic agents, such as 5-fluorouracil[161] and indocyanine green (ICG),[162] could also be loaded onto the HA-covered graphene sheets to act as anticancer nanodevices. Besides drug delivery, Lee et al. [163] made attempts to develop HA-coated GO for miR-21 translocation. Their results demonstrated that endogenous miR-21 could be knocked down after uptake and subsequently caused the suppressed proliferation and inhibited the migration of cancer cells.

1.3.4 Functionalization with other polymers

In addition to the widely used PEG, PEI, and HA, many other kinds of polymers have also been employed to functionalize graphene sheets for biological applications. These polymers could be divided into two main categories: synthesized polymers[42,164-171] and natural polymers.[172-181] The lipid bilayers-covered graphene nanosheets (lipo-GNS) were developed as a cancer theranostic nanoplatform for the co-delivery of docetaxel (DTX) and gasified perfluorohexane (PFH)).[164] It was found that ultra small lipo-GNS (40 nm) accumulated in cells 200-fold to the lipo-GNS with the diameter of 270 nm. Their results demonstrated that this multifunctional lip-GNS is a good candidate for combined gasification/chemo-thermotherapy tumor treatment. In another work, phosphorylcholine oligomer-grafted perylene (perylene-PCn), was synthesized and

covered onto rGO sheets.[42] The resulting rGO/perylene-PCn nanohybrids was water dispersible and biocompatible and was employed as nanocarriers to deliver PTX. Amino groups capped dendrimers,[166] polystyrene sulfonate sodium salt (PSS),[167,168] and poly(vinylpyrrolidone) (PVP)[169-171] have also been reported to be effective modifiers for graphene sheets and showed excellent performance for drug delivery.

Compared to the synthetic polymers, natural polymers often show higher biocompatibility and could be obtained from natural sources. Heparin is one of glycosaminoglycans that can be found in the plasma membrane of eukaryotic cells and has the ability to prevent the formation of clots and eliminate the existing clots in the blood vessel.[172] The functionalization of graphene sheets with heparin was conducted and the coverage of heparin increased the loading capacity of rGO for DOX and its accumulation in tumor site.[173] It was also found that DOX-loaded, heparin-decorated GO could mitigate the cardiotoxicity coming from DOX and the pulmonary toxicity deriving from unmodified GO.[174] Chitosan (CS) is a linear polysaccharide composed of randomly distributed β-linked D-glucosamine and N-acetyl-D-glucosamine and could be obtained from the chitin shells of shrimp and other crustaceans.[175] CS-PEG-conjugated nanodimensional GO loaded with DOX demonstrated a promising antitumor effect.[30] CS-covered GO could also be developed to deliver dicer-substrate small interfering RNA (DsiRNA) to the targeted site in the colon with the assistance of colon-targeting group pectin.[176] It has recently been reported glycyrrhetinic acid (GA) is a novel mitochondria-targeting ligand and GA-modified GO could be employed as an effective nanovehicle to delivery drugs into mitochondria.[177] Furthermore, these functional graphene sheets could also trigger the decrease of mitochondrial membrane potential and activate the mitochondria-mediated apoptosis pathway. Many other biocompatible natural polymers, such as amaranth extract,[178] alginate,[179] dextrin,[180] and inulin[181] have also been used to functionalize graphene sheets as drug delivery nanoplatforms for antitumor therapy.

1.3.5 Functionalization with protein and DNA

Protein and DNA have also been widely employed in the development of novel biomaterials including graphene-based nanomaterials. It was reported bovine serum albumin (BSA)-covered nanosized rGO displayed high stability and low cytotoxicity.[182]

The functionalized graphene sheets could be employed for both photoacoustic imaging and photothermal therapy. Additionally, the BSA-covered GO was found to specifically bind to endothelial growth factor (VEGF)-A_{165} and then inhibit the proliferation, migration, and tube formation of human vein endothelial cells.[183] Finally, VEGF-A_{165}-induced blood vessel formation could be remarkably blocked. In another interesting study, BSA-cis-aconityl pheophorbide-a(c-PheoA) conjugate was used to coat GO with different ratios.[184] Both the *in vitro* and *in vivo* results confirmed that the nanocomposite showed higher anticancer efficacy than free PheoA. Hydrophobic antitumor drug also could be loaded onto the BSA-coating GO to improve its therapeutic efficacy.[185-187] Ponpandian et al.[187] developed the hydrothermal synthesis of hydroxyapatite (HAp) nanorods on GO sheets to obtain HAp-attached GO (HAp/GO) and then BSA was covered on this nanocomplex. The resulting BSA-decorated HAp/GO demonstrated good biocompatibility and acted as a good nanoplatform for anticancer drug translocation.

Transferrin (Tf) which is an iron-transporting serum glycoprotein could bind to receptors overexpressed at the plasma membrane of glioma cells.[188-190] Tf-modified graphene(TfG) was employed as targeted delivery nanodevices and displayed a high uptake efficiency and cytotoxicity against C6 glioma cells.[188] TfG has also been used for radiofrequency ablation (RFA) against hepatocellular carcinoma (HCC).[189] Under the exposure to 100 W radiofrequency, TfG could cause 4 times more death of the cells than bare graphene. A core/shell structure was fabricated by anchoring lactoferrin onto GO nanosheets through a double emulsion method.[191] The nanocapsules were used to transport hydrophobic DOX to cancer cells and a burst-like release was achieved with NIR irradiation. Furthermore, PTT eradicated not only the tumor cells under the irradiation region but also light-omitted tumor cells, surmounting the possible tumor recurrence in other therapies.

DNA is a molecule that carry genetic information for the growth, development, functioning, and reproduction of all living creatures. Recent studies showed that DNA could also be used for the modification of nanocarriers.[192,193] Oh et al.[192] synthesized DNA polyaptamer nanothreads by rolling cycle amplification and then anchored the receptor-specific polyaptamers onto the surface of rGO. Their results demonstrated that these functionalized rGO was taken up by protein tyrosine kinase 7 receptor (PTK7) overexpressed leukemia cells with a higher efficacy and therefore exhibited stronger therapeutic efficacy compared to rGO covered with scrambled polyaptamers. In another research, GO, single-stranded DNA, and ATP aptamers were

crosslinked and ATP-responsive DNA-graphene nanoaggregates were formed and used for drug delivery.[193] The dissociation of the nanoaggregates could be triggered in the media with high concentration of ATP, which could accelerate the release of loaded drugs and is favorable for the targeted delivery of therapeutic agents.

1.3.6 Functionalization with inorganic coatings

Inorganic attachments, including Au NPs, metal oxide NPs, mesoporous silica and others, also sparked researchers' interest to produce graphene hybrids with fascinating properties. An aptamer-Au NPs-hybridized GO was fabricated and was applied for PTT with NIR light irradiation.[194] The anticancer results demonstrated that Au NPs anchored on GO could improve the photothermal effects, and the aptamer-conjugated nanocomplex exhibited significant therapeutic effects on MCF-7 cells at a low concentration without severe adverse effects for healthy cells. An cell-mediated nanoparticle delivery was proposed as an effective tumor therapeutical approach in another report.[195] Hybrid sheets composed of Au NPs and GO were obtained and stably attached to the tumor-tropic MSC. The loading capacity was largely enhanced and the cytotoxicity was effectively avoided through this functionalization. In addition, it was reported that excellent photoacoustic (PA) imaging,[118] computed tomography (CT) imaging,[168] and surface-enhanced Raman scattering (SERS) imaging[196] could be achieved with Au NPs/GO nanohybrids. A photodynamic agent[142,178] and chemotherapeutic drug[129,197-199] could also be loaded on the Au NPs/graphene nanocomposites to obtain an improved synergic theranostic effect. Targeting DNA aptamer greatly facilitated cellular internalization of nanocomposites within cancer cells.[198] It was also reported polyaniline shell could be covered on Au NPs to obtain core-shell nanocomposites with stronger NIR absorption, remarkable stability, and low cytotoxicity.[199] These nanocomposites were anchored onto GO and the resulting nanoplatforms were confirmed to be effective for chemo-photothermal ablation of cancer cells *in vitro* and *in vivo*.

Magnetic resonance imaging (MRI) was developed as a promising approach to visualize anatomical structures in clinical studies for early tumor detection.[200] It was reported iron-based magnetic nanomaterials could be applied as T2 MRI contrast agents (CAs) and they were much safer than T1 MRI CAs.[201] GO/Fe_3O_4 nanohybrids were fabricated for efficient cellular MRI and the nanohybrids displayed good hydrophilicity, less cytotoxicity, and higher MRI enhancement.[167] Furthermore, GO/Fe_3O_4

nanoconjugates showed a prolonged blood circulation half-life (~27.7 h) and outstanding tumor accumulation via an enhanced permeability and retention (EPR) effect.[202] In another work, a multimodal tumor imaging-guided, highly effective PTT was conducted with PEG-covered rGO/iron oxide NPs(IONP).[203] Triple-modal fluorescence/MRI/PA tomography *in-vivo* tumor imaging was realized with external radioactive, fluorescent labels, and magnetic properties. Together with the successful imaging process, the rGO/IONP nanocomposites were applied as nanocarriers for PTT and chemotherapy.[115,127,150,204] rGO/IONP was presented as an approach to map and eliminate regional lymph nodes (RLN), which may serve as an alternative for lymph node dissection by invasive surgery.[115]

Recently, mesoporous silica (MS) was introduced as a drug delivery nanocarrier owning to its unique properties, such as tunable pore structure, good biocompatibility, and easy surface modification.[205] However, the uncontrolled leakage of drugs from the open silica pores could cause serious toxicity to normal cells.[205] Therefore, the conjugation of MS onto graphene sheets is favorable for combining their advantages to develop more effective antitumor nanoplatforms.[128,159,160,196,206-208] Therapeutic agents could be loaded onto the graphene/MS nanosystem and polymers were conjugated as gatekeepers to avoid the unwanted release.[128,159,160,206,207] By varying pH and laser irradiation, targeted delivery and synergic therapy could be achieved.

2 Scientific goals

Hyperbranched polyglycerol (hPG), which can be easily prepared by a controlled synthesis via anionic ring-opening multi-branching polymerization (ROMBP), displays excellent biocompatibility, chemical stability, low intrinsic viscosity, tunable blood circulation, compact size, and other appealing features.[209,210] Although many kinds of polymers were used to functionalize graphene sheets to obtain nanoplatforms with better properties for biological applications, hPG seems more promising due to its bioinert properties. Recently, a novel method to functionalize graphene sheets through triazine-mediated [2+1] cycloaddition reaction was developed in our group. This method is suitable for successful conjugation of (macro)molecules including hPG onto the basal plane of graphene.[32] Therefore, in this study, I planned to prepare hPG-decorated graphene sheets with different physiochemical properties by this method and investigate their biological interactions with mammalian cells. With enough knowledge about their biological behaviors, these hPG-functionalized graphene sheets could be used to construct smart antitumor nanoplatforms.

Although fascinating progresses have been achieved with functional graphene sheets in biological applications, there were still some issues that need to be settled before further investigations. The first challenge was to investigate the cellular uptake mechanisms of graphene derivatives with different physiochemical properties and to elucidate the dominant factors at this significant biointerface. There were several above-mentioned studies that individually focused on the effects of size and surface charge of graphene derivatives on their biological behaviors.[52-56] However, it is important to combine two or more factors and simultaneously study them in one system. In the first project, we tried to address this problem by preparing water dispersible hPG-covered graphene sheets with a defined size and surface charge. Cellular uptake characteristics of graphene derivatives were carefully investigated by confocal laser scanning microscopy (CLSM) and fluorescence-activated cell sorting (FACS). Moreover, several inhibitors were applied to discover the relationship between endocytosis mechanisms and the physiochemical properties of graphene derivatives. I hoped this work could elucidate the conditions that dominated the cellular uptake pathways and efficacy of functionalized graphene sheets.

The second challenge was to understand the release features of drug-loaded-functionalized graphene sheets. Although the application of graphene derivatives as therapeutic nanocarriers has been largely studied, the correlation between their physicochemical properties and release characteristics has not been reported. The current

triggered release strategy for graphene-based nanocarriers is mainly based on the acidification inside the cells, which is not specific.[85-91] Furthermore, laser irradiation can also be used to stimulate the cargo release of graphene nanovehicles,[124-126] but this strategy is limited to the surface tissues owning to the low penetration of laser into the deeper targeted organs.[211] In the second project, we prepared functionalized graphene sheets with similar polymer coverage and size but different surface functionalities and charges. DOX was loaded onto these graphene sheets with positively and negatively charged coverage and its intracellular release was observed by Förster resonance energy transfer (FRET). I hoped this design was helpful to understand the release mechanism of therapeutic agents from the graphene surface inside the cells.

Multidrug resistance (MDR) is a serious problem nowadays as the traditional chemotherapy usually fail when they are applied for MDR cancer cells.[212,213] Therefore, another challenge of my Doctoral studies was to construct graphene-based nanomedicine for the theranostic of MDR tumors. It was reported MDR usually arose from the overexpression of ATP-binding cassette (ABC) such as P-glycoprotein (P-gP), which could decline the cellular uptake and even actively pump out therapeutic agents from the cytoplasm via an ATP-dependent manner.[212,213] As we know, mitochondria are the intracellular "energy factory" and responsible for the production of ATP which is the "biological fuel". Therefore, suppression of the production of ATP through dysfunction of mitochondria should be an effective strategy to surmount the MDR.[214,215] In the third project, we synthesized and characterized a mitochondria-targeting ligand and charge-conventional groups conjugated hPG-covered nanographene sheets (75 nm) for overcoming MDR tumors. Our hypothesis was that this multifunctional graphene-based nanoplatform could effectively target and accumulate in mitochondria and then disrupt this organelle with NIR laser irradiation. Under irradiation, anticancer drugs could be simultaneously discharged and finally the MDR would be reversed.

3 Publications

3.1 Combination of Surface Charge and Size Controls the Cellular Uptake of Functionalized Graphene Sheets

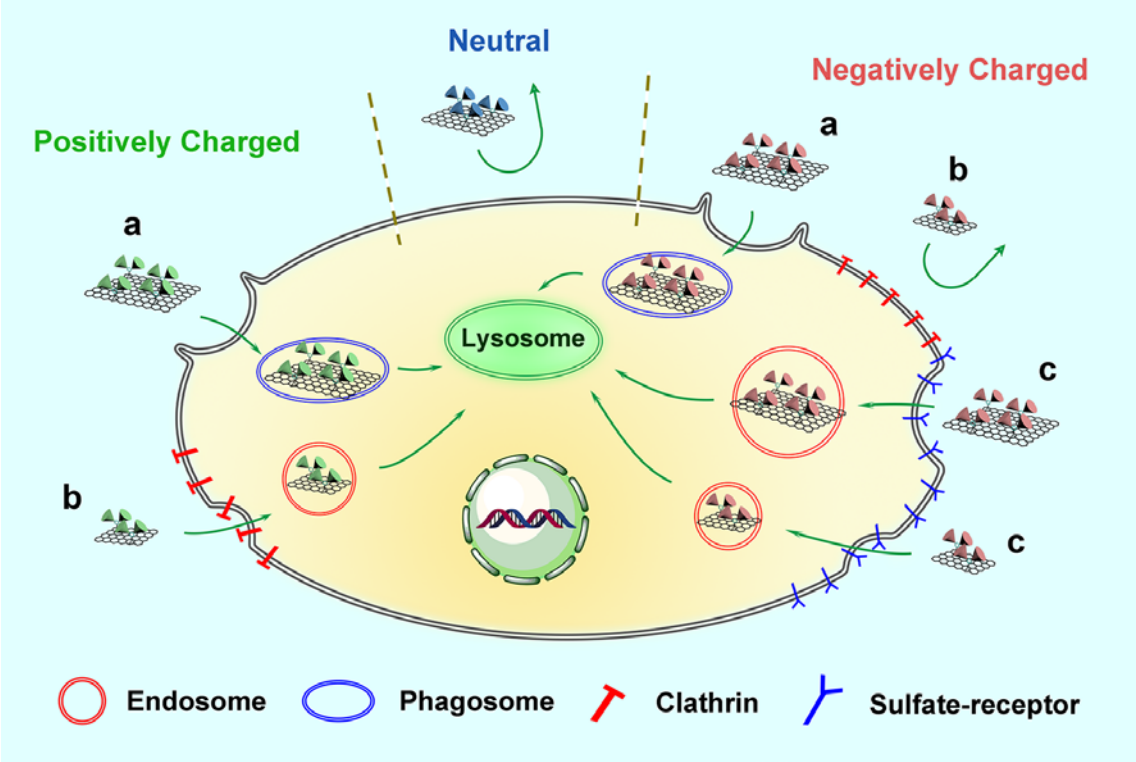

Zhaoxu Tu, Katharina Achazi, Andrea Schulz, Rolf Mülhaupt, Steffen Thierbach, Eckart Rühl, Mohsen Adeli, Rainer Haag

Adv. Funct. Mater. **2017**, *27*, 1701837

http://dx.doi.org/ 10.1002/adfm.201701837

Author contributions

Zhaoxu Tu performed the main experiments, and wrote the manuscript.

Katharina Achazi supported the biological experiments.

Andrea Schulz helped with the TEM measurements.

Rolf Mülhaupt provided the thermally reduced graphene oxide (TRGO).

Eckart Rühl instructed and Steffen Thierbach performed the Raman microscopy test.

Mohsen Adeli and Rainer Haag conceived and supervised the project, as well as corrected the manuscript.

3.2 Functionalized Graphene Sheets for Intracellular Controlled Release of Therapeutic Agents

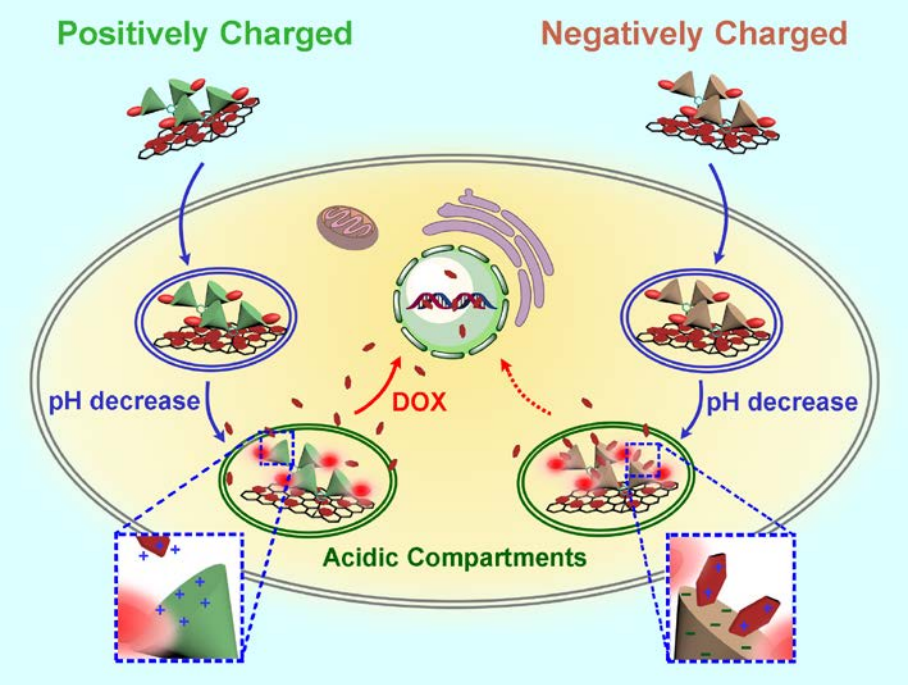

Zhaoxu Tu, Virginia Wycisk, Chong Cheng, Wei Chen, Mohsen Adeli, Rainer Haag

Nanoscale, **2017**, *9*, 18931.

http://dx.doi.org/10.1039/C7NR06588D

Author contributions

Zhaoxu Tu performed the main experiments, and wrote the manuscript.

Virginia Wycisk synthesized and provided the pH-sensitive dye.

Chong Cheng measured and analyzed the AFM images.

Wei Chen helped with the preparation of hydrophobic DOX and the measurement of release profile.

Mohsen Adeli and Rainer Haag conceived and supervised the project, as well as corrected the manuscript.

3.3 Graphene-Based Nanoplatforms for Hyperthermia Surmounting of Multiple-Drug Resistance

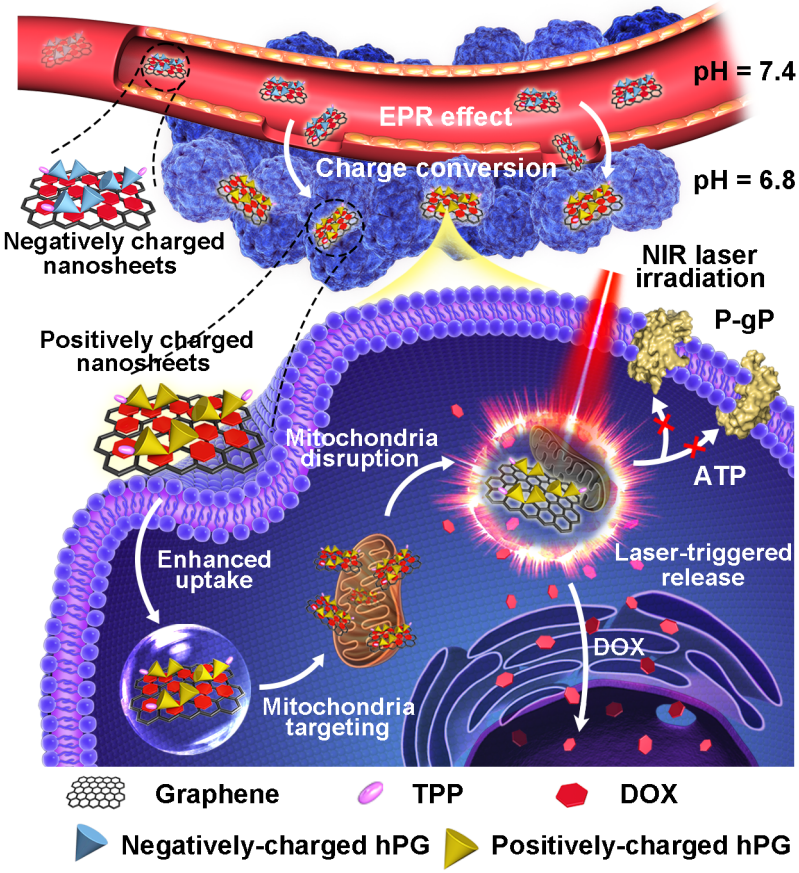

Zhaoxu Tu, Haishi Qiao, Yuting Yan, Guy Guday, Wei Chen, Mohsen Adeli, Rainer Haag

http://dx.doi.org/10.1002/anie.201804291

Author contributions

Zhaoxu Tu conceived the project and performed the main experiments, and wrote the manuscript.

Haishi Qiao and Yuting Yan performed the *in vivo* experiments, collected and analyzed the *in vivo* data.

Guy Guday measured the AFM images and analyzed the data.

Mohsen Adeli, Wei Chen and Rainer Haag conceived and supervised the project, as well as corrected the manuscript.

Directed Graphene-Based Nanoplatforms for Hyperthermia-Overcoming Multiple Drug Resistance

Zhaoxu Tu,[b] Haishi Qiao,[a] Yuting Yan,[a] Guy Guday,[b] Wei Chen,*[a] Mohsen Adeli,*[b,c] and Rainer Haag*[b]

Abstract: Multidrug resistance (MDR), which leads tumors resistance to traditional anticancer drugs, can cause the failure of chemotherapy treatments. In this work, we present a new way to overcome this problem using smart multifunctional graphene-based drug delivery systems which can target subcellular organelles and show synergistic hyperthermia and chemotherapy. Mitochondria-targeting ligands are conjugated onto the doxorubicin-loaded, polyglycerol-covered nanographene sheets to actively accumulate them inside the mitochondria after charge-mediated cellular internalization. Upon near-infrared irradiation (NIR), adenosine triphosphate (ATP) synthesis and mitochondrial function were inhibited and doxorubicin released into the cellular interior. The hyperthermia-accelerated drug release led to a highly selective anticancer efficiency, confirmed by *in vitro* and *in vivo* experiments.

2D nanomaterials including graphene, transition-metal dichalcogenides, black phosphorus, and others have recently gained tremendous interest for biomedical applications and provide new insights for future cancer therapies.[1] In addition to photothermal effect and high cellular uptake, 2D nanomaterials exhibit an extremely high loading capacity for therapeutic agents as compared with the traditional polymer-based nanocarriers.[2] Accordingly, graphene derivatives and their hybrid systems have been used to produce nanosystems for controlled delivery of therapeutic agents in cancer therapy.[3] Although appealing therapeutic effects and remarkable progress in cancer therapy have been demonstrated, control over the functionality and physicochemical properties of these graphene-based nanoplatforms is crucial to address challenges such as MDR.[4]

MDR usually arises from the overexpression of ATP-binding cassette (ABC) such as P-glycoprotein (P-gP), and results in the failure of traditional chemotherapy.[4] P-gP remarkably inhibits the cellular uptake and even causes an active removal of anticancer drugs from the cytoplasm to the extracellular surroundings via ATP-dependent pathways.[4] The combination of suppressing ATP production through mitochondrial dysfunction triggered by hyperthermia, along with releasing therapeutic agents, should be an effective strategy to surmount MDR.[5] For example, it has been found that tumor-triggered nanomedicine composed of proapoptotic peptide KLA[5b] or gold nanostars are able to disrupt mitochondria with NIR irradiation and greatly increase the anti-MDR efficacy.[5c] However, side effects, poor stability, as well as low uptake and loading capacity are factors which limit the efficacy of these systems.[5]

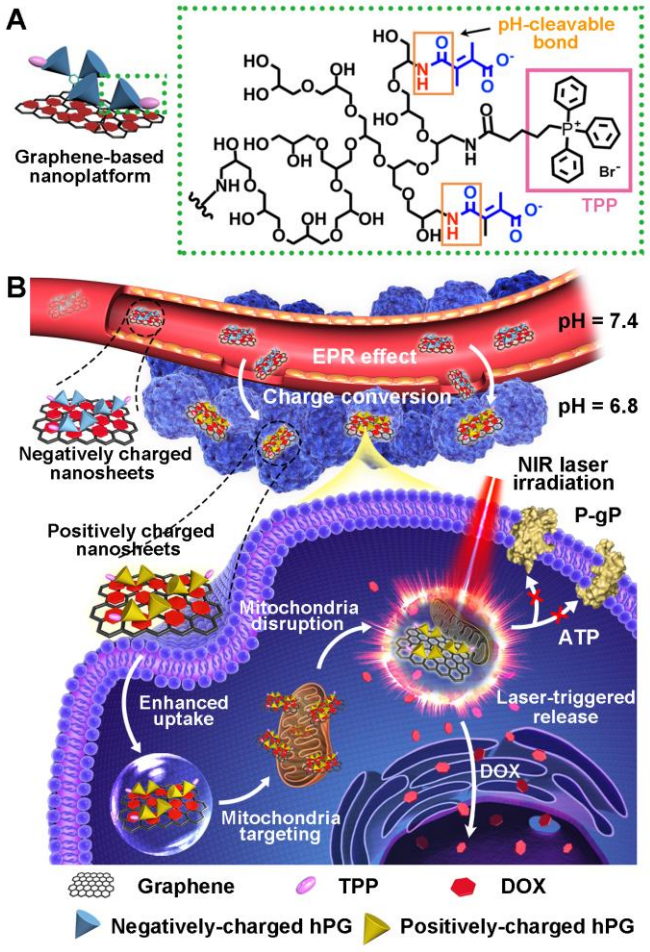

Scheme 1. (A) The chemical structure of functionalized nanographene sheets; (B) Hyperthermia surmounting of MDR by functionalized graphene sheets. After charge-mediated cellular internalization, graphene sheets accumulate into the mitochondria by targeting ligands. Mitochondrial dysfunction and accelerated drug release through hyperthermia result in MDR suppression and efficient chemotherapy.

Due to their stability and good photothermal properties,[2a,3a] high loading capacity,[2c,2d] and fast cellular uptake,[2b-2d,6] functionalized graphene derivatives are promising candidates for inducing mitochondrial dysfunction. However, their size, functionality, and dispersability in aqueous solutions are factors that have to be optimized before proceeding for any biomedical study. Our previous work proved that hyperbranched polyglycerol (hPG) coverage could effectively improve the

[a] Dr. H. Qiao, Y. Yan, Prof. W. Chen
Department of Pharmaceutical Engineering, China Pharmaceutical University, Nanjing, 210009, China
E-mail: w.chen@cpu.edu.cn
[b] Z. Tu, G. Guday, Prof. M. Adeli, Prof. R. Haag
Institut für Organische Chemie und Biochemie, Freie Universität Berlin, Takustraße 3, 14195 Berlin, Germany
E-mail: haag@chemie.fu-berlin.de
[c] Prof. M. Adeli
Department of Chemistry, Faculty of Science, Lorestan University, Khorram Abad, Iran
E-mail: aadeli@zedat.fu-berlin.de

Supporting information for this article is given via a link at the end of the document.

biocompatibility of graphene sheets, which provide a new idea for the biological application of functional graphene sheets.[6]

Recently, we have developed a method[7] to produce high quality nanographene sheets (nG) with narrow size distribution, in a suitable regime (50 nm - 100 nm) for *in vivo* administration. According to Raman spectra and other characterizations, the composition and structure of the produced nG is close to CVD samples,[7] leading to outstanding optoelectronic properties. However, poor water dispersibility and functionality of the nG is a challenge and hampers *in vivo* studies.[7] Recently, we implemented a new method for the controlled nondestructive functionalization of carbon based nanomaterials through nitrene [2+1] cycloaddition reaction at ambient conditions.[6,8] Controlled post-modification of the triazine-functionalized graphene sheets by different (macro)molecules resulted in graphene sheets with desired functionalities.[8c,8d] In this work, nG was produced and functionalized by triazine, and consequently post-modified with hyperbranched polyglycerolamine (hPG_{NH2}) according to previously reported methods.[6] Afterwards, triphenylphosphonium (TPP), a mitochondrial targeting ligand,[9] was conjugated to the surface of the nanosystem. Polyglycerol-functionalized nG (GP) and their analogs with TPP ligands (GPT) were further functionalized by 2,3-dimethylmaleic anhydride (DA) to obtain graphene derivatives with pH-triggering surface charge conversion (GPD and GPTD, respectively).[10] In order to investigate the pH-triggered surface charge conversion of GPTD, succinic anhydride-modified GPT (GPTS) was also synthesized and used as a reference. Information concerning the synthetic procedures can be found in the ESI (Scheme S1).

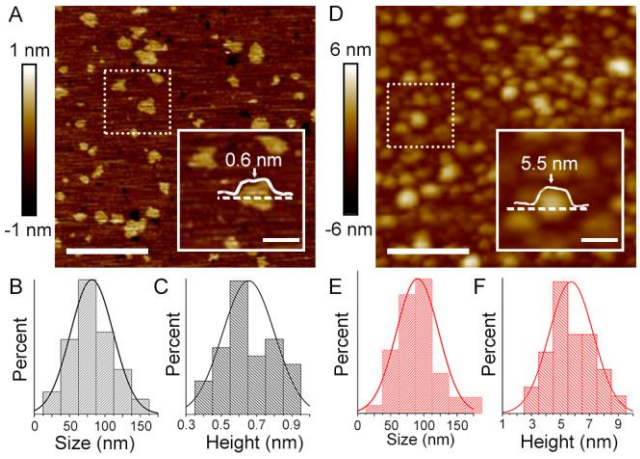

Figure 1. AFM images of nG (A) and their size distribution (B) and height profile (C); AFM images of GPTD (D) and their size distribution (E) and height profile (F); Scale bars in full images correspond to 500 nm and the scale bars in the amplified sections correspond to 100 nm.

The functionalized graphene sheets were characterized by different methods (Figure 1 and Figures S1-S4). AFM images, size and height distribution histograms of nG, GPD, GPTS, and GPTD are displayed in Figure 1 and S2. The diameter of products before and after functionalization is almost the same and shows a narrow size distribution with a mean value of 75 nm. However, the average height of the graphene sheets rose from 0.65 nm to 5-6 nm upon functionalization. The efficacy of surface charge conversion was investigated by measuring the zeta potential of graphene sheets at different pHs (Figure S4). While GPT and GPTS exhibited positive and negative charges in a broad range of pH, the zeta potential of their GPTD analogues with charge conversion ability changed abruptly from negative to positive upon decreasing pH from 7.4 to 6.8 (Figure 2A and 2B). Therefore, GPTD should be negatively charged in the blood stream, leading to a longer-term circulation in body and a higher enhanced permeability and retention (EPR) effect.[10b] After accumulation in tumor, the surface charge will become positive, accelerating cellular uptake and inducing efficient therapeutic delivery.[6,11]

The toxicity of graphene derivatives against P-gP overexpressed (Figure S5) multidrug resistant HeLa (HeLa-R) cells was investigated. Positively charged GP and GPT exhibited significant cytotoxicity at concentrations above 100 μg/mL (ESI, Figure S6). However, negatively charged GPD, GPTD, and GPTS displayed low toxicity up to 1.0 mg/mL. The higher toxicity of the positively charged sheets is due to their stronger interaction with the plasma membrane and higher cellular uptake.[6,11] In order to investigate the cellular uptake of graphene sheets and efficiency of the conjugated mitochondrial targeting ligands, fluorescein isothiocyanate (FITC) labeled GPD, GPTS, and GPTD (GPD_F, $GPTS_F$, and $GPTD_F$, respectively) were incubated with HeLa-R cells at both physiological and tumor pH. Confocal laser scanning microscopy (CLSM) and fluorescence-activated cell sorting (FACS) showed a significant increase in the cellular uptake of GPD and GPTD upon a minor reduction in pH (Figure 2C, 2D, S7 and S8). Clearly, this effect was much lower for GPTS. This result confirms the efficiency of surface charge conversion to improve the cellular uptake of graphene sheets.

Intensive accumulations of GPTD in mitochondria, in comparison with GPD, showed the efficiency of TPP as a mitochondria targeting ligand (Figure 2E).[9] Intracellular ATP concentration of HeLa-R cells after incubation with GPD and GPTD and exposing to NIR (808 nm) irradiation for 5 min and 10 min was investigated (Figure 2F). While ATP values were relatively constant after irradiation in the case of GPD, it plunged for the GPTD incubated cells. JC-1 assays also confirmed significant disruption of mitochondrial membranes in GPTD-incubated cells after 5 min NIR irradiation (Figure S10).

Doxorubicin (DOX) was loaded on GPD and GPTD to produce the corresponding drug delivery nanoplatforms (GPD_D and $GPTD_D$). Loading capacity of GPD_D and $GPTD_D$ was 41.3 wt% and 38.8 wt%, respectively (Figure S11). Their release profiles were measured in various conditions including pH 7.4, pH 6.8, with and without laser irradiation (Figure S12 and S13). Rate of drug release from graphene derivatives was accelerated by NIR irradiation,[2c,3d] which could result in an amplified chemotherapy after destroying the mitochondria. In order to investigate the anticancer activity of the free DOX, GPD_D, and $GPTD_D$, they were incubated with HeLa-R cells and fluorescence intensity of drug inside the cells with or without NIR irradiation was evaluated by CLSM and FACS (Figure 3A, 3B, S14 and S15).

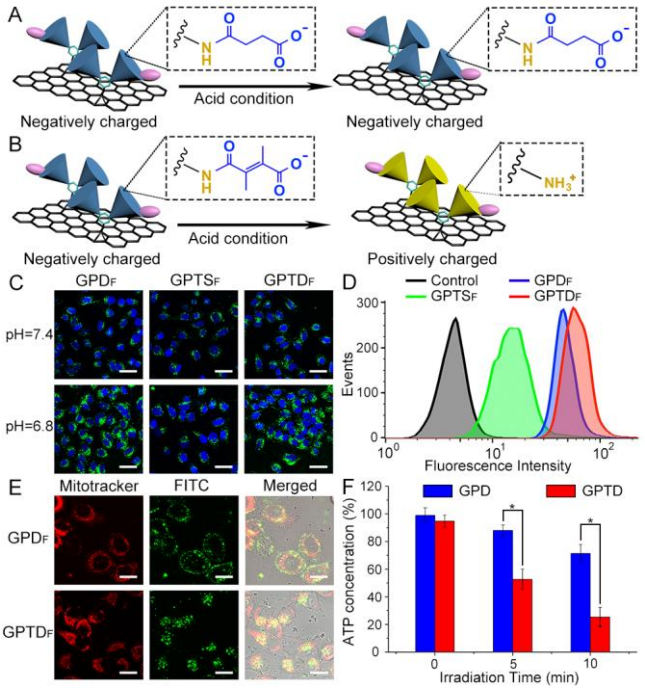

Figure 2. The structure and surface charge conversion of GPTS (A) and GPTD (B) under acid conditions; (C) CLSM images of HeLa-R cells incubated with GPD_F, $GPTS_F$, and $GPTD_F$ in pH 7.4 and 6.8 for 24 h. Scale bars correspond to 50 μm. (D) FACS results of HeLa-R cells after incubation with GPD_F, $GPTS_F$, and $GPTD_F$ in pH 6.8 for 24 h. (E) CLSM images of HeLa-R cells incubated with GPD_F and $GPTD_F$ for 30 min. Images were recorded 6 h after a washing step. Mitotracker (red) was applied to label mitochondria. Scale bars correspond to 25 μm. (F) Relative intracellular ATP concentration in HeLa-R cells after incubation with GPD and GPTD for 6 h. Cells were treated with NIR laser (808 nm, 0.5 W/cm^2) for 0, 5, and 10 min, and then their intracellular ATP concentrations were measured. Data are shown as the average ± standard deviation (n = 3, student's test, *p < 0.001).

It is reported that pretreatment of cells with graphene quantum dots downregulates multidrug-resistant genes and improves the chemotherapeutic efficiency intrinsically.[12] However, the toxicity of GPD_D and $GPTD_D$ without laser irradiation was low and a strong MDR effect was observed (Figure 3C). The reasons for such different results can be different surface coatings, concentration, and size of graphene derivatives as well as incubation times between our experiments and the reported work. Figures S14 and S15 show CLSM and FACS results, respectively, for cells without laser irradiation. Poor fluorescence intensity of DOX confirmed low intracellular concentrations of the drug, attributed to the powerful P-gP pumping system[4,5], although fluorescence quenching by graphene sheets should not be ignored as a factor.[3d,11] Due to the MDR effect, the toxicity of the free drug, GPD_D and $GPTD_D$ without irradiation was low, as was expected (Figure 3C).

Intracellular fluorescence intensity and therapeutic efficiency of DOX delivered by GPD_D and $GPTD_D$ improved dramatically upon laser irradiation (Figure 3). While almost no difference was found in the case of DOX·HCl, many therapeutic agents were discharged from GPD_D and $GPTD_D$ (Figure 3A). However, in the case of $GPTD_D$, a large quantity of DOX entered the nucleus while very little could be found in the corresponding GPD_D-incubated cells. The quantitative FACS results (Figure 3B) were also in accordance with the CLSM results. $GPTD_D$ also showed the highest toxicity (Figure 3D), successfully overcoming MDR. Due to TPP-mediated targeting, $GPTD_D$ accumulated in mitochondria and disrupted these organelles after NIR irradiation, resulting in ATP suppression. This effect together with the accelerated drug release, triggered by laser irradiation, led to DOX uptake into the nucleus before the drug could be pumped out to the extracellular medium. In the case of GPD_D, mitochondria were active and a major part of the released drugs was pumped out from the intracellular medium.

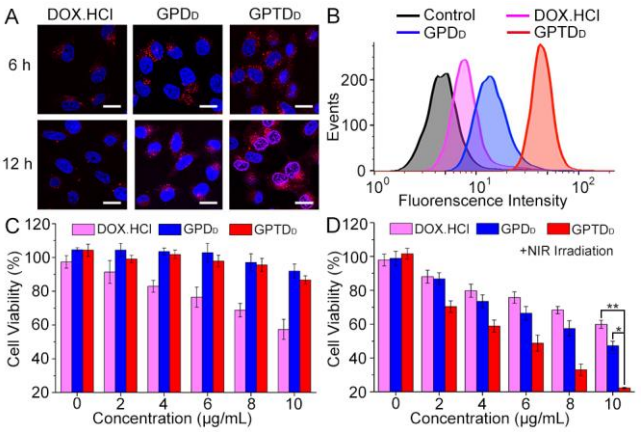

Figure 3. (A) CLSM images of HeLa-R cells incubated with DOX.HCl, GPD_D, and $GPTD_D$ for 6 h and 12 h. Cells were irradiated by NIR laser (808 nm, 0.5 W/cm^2) for 5 min after 6 h incubation times. Scale bars correspond to 25 μm. (B) FACS results of HeLa-R cells after 12 h incubation with DOX.HCl, GPD_D, and $GPTD_D$, respectively. NIR laser (808 nm, 0.5 W/cm^2) irradiation was performed for 5 min after the incubation of 6 h. Anticancer efficacy for HeLa-R cells incubated with different concentrations of DOX.HCl, GPD_D, and $GPTD_D$ for 24 h without (C) and with (D) laser irradiation. Cells were irradiated by NIR laser (808 nm, 0.5 W/cm^2) for 5 min after 6 h incubation times. Data are shown as the average ± standard deviation (n = 3, student's test, *p < 0.001, **p < 0.0001).

Biodistribution and *in vivo* antitumor activity of GPD_D and $GPTD_D$ with and without laser irradiation were investigated. Figure 4A shows accumulation of Cy5-labeled GPD_D and Cy5-labeled $GPTD_D$ in tumor 24 h following injection, attributed to EPR effect.[3a,3d,13]

In order to elucidate the factors contributing to tumor suppression, saline and DOX·HCl were employed as negative and positive control groups, respectively. Furthermore, GPTD without loaded DOX and $GPTD_D$ without laser irradiation serve as additional controls. After laser irradiation (808 nm, 0.5 W/cm^2, 5 min) the local temperature at tumor sites boosted to 60.5 °C and 61.2 °C for GPD_D and $GPTD_D$-treated mice, respectively. In the case of saline- and DOX·HCl-treated mice, the temperature increase was much less substantial, at 40.5 and 40.7 °C, respectively (Figure 4B). Tumor growth and body weight were recorded after administration and irradiation (Figure 4C and 4D). The tumor growth inhibition was very efficient in the case of $GPTD_D$ boosted with laser irradiation. The average tumor volume diminished to 3.7% in comparison with DOX.HCl group. This result confirms the inadequacy of free anticancer drug and

efficiency of our system for destruction of MDR HeLa cells.[4,5] Tumors were extracted from the bodies of mice and their sizes were visually evaluated (Figure S18). Tumors from mice treated with $GPTD_D$/Laser were much smaller than others and in some cases they were too small to be extracted. Furthermore, free drug exhibited considerable side effects, especially for heart tissue (Figure S19).[13] Accordingly, the body weight of the mice decreased after injection of free DOX. This effect was negligible for other groups (Figure 4D).

In addition, histological staining analyses demonstrated remarkable reduction of tumor cells and more vacancies in hematoxylin & eosin (H&E) staining slices of tumor tissue upon $GPTD_D$ administration (Figure S20).[5,9d] However, compact tumor tissue was observed for saline- and DOX-treated mice. According to immunohistochemical staining analysis, the highest vessel (CD31-positive staining)[3d] damage occurred for the $GPTD_D$-administrated group (Figure S20). This group also showed the lowest tumor proliferation (Ki-67-positive cells)[13a] and the most efficient apoptosis (TUNEL-positive cells)[13a] of HeLa-R cells (Figure 4E).

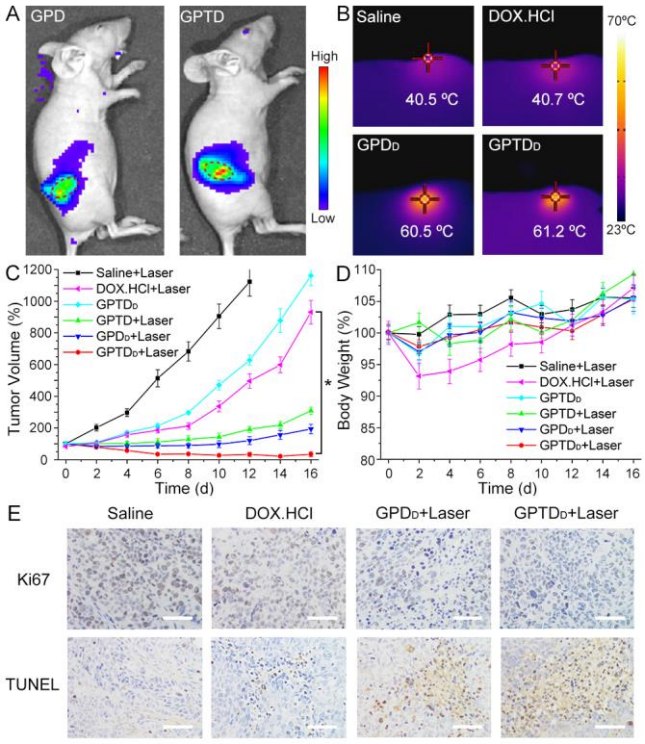

Figure 4. (A) *In-vivo* fluorescent imaging of HeLa-R tumor-bearing nude mice 24 h after intravenous injection of Cy5-labeled GPD and GPTD. The tumors were masked by red circles; (B) Thermographic images of HeLa-R tumor-bearing nude mice injected with saline, DOX.HCl, GPD_D, and $GPTD_D$ after exposure to NIR irradiation (808 nm, 0.5 W/cm^2) for 5 min. Variations in tumor volumes (C) and body weights (D) of HeLa-R tumor-bearing nude mice, 24 h after intravenous injection of saline (1), DOX.HCl (2), $GPTD_D$ (3), GPTD (4), GPD_D (5), and $GPTD_D$ (6) with and without laser irradiation. NIR irradiation (5 min, 808 nm, 0.5 W/cm^2) was applied for group 1, 2, 4, 5, and 6. Each group of nude mice (n = 6) was administered at a dose of 5 mg/kg (DOX content) at the beginning of this therapy. Statistical significance: *p < 0.001. (E) Immunohistochemical analysis for HeLa-R tumors. Ki-67-positive cells, and TUNEL-positive cells are stained brown. Scale bars correspond to 500 μm.

In summary, graphene-based drug delivery systems with the ability to disrupt mitochondria and suppress ATP production, as well as high chemotherapeutic efficacy, were synthesized. Despite of their high loading capacity for DOX, fast drug release and good photothermal properties, nanographene derivatives without mitochondrial targeting ligands did not show a significant chemotherapeutic effect. However, graphene derivatives with TPP ligands were able to efficiently and selectively deliver drug to the nucleus of cells, leading to a high anticancer effect. Precise functionalization of graphene nanosheets by bioligands in combination with triggered release of cytotoxic drugs can overcome the current challenges in MDR chemotherapy.

Acknowledgements

Dr. Rainer Haag would like to thank SFB 765 and the Focus Area Nanoscale of Freie Universität Berlin for the financial support. Dr. Wei Chen acknowledges the National Natural Science Foundation of China (NSFC 51703244), and the Natural Science Foundation of Jiangsu Province (BK20170730). Dr. Haishi Qiao would like to thank the National Natural Science Foundation of China (NSFC 81600178). China Scholarship Council (CSC) was appreciated for the financial support. Dr. Pamela Winchester is acknowledged for proofreading the manuscript and Yan Li for performing the Western Blot assay.

Keywords: graphene • drug delivery • multidrug resistance • mitochondria • hyperthemia

[1] a) K. S. Novoselov, V. I. Fal, L. Colombo, P. R. Gellert, M. G. Schwab, K. Kim, *Nature* **2012**, *490*, 192–200; b) D. Bitounis, H. Ali-Boucetta, B. H. Hong, D. Min, K. Kostarelos, *Adv. Mater.* **2013**, *25*, 2258–2268; c) G. Reina, J. M. González-Domínguez, A. Criado, E. Vázquez, A. Bianco, M. Prato, *Chem. Soc. Rev.* **2017**, *46*, 4400–4416; d) Z. Tu, G. Guday, A. Mohsen, R. Haag, *Adv. Mater.* **2018**, *30*, accepted; e) Y. Chen, C. Tan, H. Zhang, L. Wang, *Chem. Soc. Rev.* **2015**, *44*, 2681–2701.

[2] a) Y.-W. Chen, Y.-L. Su, S.-H. Hu, S.-Y. Chen, *Adv. Drug Deliv. Rev.* **2016**, *105*, *Part B*, 190-204; b) H. Y. Mao, S. Laurent, W. Chen, O. Akhavan, M. Imani, A. A. Ashkarran, M. Mahmoudi, *Chem. Rev.* **2013**, *113*, 3407–3424; c) K. Yang, L. Feng, Z. Liu, *Adv. Drug Deliv. Rev.* **2016**, *105*, *Part B*, 228–241; d) G. Shim, M.-G. Kim, J. Y. Park, Y.-K. Oh, *Adv. Drug Deliv. Rev.* **2016**, *105*, *Part B*, 205–227.

[3] a) K. Yang, S. Zhang, G. Zhang, X. Sun, S.-T. Lee, Z. Liu, *Nano Lett.* **2010**, *10*, 3318–3323; b) R. Mo, T. Jiang, W. Sun, Z. Gu, *Biomaterials* **2015**, *50*, 67–74; c) S. Kang, J. Lee, S. Ryu, Y. Kwon, K.-H. Kim, D. H. Jeong, S. R. Paik, B.-S. Kim, *Chem. Mater.* **2017**, *29*, 3461–3476; d) Y. Su, T. Yu, W. Chiang, H. Chiu, C. Chang, C. Chiang, S. Hu, *Adv. Funct. Mater.* **2017**, *27*; e) G. Liu, H. Qin, T. Amano, T. Murakami, N. Komatsu, *ACS Appl. Mater. Interfaces* **2015**, *7*, 23402–23406; f) C. Zhang, Z. Liu, Y. Zheng, Y. Geng, C. Han, Y. Shi, H. Sun, C. Zhang, Y. Chen, L. Zhang, *Small* **2018**, *14*, 1703306.

[4] a) Z. Chen, T. Shi, L. Zhang, P. Zhu, M. Deng, C. Huang, T. Hu, L. Jiang, J. Li, *Cancer Lett.* **2016**, *370*, 153–164; b) M. Bar-Zeev, Y. D. Livney, Y. G. Assaraf, *Drug Resist. Updat.* **2017**, *31*, 15-30.

[5] a) A. G. Assanhou, W. Li, L. Zhang, L. Xue, L. Kong, H. Sun, R. Mo, C. Zhang, *Biomaterials* **2015**, *73*, 284–295; b) W.-H. Chen, G.-F. Luo, W.-X. Qiu, Q. Lei, L.-H. Liu, D.-W. Zheng, S. Hong, S.-X. Cheng, X.-Z. Zhang, *Chem. Mater.* **2016**, *28*, 6742–6752; c) S. Chen, Q. Lei, W.-X. Qiu, L.-H. Liu, D.-W. Zheng, J.-X. Fan, L. Rong, Y.-X. Sun, X.-Z. Zhang, *Biomaterials* **2017**, *117*, 92–104.

[6] Z. Tu, K. Achazi, A. Schulz, R. Mülhaupt, S. Thierbach, E. Rühl, M. Adeli, R. Haag, *Adv. Funct. Mater.* **2017**, *27*, 1701837.

[7] G. Guday, I. S. Donskyi, M. F. Gholami, A. Lippitz, W. E. S. Unger, J. P. Rabe, M. Adeli, R. Haag, **2018**, in submission.

[8] (a) A. Setaro, M. Adeli, M. Glaeske, D. Przyrembel, T. Bisswanger, G. Gordeev, F. Maschietto, A. Faghani, B. Paulus, M. Weinelt, *Nat. Commun.* **2017**, *8*, 14281; (b) Z. Beiranvand, A. Kakanejadifard, I. S. Donskyi, A. Faghani, Z. Tu, A. Lippitz, P. Sasanpour, F. Maschietto, B. Paulus, W. E. S. Unger, *RSC Adv.* **2016**, *6*, 112771–112775; (c) A. Faghani, I. S. Donskyi, M. Fardin Gholami, B. Ziem, A. Lippitz, W. E. S. Unger, C. Böttcher, J. P. Rabe, R. Haag, M. Adeli, *Angew. Chemie Int. Ed.* **2017**, *56*, 2675–2679; *Angew. Chem.* **2017**, *129*, 2719-2723; (d) M. F. Gholami, D. Lauster, K. Ludwig, J. Storm, B. Ziem, N. Severin, C. Böttcher, J. P. Rabe, A. Herrmann, M. Adeli, *Adv. Funct. Mater.* **2017**, *27*, 1606477.

[9] a) S. E. Weinberg, N. S. Chandel, *Nat. Chem. Biol.* **2015**, *11*, 9–15; b) C. Dong, Z. Liu, J. Liu, C. Wu, F. Neumann, H. Wang, M. Schäfer-Korting, B. Kleuser, J. Chang, W. Li, *Adv. Healthc. Mater.* **2016**, *5*, 2214–2226; c) C. Zhang, J. Wang, J. Zhang, Y. M. Lee, G. Feng, T. K. Lim, H. Shen, Q. Lin, B. Liu, *Angew. Chem. Int. Ed.* **2016**, *55*, 13770-13774; *Angew. Chem.* **2016**, *128*, 13974–13978; d) J. Mou, T. Lin, F. Huang, J. Shi, H. Chen, *Theranostics* **2017**, *7*, 1531.

[10] a) Y. Lee, S. Fukushima, Y. Bae, S. Hiki, T. Ishii, K. Kataoka, *J. Am. Chem. Soc.* **2007**, *129*, 5362–5363; b) L. Jiang, L. Li, X. He, Q. Yi, B. He, J. Cao, W. Pan, Z. Gu, *Biomaterials* **2015**, *52*, 126–139.

[11] a) Z. Tu, V. Wycisk, C. Cheng, W. Chen, M. Adeli, R. Haag, *Nanoscale* **2017**, *9*, 18931–18939; b) N. Luo, D. Ni, H. Yue, W. Wei, G. Ma, *ACS Appl. Mater. Interfaces* **2015**, *7*, 5239–5247.

[12] C. Luo, Y. Li, L. Guo, F. Zhang, H. Liu, J. Zhang, J. Zheng, J. Zhang, S. Guo, *Adv. Healthc. Mater.* **2017**, *6,* 1700328.

[13] a) N. Li, N. Li, Q. Yi, K. Luo, C. Guo, D. Pan, Z. Gu, *Biomaterials* **2014**, *35*, 9529–9545; b) W. Chen, Y. Zou, Z. Zhong, R. Haag, *Small* **2017**, *13*.

COMMUNICATION

Multiple functionalized nanographene sheets accumulate in mitochondria after cellular uptake, and disrupt mitochondrial function upon laser irradiation, leading to a drop in ATP levels and the dysfunction of P-glycoprotein. This enables more of the released DOX to be delivered into the nucleus. Our results show these multiple functionalized graphene sheets could overcome multidrug resistance and achieve effective synergistic tumor therapy.

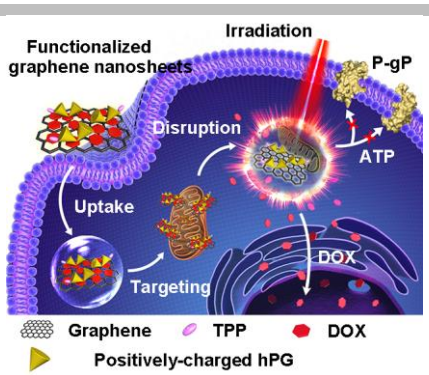

Zhaoxu Tu, Haishi Qiao, Yuting Yan, Guy Guday, Wei Chen, Mohsen Adeli,* and Rainer Haag**

Page No. – Page No.

Directed Graphene-based Nanoplatforms for Hyperthermia-Overcoming Multiple Drug Resistance

Supporting Information

Directed Graphene-Based Nanoplatforms for Hyperthermia-Overcoming Multiple Drug Resistance

Zhaoxu Tu, Haishi Qiao, Yuting Yan, Guy Guday, Wei Chen,* Mohsen Adeli,* and Rainer Haag*

Dr. H. Qiao, Y. Yan, Prof. W. Chen
Department of Pharmaceutical Engineering, China Pharmaceutical University, Nanjing 210009, China
E-mail: w.chen@cpu.edu.cn

Z. Tu, G. Guday, Prof. M. Adeli, Prof. R. Haag
Institut für Organische Chemie und Biochemie, Freie Universität Berlin, Takustraße 3, 14195 Berlin, Germany
E-mail: haag@chemie.fu-berlin.de

Prof. M. Adeli
Department of Chemistry, Faculty of Science, Lorestan University, Khorram Abad, Iran
E-mail: aadeli@zedat.fu-berlin.de

Table of contents

1. Experimental

Material: Hyperbranched polyglycerol (hPG) with Mn ≈ 100,000 g·mol^{-1} was synthesized by one-pot, ring-opening anionic polymerization (ROAP), according to a reported procedure.[1] Graphite, cyanuric chloride, triethylamine (TEA), sodium azide, methanesulfonyl chloride, triphenylphosphine (PPh3), (4-Carboxybutyl)triphenylphosphonium bromide (TPP), 2-(N-morpholino)ethanesulfonic acid (MES), N-(3-Dimethylaminopropyl)-N'-ethylcarbodiimide hydrochloride (EDC.HCl), 2,3-dimethylmaleic anhydride (DA), succinic acid (SA), fluorescein isothiocyanate isomer I (FITC), human serum albumin (HSA), 1-methyl-2-pyrrolidinone (NMP), N,N-dimethylformamide (DMF) and tetrahydrofuran (THF) were purchased from Sigma-Aldrich and used directly without any further purification. Cell counting kit-8 (CCK-8) assay, ATP determination kit (A22066), cell lysis buffer (16189) and CellLight® fluorescent protein labeling (red) for mitochondria was bought from Thermo Fisher Scientific. Milli-Q water was applied in all experiments.

Methods: Nuclear magnetic resonance spectroscopy (NMR) spectra were measured on a Jeol Eclipse 500 MHz. Fourier transform infrared spectroscopy (FT-IR) spectra data were obtained from a Jasco FT/IR-4100 spectrometer. Thermal gravimetric analysis (TGA) were recorded on Linseis STA PT 1600 with a 10 ºC/min heating rate under argon gas. Atomic force microscopy (AFM) was performed with a MultiMode Nanoscope V scanning probe microscopy (SPM) system (Bruker, USA). Fluorescence was measured with a JASCOFP-6500 spectrofluorometer. Zeta potential data were obtained by NANO ZSPO (Malvern) in PBS solution. The cell viability and ATP determination were measured using a TECAN Infinite M200 Pro microplate reader. Confocal laser scanning microscopy (CLSM) was recorded by Leica TCS SP8 with 63× oil-immersion objective lens and disposed by Leica confocal software. Fluorescence-activated cell sorting (FACS) was measured with BD FACS calibur flow cytometer (Beckton Dickinson) and processed with Flowjo software. The in *vivo*

and *ex vivo* biodistribution imaging was measured by IVIS® spectrum, PerkinElmer (USA). The laser irradiation was performed with diode infrared laser module (808 nm), Changchun New Industries, CNI.

Synthesis of 30% amino-functionalized hPG (hPG(NH_2)$_{30\%}$): hPG (Mn ≈ 10000 g/mol) (10.0 g, 1 mmol, 135 mmol hydroxyl groups) was dissolved in DMF (200 mL) and stirred at room temperature for 1 h. Then methanesulfonyl chloride (4.18 mL, 54 mmol) and TEA (22.5 mL, 160 mmol) were added to the hPG solution at room temperature. The mixture was stirred under nitrogen atmosphere at room temperature for 24 h. Then DMF was evaporated and product was dissolved in methanol and dialyzed against this solvent for 24 h to obtain purified hPG(OMs)$_{30\%}$. In the second step, hPG(OMs)$_{30\%}$ (5.0 g, 0.5 mmol) was dissolved in DMF (200 mL) and sodium azide (6.52 g, 100 mmol) was added to this solution at room temperature. The mixture was stirred at 80 ºC for 24 h. The produced 30% azido-functionalized hPG (hPG(N_3)$_{30\%}$) was purified by dialysis in acetone for 24 h. In the last step, hPG(N_3)$_{30\%}$ (5.0 g, 0.5 mmol) was dissolved in a mixture of THF and water (THF:H_2O=2:1) and PPh_3 (10.48 g, 40 mmol) was dissolved in the same solvent. Afterwards, the solutions were mixed and the reaction was conducted at 45 ºC for 48 h to reduce the azido groups to amino groups. Then the reaction was cooled down and the solvent was evaporated. The product was dissolved in methanol and dialyzed against the same solvent for 24 h to obtain hPG(NH_2)$_{30\%}$. The yield was about 40%.

Conjugation of hPG to nanographene sheets (nG): nG and triazine-functionalized nG (nG-Trz) was synthesized according to a method developed in our group.[2,3] hPG decorated nG (GP) was also prepared according to a protocol developed in our group.[4] nG-Trz (500 mg) was dispersed in NMP (200 mL) and sonicated for 20 min to obtain a fine dispersion. Then hPG(NH_2)$_{30\%}$ (10 g, 1 mmol) was dissolved in NMP (50mL) and added to this dispersion at

room temperature. The mixture was stirred in an ice bath for 1 h. Then the ice bath was removed and the mixture was stirred at room temperature for 1 day. Afterwards, the reaction temperature was raised to 100 ºC for 1 day. Finally, the reaction was cooled down and the non-functionalized and low-functionalized nG-Trz was removed by centrifugation at 2000 rpm for 10 min. The supernatant was dialyzed in water for 2 days to obtain GP. The yield was about 50%.

Preparation of TPP-modified GP (GPT): GP (1 g) was dispersed in MES solution (0.1 mM) with EDC.HCl (1.29 g, 6.75 mmol). Then TPP (600 mg, 1.35 mmol) was added to the solution and the mixture dispersion was stirred at room temperature for 24 h. Finally, the dispersion was centrifuged at 11,000 rpm for 10 min and the precipitate was washed with Milli-Q water by the same process to obtain GPT. The yield was about 70%.

Preparation of DA-functionalized GPT (GPTD), DA-functionalized GP (GPD) and SA-functionalized GPT (GPTS): GPT (500 mg) was dispersed in Milli-Q water (100 mL) and then the pH was adjusted to 8.5 with NaOH solution (0.1 M). After stirring at room temperature for 10 min, DA (378 mg, 3.0 mmol) solution was added dropwise into the solution. During the addition of DA, the NaOH solution (0.1 M) was added to maintain pH in the range of 8.0-8.5. Three hours later, DA was removed by centrifugation (11,000 rpm, 10 min) and GPTD was obtained. The yield was about 70%.

GPD and GPTS were obtained through almost the same process but with different reagents.

Conjugation of fluorescence dye (FITC) onto the surface of graphene derivatives: GPD, GPTS and GPTD (100 mg) were dispersed in PBS (pH = 7.4) with a concentration of 1.0 mg/mL. Then FITC (1 mg) was added to this dispersion at room temperature. Subsequently,

the mixture was stirred at room temperature for 24 h. Then the dispersion was dialysis in Milli-Q water for 1 day to remove all free dye. The resultant products are called GPD_F, $GPTS_F$, and $GPTD_F$, respectively.

Preparation of DOX-loaded GPD, GPTS and GPTD: Hydrophobic doxorubicin (DOX) was obtained according to the reported method.[5] GPTD (10 mg) was dispersed in PBS (7.4, 20 mL) and then DOX (20 mg, dissolved in 2 mL DMSO) was added dropwise into the GPTD dispersion under stirring. The mixture was stirred overnight at room temperature and then was dialyzed in Milli-Q water for 24 h with dialysis membrane tube (Spectra/Por MWCO = 2000). After that the dispersion was centrifuged at 11,000 rpm for 10 min. The supernatant was discarded and the precipitate was DOX-loaded GPTD ($GPTD_D$). DOX-loaded GPD (GPD_D) and DOX-loaded GPTS ($GPTS_D$) were obtained with the same protocol.

The drug loading capacity of DOX in GPD_D, $GPTS_D$, and $GPTD_D$ was calculated by UV-vis absorption at 545 nm (Figure S10) and the calibration curve was obtained from DOX solution with a series of DOX concentrations. The following equation was adopted to calculate drug-loading capacity (LC):

$$\mathrm{LC} = \frac{\text{mass of drug in nanocarriers}}{\text{total mass of DOX loaded nanocarriers}} \times 100\%$$

Release Profile of GPD_D and $GPTD_D$: 1200 μg $GPTD_D$ was dispersed in 4 mL PBS (pH = 7.4) and then equally distributed into 4 dialysis membrane tubes (Spectra/Por MWCO = 2000). Subsequently, the tubes were immersed in 4 vials with each one containing 30 mL PBS solution (with 0.1 M HSA) (2 vials with pH = 7.4 and 2 vials with pH = 5.6, respectively). The vials were set in a thermostatic water bath (37 °C) on a heating rotator. During the whole experiment, 0.1 mL of media from each vial was collected for sampling every 30 min, and 0.1 mL fresh media was replenished. For two of the vials (one with pH = 7.4 and one with pH =

5.6), near-infrared (NIR) laser irradiation (808 nm, 0.5 W/cm^2) was performed for 1 min every 30 min. The quantity of released DOX was measured by a fluorometer with excitation at 480 nm and emission at 550 nm. The release experiments for $GPTD_D$ in each condition were performed in triplicate and the mean value was employed. The release experiments of GPD_D were conducted with the same protocol.

Cell culture: All cell experiments were conducted in accordance with the German genetic engineering law and German biosafety guidelines in an approved biosafety level 1 laboratory. Dulbecco's modified eagle's medium (DMEM) and fetal bovine serum (FBS) were applied for the following tests. Human cervical cancer cells (HeLa cells) and multidrug-resistant HeLa cells (HeLa-R cells) were obtained from Leibnitz Institute DSMZ - German Collection of Microorganisms and Cell Cultures. HeLa-R cells were cultured in DMEM with 10% (v/v) FBS and 1% penicillin-streptomycin and were incubated in a humidified atmosphere with 5% CO_2 at 37 °C. In addition, DOX.HCl (0.5 μg/mL) was added in the culture medium to maintain the drug-resistant characteristics.

Western Blot Analysis: The HeLa cells and HeLa-R cells was harvested and lysed on ice before the following experiments. The mixture was centrifuged at 13000 rpm for 30 min at 4°C, and then the protein concentration in supernatant was determined with the Pierce BCA Protein Assay Kit (Thermo Fisher Scientific, USA). 40 μg total protein from each sample was separated on a sodium dodecyl sulfate polyacrylamide gel and transferred onto a polyvinylidene fluoride (PVDF) membrane. 5% (w/v) BSA was applied to block the PVDF membrane and then the membrane was incubated with primary antibody (Anti-ABCB1 rabbit antibody, SAB2702025, Sigma USA; Anti-GAPDH, rabbit mAb, 2118S, CST, USA) in dilution buffer overnight at 4 °C. The membranes were rinsed with Tris-buffered saline Tween three times and incubated with goat anti-rabbit IgG HRP (Abcam, UK). The

luminescence was detected by an enhanced ECL Western Blotting Detection kit (Thermo Fisher Scientific, USA) with a ChemiDoc XR+UV illuminator (Bio-Rad, USA).

CCK-8 assay: HeLa-R cells (5×10^3 cells/well) were seeded in 96-well plates with 100 μL DMEM and incubated for the following 24 h before the biocompatibility tests. GP, GPT, GPD, GPTS and GPTD were firstly dispersed in the culture medium (pH=7.4) and then added to the medium-removed 96-well plates with different concentrations (from 0.1 to 1000 μg/mL). After another 34 h incubation, all of the culture medium solutions were removed and the wells were rinsed with PBS twice. Subsequently, 100 μL culture medium containing 10 μL CCK-8 was added to each well. After the following 4-hour incubation, 75 μL medium was carefully transferred to a new plate in case of the influence of graphene derivatives on final results, and the absorbance was measured at wavelength of 450 nm. Cells without any treatment were applied as a negative control and the cytotoxicity of DOX.HCl (2 and 20 μg/mL) was tested in the same way as a positive control. Each sample was tested 3 times.

The anti-tumor test for GPD_D and $GPTD_D$ was conducted by almost the same protocol with just a change in DOX concentration from 0 to 10 μg/mL. DOX.HCl with the corresponding concentrations was employed as a positive control. The experiments were replicated as 2 groups and NIR laser irradiation (808 nm, 0.5 W/cm^2) was applied to one the group after 6 h incucbation for 5 min.

ATP determination assay: The standard curve for a series of ATP concentration by ATP determination kit was calculated before the following experiments.

HeLa-R cells (1×10^4 cells/well) were seeded in 96-well plates with 100 μL DMEM and incubated for the following 24 h before the ATP determination tests. GPD and GPTD were dispersed in the culture medium (pH=6.8, 10 μg/mL) and then added to cells. All of the experiments were replicated as 2 groups. After the incubation of the following 6 h, the culture

medium of the first group was removed and the cells were treated with lysis buffer. However, the cells of the other group were treated with NIR laser irradiation (808 nm, 0.5 W/cm^2) for 5 min and 10 min, respectively. Then the culture medium was removed and the cells were also treated with lysis buffer. Subsequently, the ATP determination kit was added to these cell lysis solutions and the luminescence was measured to calculate the ATP concentration with Platereader. Each experiment was repeated 3 times and the mean value was adopted.

Confocal Laser Scanning Microscopy (CLSM): HeLa-R cells were seeded on 8-well plates at the density of 3×10^4 cells/well and incubated for 24 h before the following CLSM experiments.

Cellular uptake of GPD, GPTS, and GPTD: GPD_F, $GPTS_F$, and $GPTD_F$ were dispersed in culture medium (10 μg/mL) and then added to the cells. The cells were incubated in different pH conditions (6.8 and 7.4) at 37 °C for 3 h and 24 h, respectively. After the desired incubation time, the culture medium was removed, and the wells were rinsed with PBS. The nuclei of HeLa-R cells were subsequently stained with Hoechst for 30 min before the cells were observed with CLSM (Leica TCS SP8). Hoechst was excited at 350 nm with the emission at 460 nm and FITC was excited at 488 nm with the emission at 520 nm.

Intracellular localization of GPD_F, $GPTS_F$, and $GPTD_F$: CellLight fluorescence protein labeling (mitochondria tracker, red) was applied (2 μL per 10^4 cells) to label the mitochondria of the cells 24 h before the following tests. GPD_F, $GPTS_F$, and $GPTD_F$ were dispersed in culture medium (pH=6.8, 10 μg/mL) and then added to the cells. The culture medium was removed after 0.5 h incubation and fresh medium was supplemented. Subsequently, cells were incubated at 37 °C for another 6 h before the cells were observed with CLSM (Leica TCS SP8). FITC was excited at 488 nm with the emission at 520 nm and CellLight labeling protein (red) was excited at 560 nm with the emission at 590 nm.

JC-1 assay: The culture medium was removed and the well was rinsed with PBS before

adding of JC-1 (20 μM in PBS). The cells were incubated with JC-1 in 37 °C for 10 min and then rinsed with PBS twice. Subsequently, GPD, GPTS, and GPTD, which were dispersed in culture medium (pH=6.8), were added and the test was replicated as 2 groups. After 6 hours, one group was treated with NIR laser irradiation (808 nm, 0.5 W/cm^2) for 5 min. After that, all of the medium was removed and rinsed with PBS twice before the cells were observed with CLSM (Leica TCS SP8). JC-1 monomer was excited at 488 nm with the emission at 530 nm.

Intracellular DOX release: DOX.HCl, GPD_D and $GPTD_D$ were dispersed in culture medium (pH=6.8, DOX concentration: 4 μg/mL) and then added to the cells. These experiments were replicated as 2 groups. The first group was incubated for 6 h and then changed with fresh culture medium. The second group was incubated for 6 hours before they were treated with NIR laser irradiation (808 nm, 0.5 W/cm^2) for 5 min and then the cells were further incubated with fresh medium for 24 h. Finally, all of the wells were rinsed with PBS and the nuclei was stained with Hoechst before observation by CLSM. Hoechst was excited at 350 nm with the emission at 460 nm and DOX was excited at 488 nm with the emission at 550 nm.

Flow Cytometer: HeLa-R cells were seeded in 24-well plates (1×10^5 cells/well) and they were incubated for 24 h before the following test. GPD_F, $GPTS_F$ and $GPTD_F$ were dispersed in culture medium (10 μg/mL) and then added to the cells. The cells were incubated for 24 hours in medium with different pH (6.8 and 7.4), respectively. After that, the culture medium was removed and the cells were rinsed with PBS twice and then treated with trypsin/EDTA. Cells were re-suspended in PBS after centrifugation to discard the supernatant, and then fluorescence intensity was measured (excitation: 488 nm; emission: 520 nm) using a BD FACS calibur flow cytometer (Beckton Dickinson).

In another intracellular DOX accumulation test, DOX.HCl, GPD_D, and $GPTD_D$ were

dispersed in culture medium (pH=6.8, DOX concentration: 4 μg/mL) and then added to the cells. The cells were replicated as 2 groups and the first group was incubated for another 24 h with a change to fresh medium at 6 h point. While the second group was treated with NIR laser irradiation (808 nm, 0.5W/cm^2) for 5 min after 6 h incubation and then they were put in incubator for another 18 h. After that, all of the culture medium was removed and the cells were rinsed with PBS twice and then treated with trypsin/EDTA. Cells were re-suspended in PBS after centrifugation to discard the supernatant, and then fluorescence intensity was measured (excitation: 488 nm; emission: 550 nm) using a BD FACS caliber flow cytometer (Beckton Dickinson).

Animal and Tumor Xenograft Models: Female BALB/c nude mice (four to six weeks old) were purchased from Model Animal Research Center Of Nanjing University (Nanjing, China), and all animals were treated in accordance with the National Institute of Health Guide for the Care and Use of Laboratory Animals. HeLa-R cells (1×10^6 cells per mouse) were subcutaneously inoculated into the right flank of nude mice to prepare the tumor-bearing mice. Electronic caliper was used to measure the tumor size and the tumor volumes (V) were calculated as $V = a^2\times b/2$ (a and b were the width and length of the tumor, respectively). And the body weight of the nude mice also was recorded by an electronic balance.

In Vivo Antitumor Efficiency: When the tumor volume reached about 100 mm^3, the tumor-bearing mice were randomly divided into 6 groups (n = 6) and administrated with saline (group 1), $GPTD_D$ (group 2), GPTD (group 3), GPD_D (group 4), $GPTD_D$ (group 5), and DOX.HCl (group 6). 24 h later, the tumors of mice in groups 1, 2, 3, 4, and 6 were irradiated with NIR (808 nm, 0.5 W/cm^2) for 5 min. The tumor size and body weight were monitored every 2 days during the treatment. After 16 days, the mice were sacrified and the tumors and

major organs were excised, followed by hematoxylin and eosin (H&E) staining. Furthermore, for all of the tumors, CD31, Ki67, and TUNEL immunostaining were also applied.

2. Elemental analysis of nG and nG-Trz

Table S1. Elemental analysis of nG and nG-Trz.

Elemental Analysis	N (%)	C (%)	H (%)	S (%)
nG	0.022	98.2	0.338	0
nG-Trz	2.892	97.93	0.494	0

Degree of functionalization (DF) of triazine:

$$\mathrm{DF} = \frac{\text{number of triazine groups}}{\text{number of carbon atoms of graphene}}$$

1. Number of triazine groups: calculated by nitrogen percent (N wt.%) in elemental analysis;

2. Number of carbon atoms of TRGO: calculated by carbon percent (C wt.%) in elemental analysis.

Mass of a building block (MB) in nG-Trz:

$$\mathrm{MB} = \frac{100 * 56(\text{Mass of N atoms of one triazine group})}{2{,}892(\text{percentage of N in TRGO} - \text{Trz})} = 1936.4$$

$$\mathrm{DF} = \frac{14(\text{Mass of one N atom})}{1936.4\ (\mathrm{MB}) - 163.5(\text{Mass of one triazine group})} = {}^{1}\!/_{127}$$

3. Synthesis of GPT, GPD, GPTS and GPTD

Scheme S1 displays an overview of the synthesis route of GPT, GPD, GPTS and GPTD. nG was modified with $hPG(NH_2)_{30\%}$ through a [2 + 1] nitrene cycloaddition reaction and nucleophilic substitution and the resulted $hPG(NH_2)_{30\%}$ covered nG is GP. GPT, GPD, GPTS and GPTD were prepared based on GP according to the process in Experimental Section.

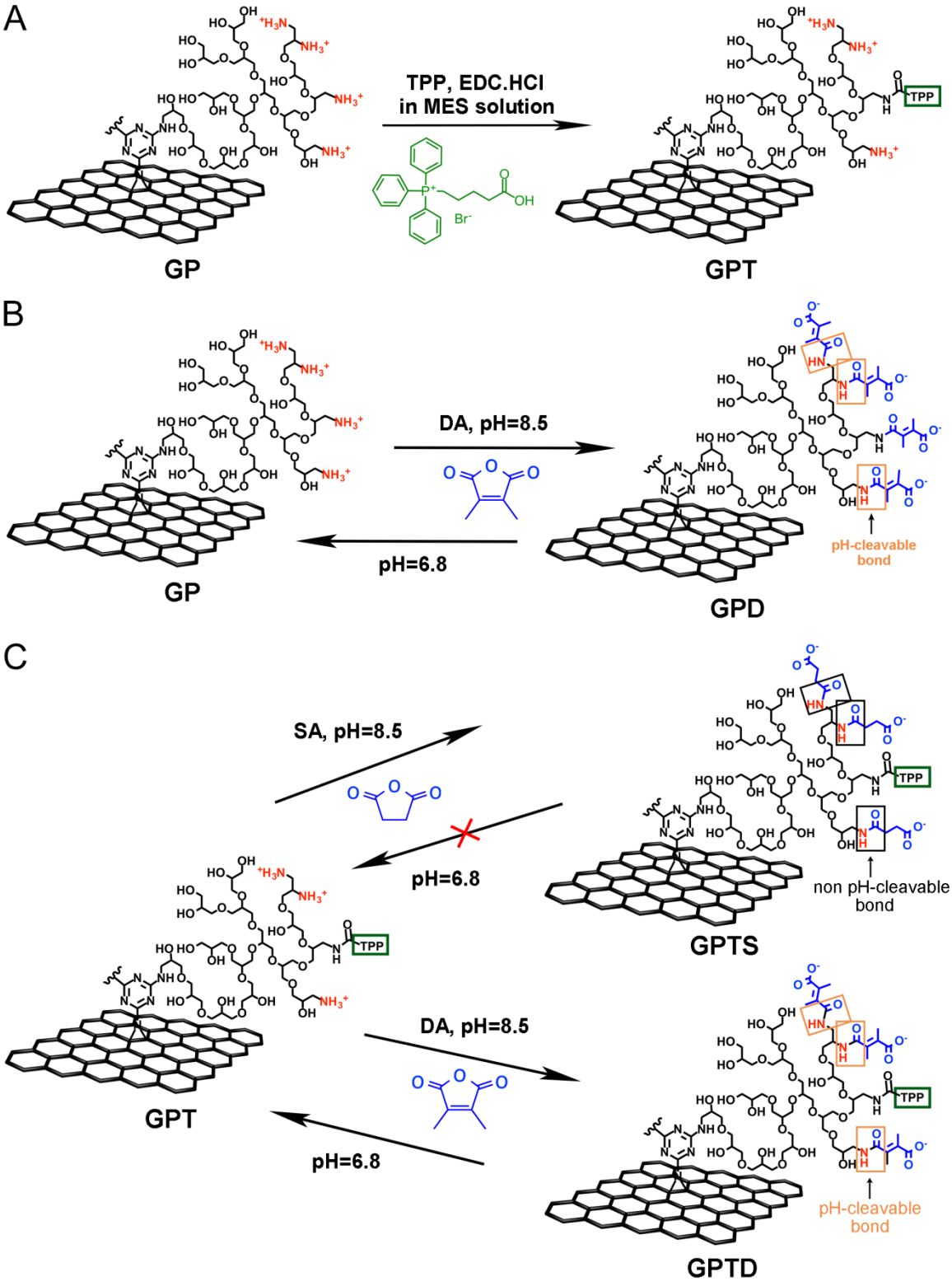

Scheme S1. Synthesis route of GPT (A), GPD (B), GPTS (C) and GPTD (C).

4. ^{1}H NMR spectra of the GPT

The signals at 3.4 - 4.2 ppm and 7.6 - 8.0 ppm were attributed to the protons of hPG backbone and benzene ring of TPP group, respectively. Based on the peak area ratio, the functionalized ratio of TPP on GPT is 4.87% (Figure S1). The singles at 3.2 – 3.4 ppm and 4.8 – 5.0 ppm were attributed to the protons of D-methanol and D_2O, respectively.

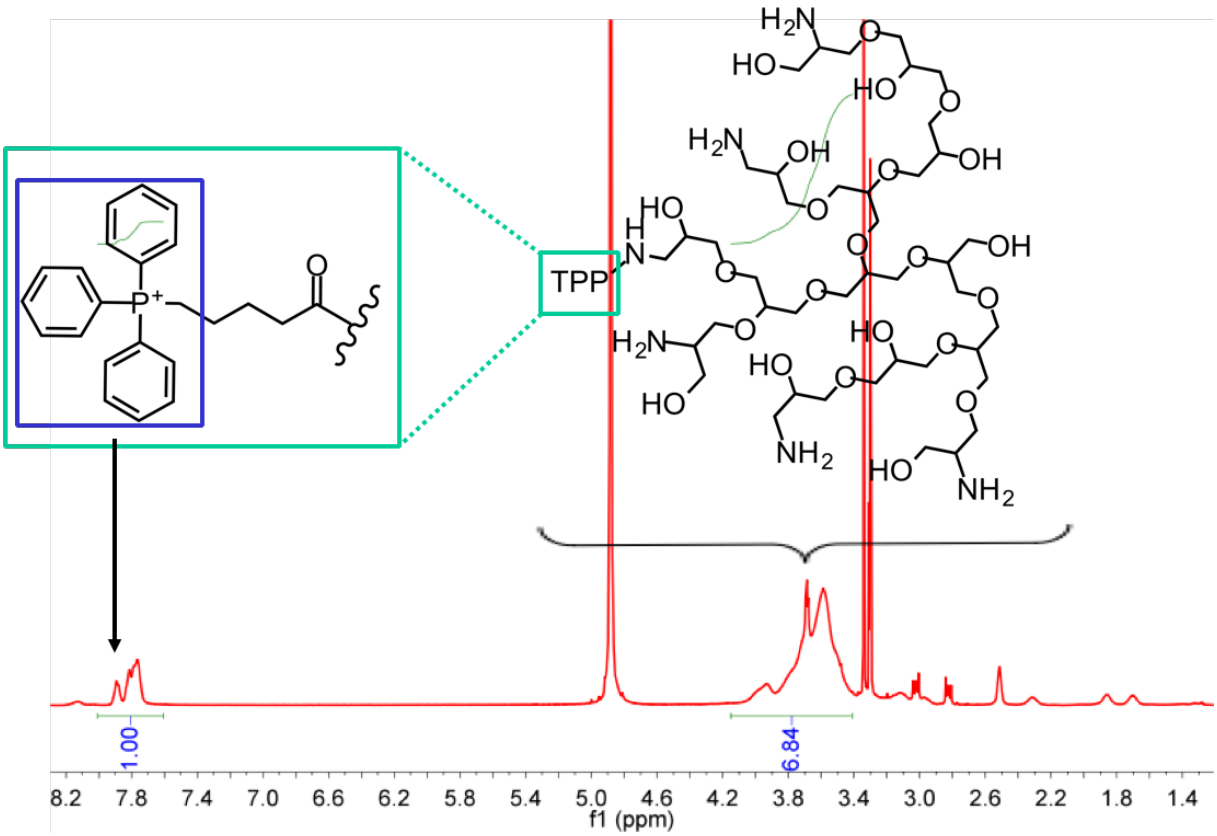

Figure S1. The ^{1}H NMR spectrum of GPT in D_2O and D-methanol.

5. Height-distribution histograms of nG, GPD, GPTS and GPTD

The average height of nG is around 0.65 nm, however this value increase to around 5.5 nm, 5.5 nm and 6.0 nm for GPD, GPTS and GPTD, respectively. The changes of height confirm the successful conjugation of polymers on the surface of nanographene sheets.

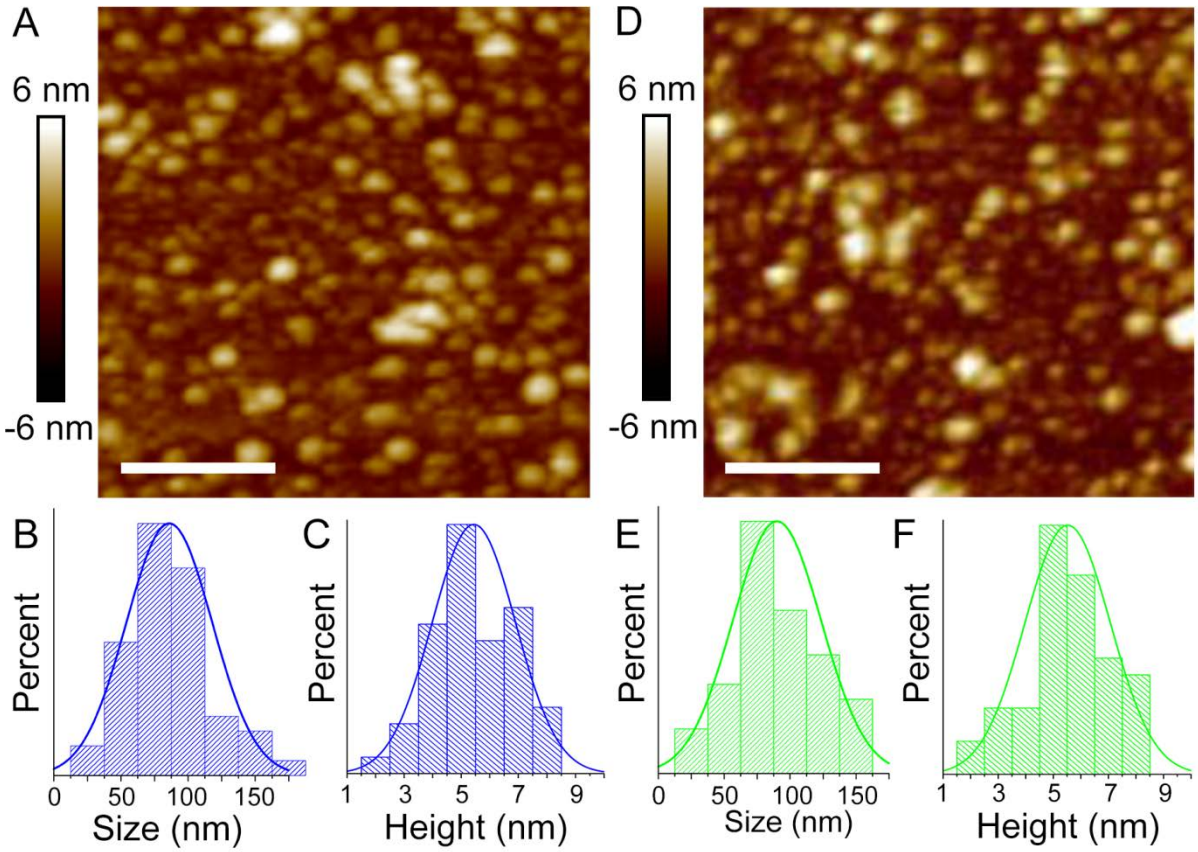

Figure S2. AFM images of GPD (A) and their size distribution (B) and height profile (C); AFM images of GPTS (D) and their size distribution (E) and height profile (F); Scale bars correspond to 500 nm.

6. TGA of GPD, GPTS and GPTD

According to the TGA results, the percent of polymers in GPD, GPTS and GPTD is around 74%, 77% and 79%, respectively. The TGA data proves the percent of coating polymers on the functionalized graphene sheets is quite high, which is favorable for the further biological applications.

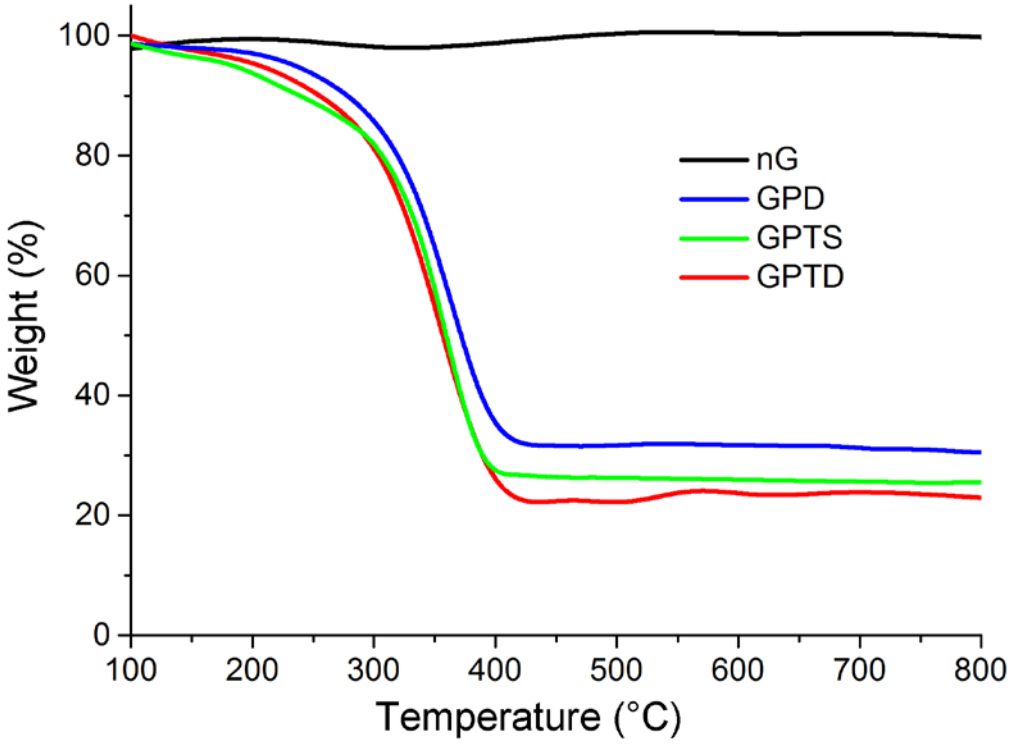

Figure S3. The TGA of nG, GPD, GPTS and GPTD.

7. Zeta potential of GPD, GPTS, GPTD

The zeta potential variations demonstrated GPT and GPTS exhibited positive and negative charges in a broad range of pH, while GPTD changes from negative to positive upon decreasing pH from 7.4 to 6.8. This pH-conventional characteristic is helpful for the long circulation in the blood stream (pH=7.4), while enhance the cellular uptake efficacy after accumulation in tumor (pH=6.8).[6]

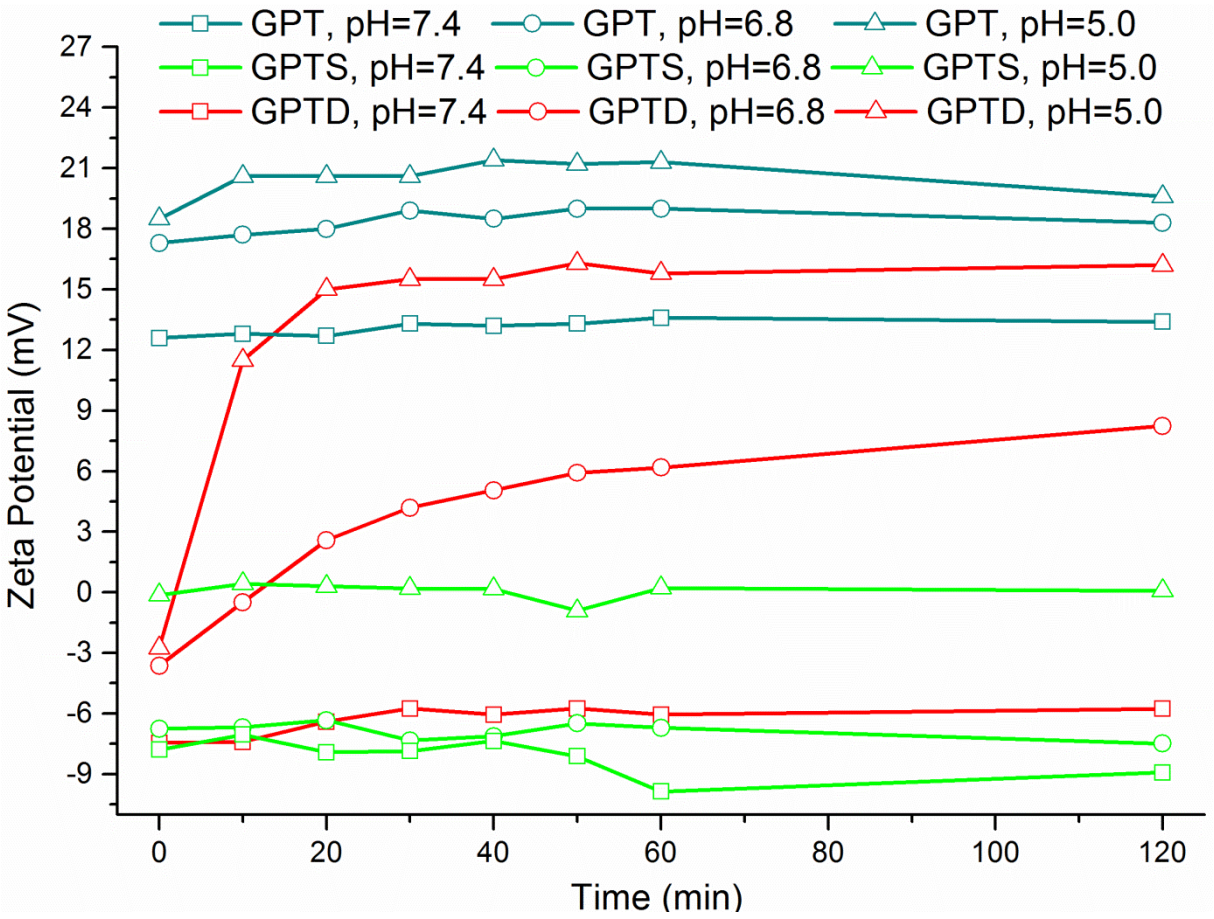

Figure S4. Zeta potentials of GPT, GPTS and GPTD with different incubation time at pH 7.4, 6.8, and 5.0.

8. Western blot assay

The overexpression of P-glycoprotein (P-gP) on the plasma membrane of HeLa-R cells was confirmed by western blot assay.

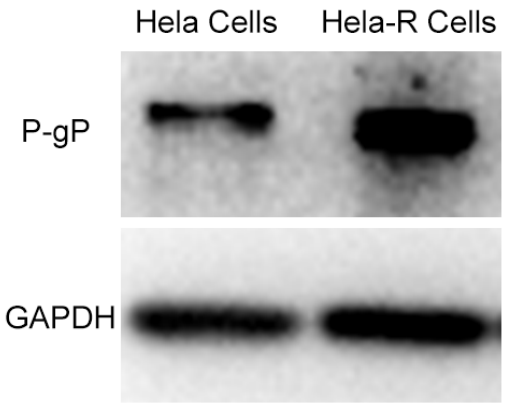

Figure S5. Western blotting analysis of P-gP among HeLa and HeLa-R cell lines.

9. Biocompatibility tests

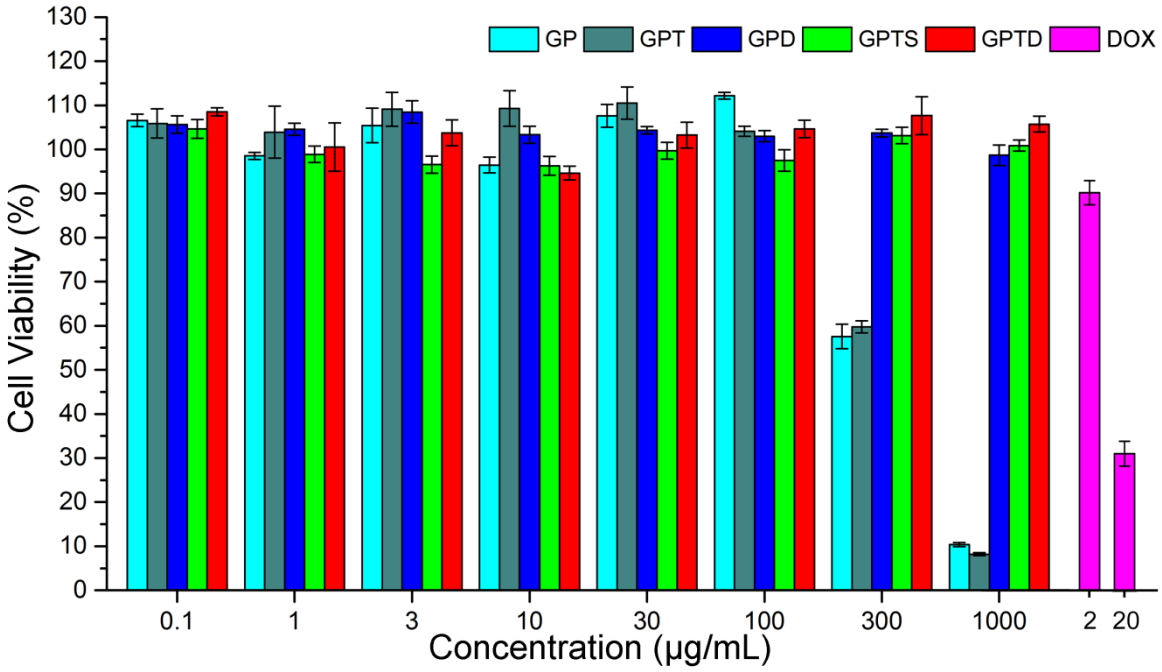

Figure S6. The biocompatibility tests of GP, GPT, GPD, GPTS and GPTD obtained from the CCK-8 assay of HeLa-R cells after 24 h treatment. The cells without any treatments was considered as negative control and the cells treated with DOX.HCl (2 μg/mL and 20 μg/mL) was considered as positive control.

10. Cellular uptake efficiency

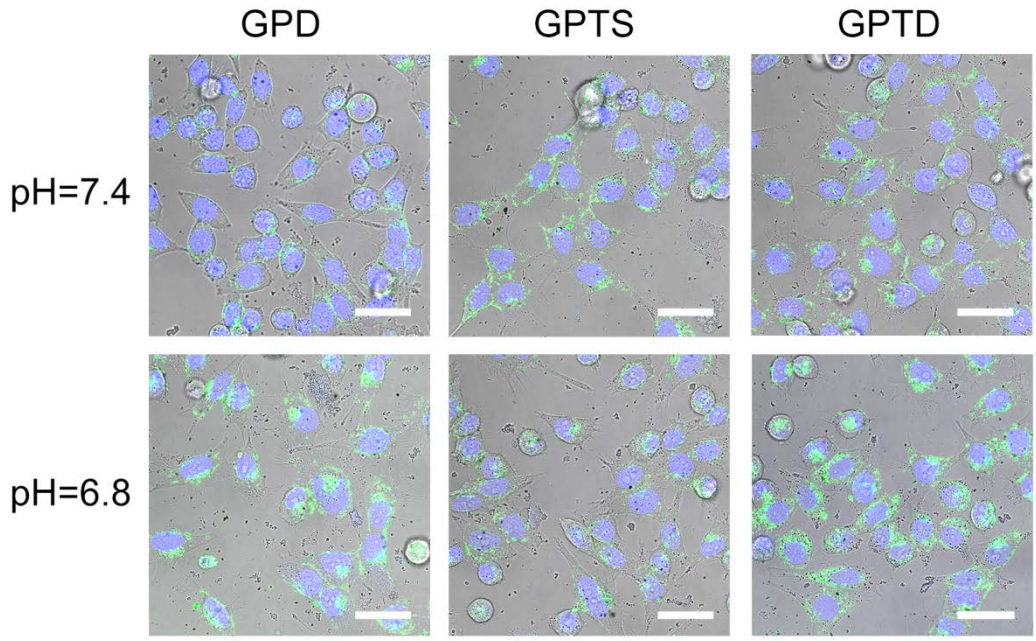

Figure S7. CLSM images of HeLa-R cells incubated for 3 h with GPD_F, $GPTS_F$, and $GPTD_F$ (10 μg/mL) in pH 7.4 and pH 6.8 culture medium, respectively. Scale bars correspond to 50 μm.

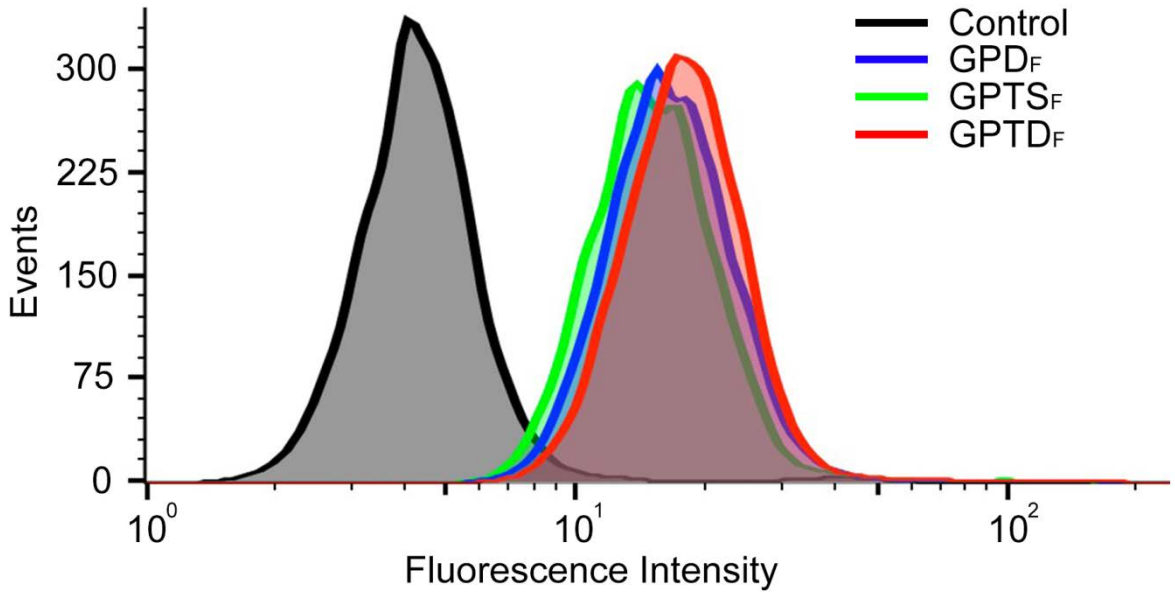

Figure S8. FACS results of HeLa-R cells after 24 h incubation with GPD_F, $GPTS_F$, and $GPTD_F$ (10 μg/mL) in culture medium (pH 7.4), respectively.

11. Photothermal effect

The temperature of the GPD and GPTD solution (100 and 1000 μg/mL in PBS) rapidly increased under the NIR irradiation (808 nm, 0.5 W/cm^2) while the temperature of GPD and GPTD with low concentration (15 μg/mL in PBS) only displayed mild increase under the same condition.

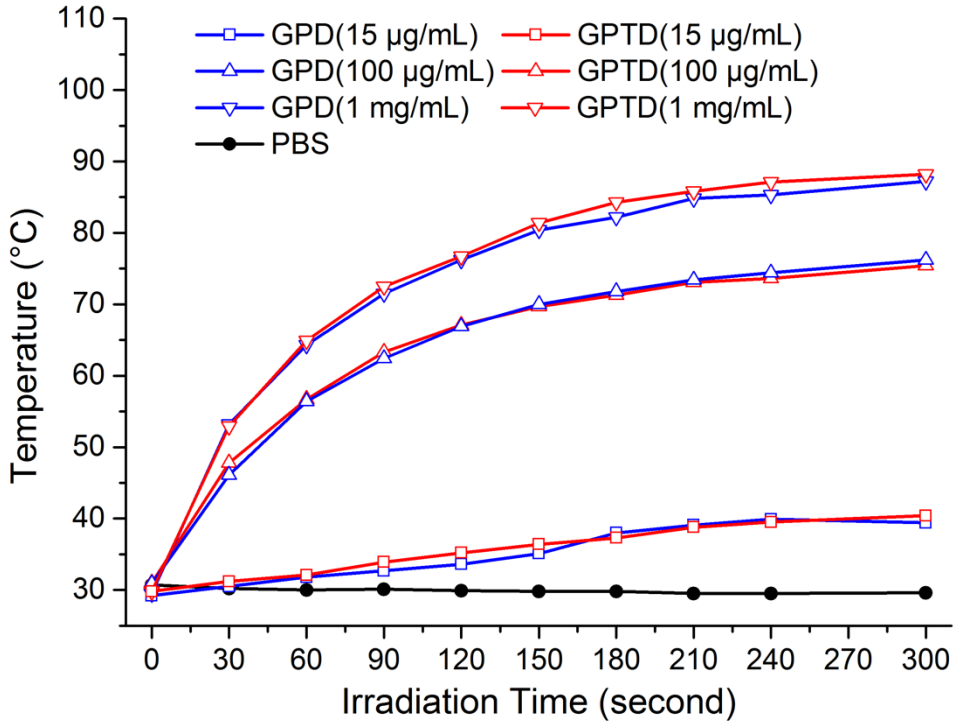

Figure S9. Heat-generation kinetics of GPD and GPTD dispersed in PBS with different concentrations under NIR irradiation (808 nm, 0.5 W/cm^2). Pure PBS was used as control.

12. JC-1 assay

The disruption of mitochondrial membranes was studied by JC-1 assay. As a cationic dye, JC-1 can accumulate in mitochondria to form aggregates (red fluorescence) in healthy cells, and disperse in cytoplasm as monomer (green fluorescence) if mitochondria was damaged.[7] As shown in Figure S10, the green fluorescence enhanced a lot after the treatment with GPTD and irradiation. These variations confirmed the mitochondria-targeting and the following mitochondria-disruption (with irradiation) ability of TPP-conjugated graphene derivatives.

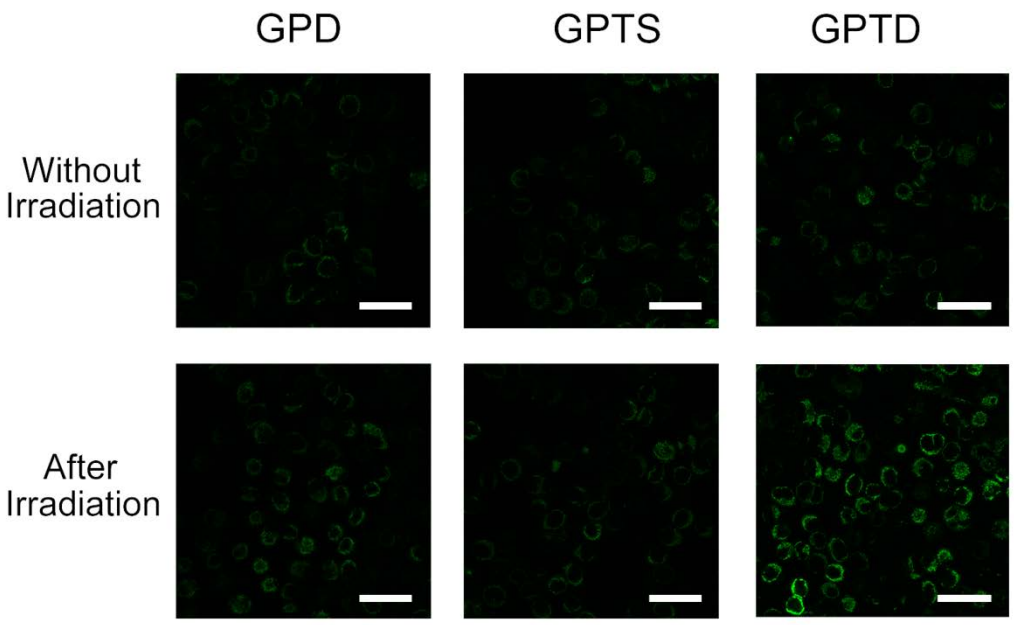

Figure S10. The CLSM images of HeLa-R cells after 6 h incubation with GPD, GPTS and GPTD (10 μg/mL). Scale bars correspond to 50 μm.

13. Characterization of GPD_D and $GPTD_D$

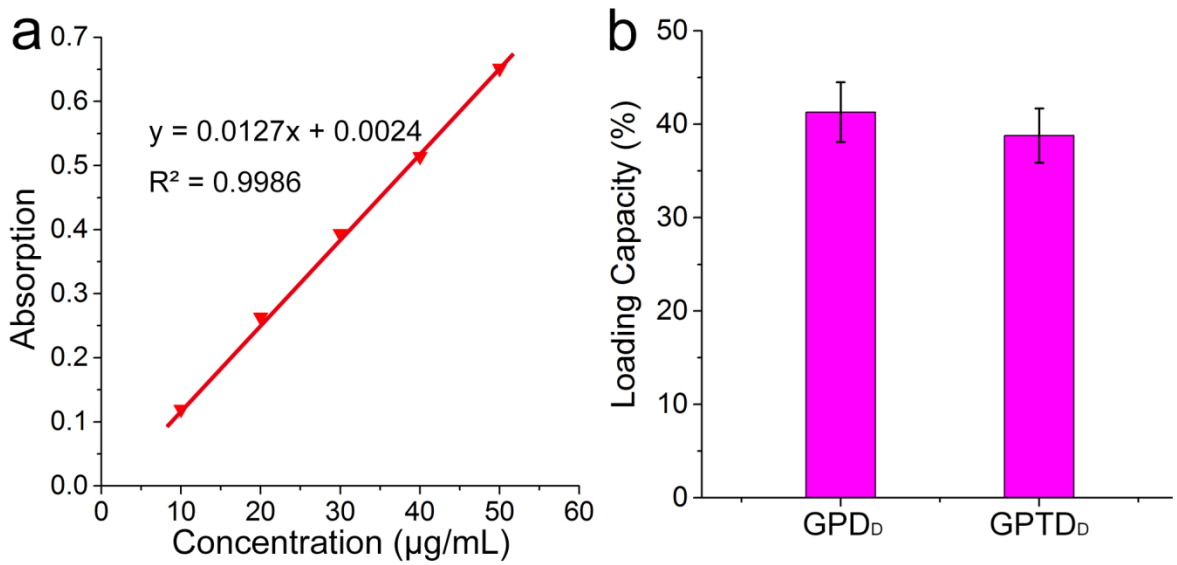

Figure S11. (a) The calibration curve of DOX in PBS with the absorption at 545 nm; (b) the loading capacity of GPD_D and $GPTD_D$, the data was calculated by UV-vis absorption.

14. Release profile

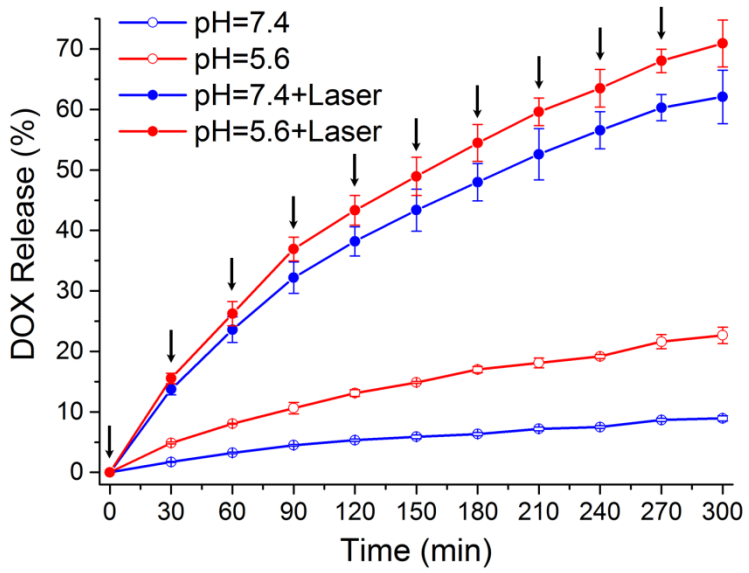

Figure S12. In vitro release profile of DOX from the GPD_D at 37 °C in various conditions. NIR laser irradiation (808 nm, 0.5 W/cm^2) was applied 1 min every 30 min for two of the profiles. Means ± SD (n = 3).

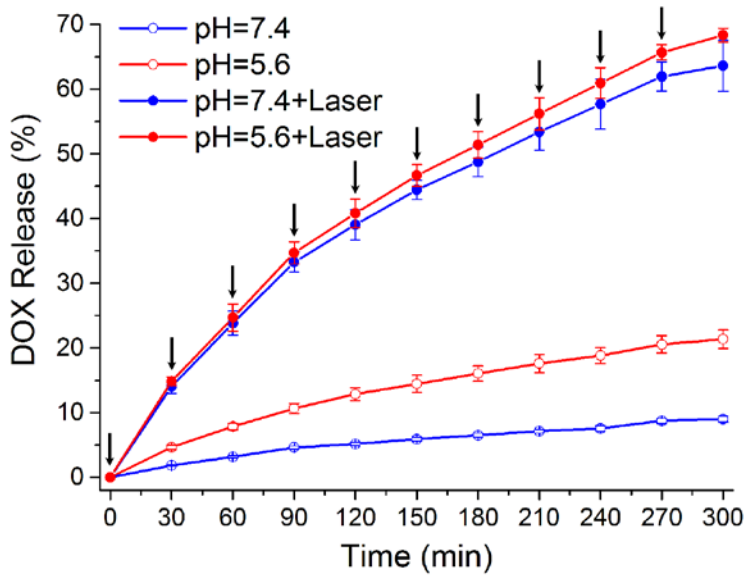

Figure S13. In vitro release profile of DOX from the $GPTD_D$ at 37 °C in various conditions. NIR laser irradiation (808 nm, 0.5 W/cm^2) was applied 1 min every 30 min for two of the profiles. Means ± SD (n = 3).

15. Intracellular DOX release

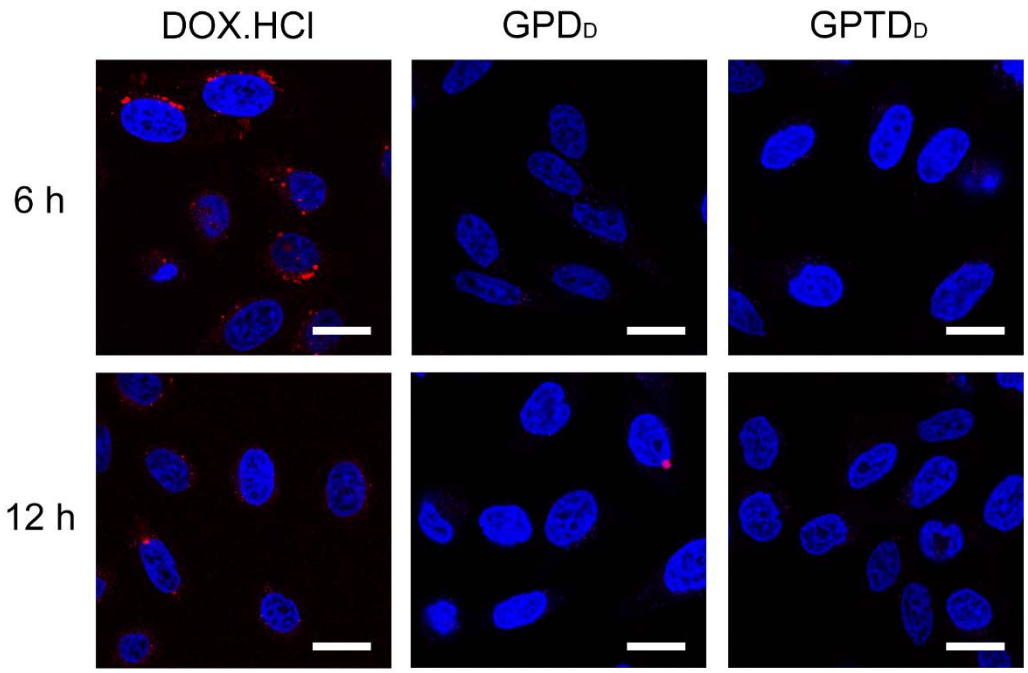

Figure S14. CLSM images of HeLa-R cells incubated for 6 h and 24 h with DOX.HCl, GPD_D and $GPTD_D$ (DOX concentration is 4 μg/mL), respectively. No NIR laser irradiation was performed during the whole incubation. Scale bars correspond to 25 μm.

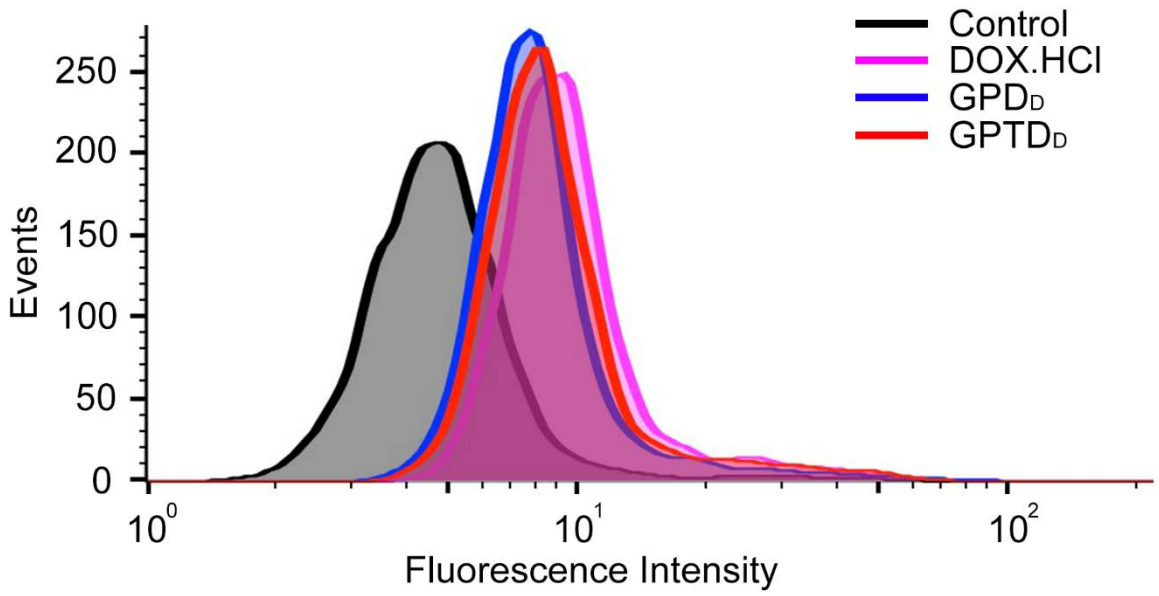

Figure S15. FACS results of HeLa-R cells after 24 h incubation with DOX.HCl, GPD_D and $GPTD_D$ (DOX concentration is 4 μg/mL), respectively. No NIR laser irradiation was performed during the whole incubation.

16. Photothermal effect of GPD and GPTD

The photothermal therapeutic effect of GPD and GPTD is not significant when their concentration is below 15 μg/mL, which could be attributed to their limited photothermal effect in low concentration (Figure S9). This result certified the function of graphene sheets in the synergic therapy is mainly disruption of mitochondria and enhance the chemotheraputical effect of DOX.

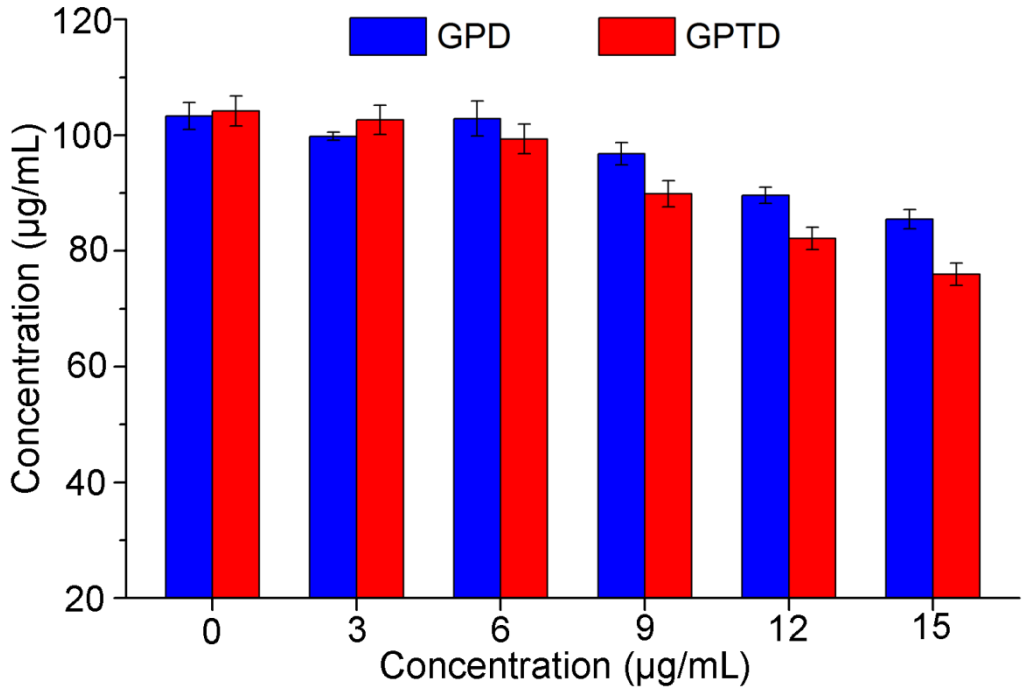

Figure S16. Anticancer therapeutic efficacy of GPD, and GPTD against HeLa-R cells after incubation of 24 h with different concentrations. NIR laser (808 nm, 0.5 W/cm^2) irradiation was performed for 5 min after the incubation of 6 h. Data are showed as the average ± standard deviation (n = 3, student's test).

17. In vivo photothermal effect

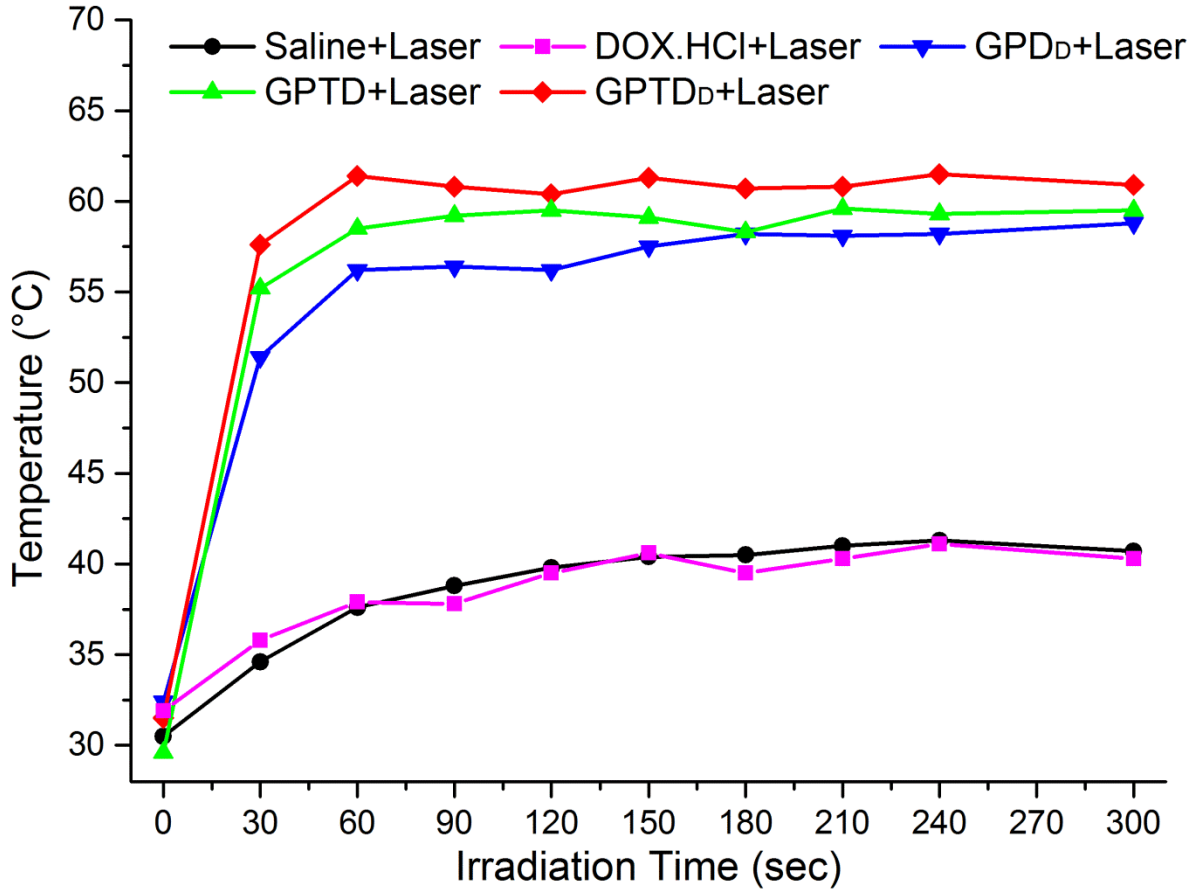

Figure S17. In vivo heat generation kinetics of tumors in nude mice injected with saline, GPD_D, GPTD and $GPTD_D$ (5 mg/kg DOX) under NIR irradiation (808 nm, 0.5 W/cm^2).

18. Ex vivo tumor photos

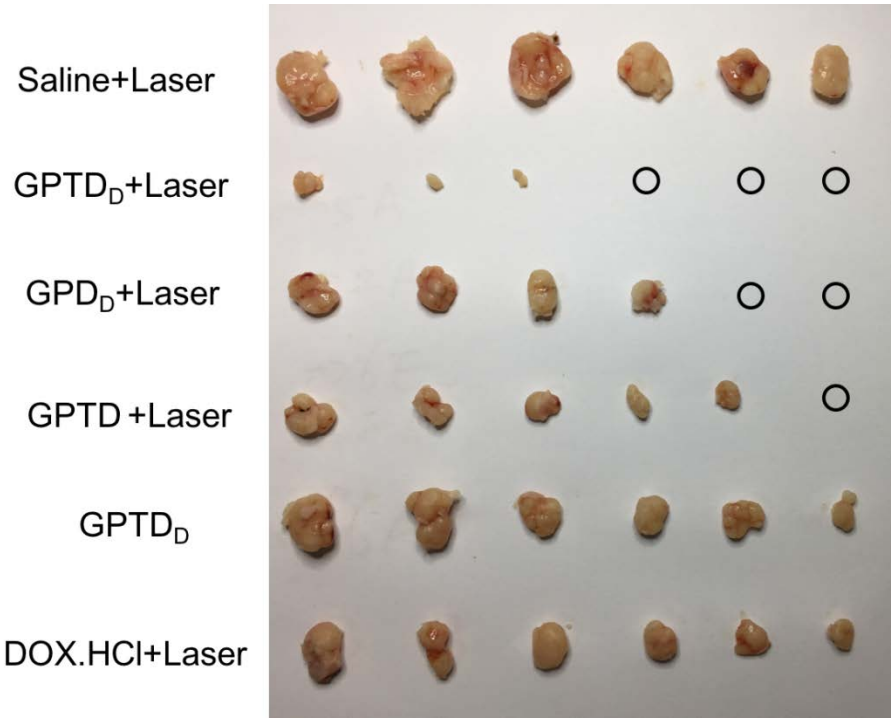

Figure S18. Photos of the tumors extracted from the mice bearing HeLa-R tumor at the end of the experiment. The circles mean the tumors were too small to be isolated.

19. Tissue staining

The damage for heart tissue is obvious in DOX.HCl treated mice while this side effect is hard to find in other experimental groups.

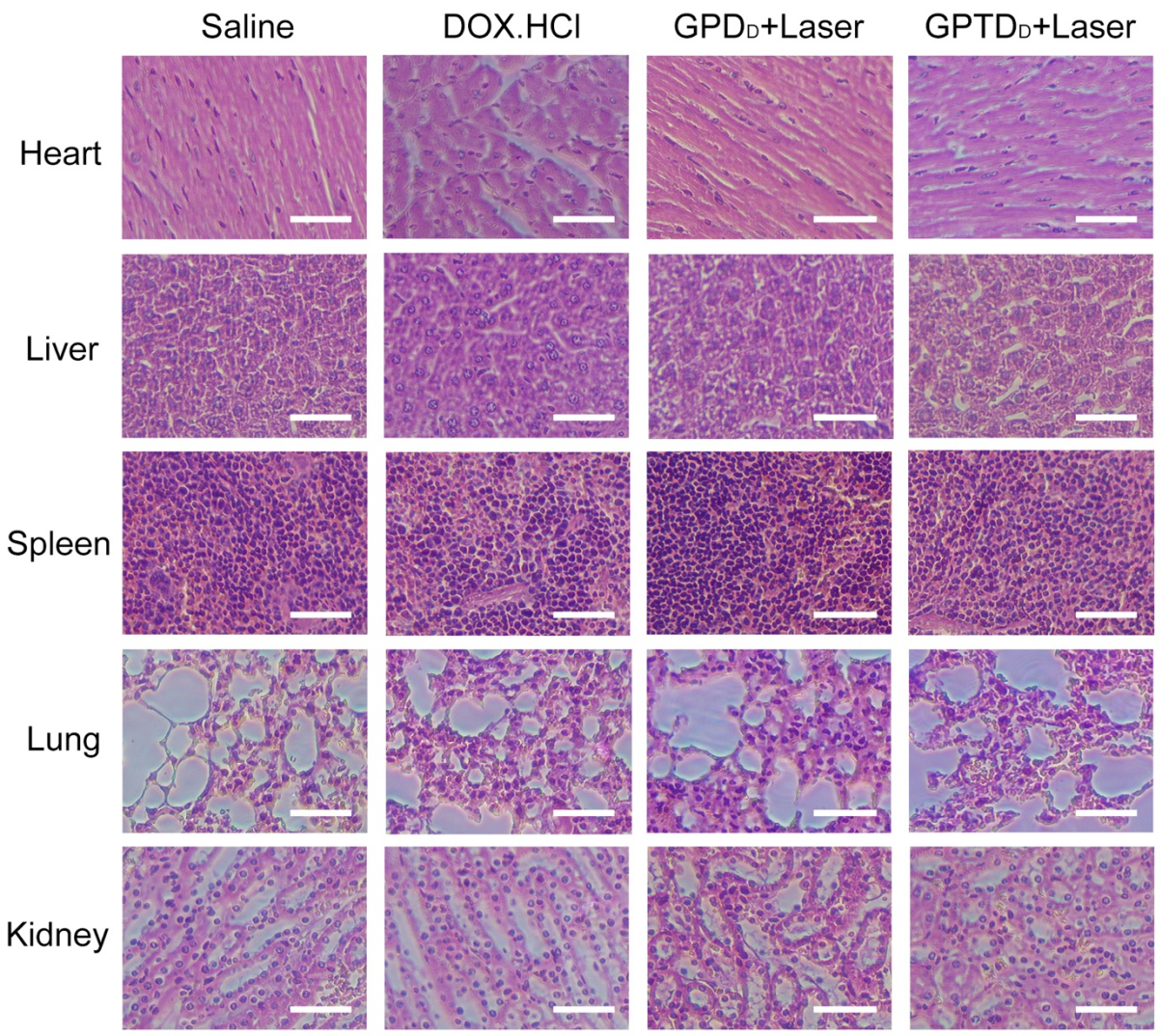

Figure S19. Hematoxylin & eosin (H&E) staining images of heart tissues, liver tissues, spleen tissues, lung tissues and kidney tissues under light microscopy. Scale bars correspond to 500 μm.

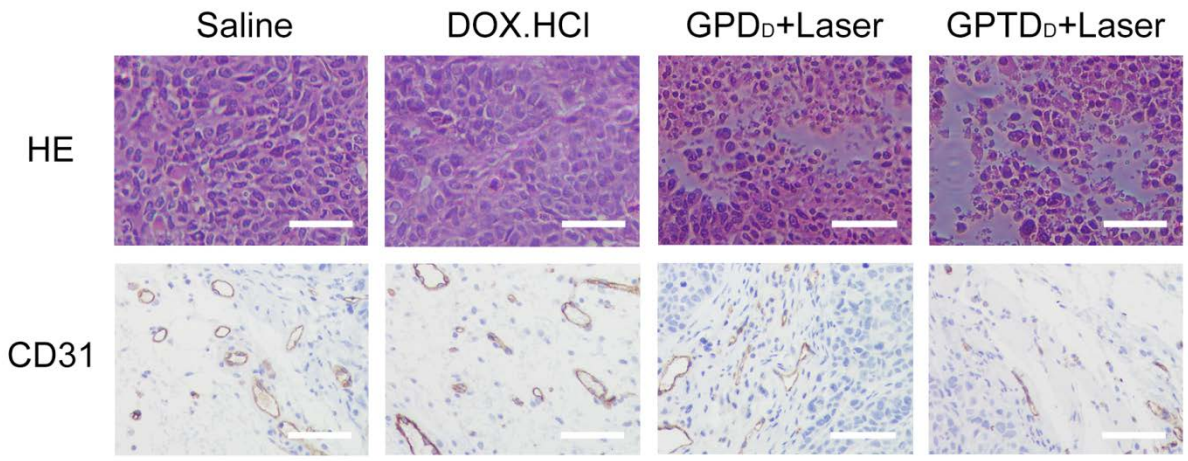

Figure S20. H&E staining and CD31 staining images of tumor tissues under light microscopy. Scale bars correspond to 500 μm.

20. References

[1] M. Calderón, M. A. Quadir, S. K. Sharma, R. Haag, *Adv. Mater.* **2010**, *22*, 190–218.

[2] G. Guday, I. S. Donskyi, M. F. Gholami, A. Lippitz, W. E. S. Unger, J. P. Rabe, M. Adeli, R. Haag, **2018**, in submission.

[3] A. Faghani, I. S. Donskyi, M. Fardin Gholami, B. Ziem, A. Lippitz, W. E. S. Unger, C. Böttcher, J. P. Rabe, R. Haag, M. Adeli, *Angew. Chemie Int. Ed.* **2017**, *56*, 2675–2679; *Angew. Chem.* **2017**, *129*, 2719-2723..

[4] Z. Tu, K. Achazi, A. Schulz, R. Mülhaupt, S. Thierbach, E. Rühl, M. Adeli, R. Haag, *Adv. Funct. Mater.* **2017**, *27*, 1701837.

[5] Z. Tu, V. Wycisk, C. Cheng, W. Chen, M. Adeli, R. Haag, *Nanoscale* **2017**, *9*, 18931–18939.

[6] Y. Lee, S. Fukushima, Y. Bae, S. Hiki, T. Ishii, K. Kataoka, *J. Am. Chem. Soc.* **2007**, *129*, 5362–5363

[7] K. Han, J.-Y. Zhu, H.-Z. Jia, S.-B. Wang, S.-Y. Li, X.-Z. Zhang, H.-Y. Han, *ACS Appl. Mater. Interfaces* **2016**, *8*, 25060−25068

4 Summary and outlook

In this thesis, functionalized graphene sheets were synthesized and their cellular uptake features, drug release properties, and anti-MDR ability were investigated and some significant conclusions were obtained. Hyperbranched polyglycerol (hPG) was successfully conjugated to the graphene backbone that was functionalized by nitrene through a [2+1] cycloaddition reaction. The resulting hPG-coating graphene sheets showed high polymer coverage, controllable size, good water dispersibility, excellent biocompatibility and can be easily post-functionalized. Amination and sulfation was applied to obtain positively charged and negatively charged graphene sheets, respectively. Furthermore, functionalized graphene sheets could be broken down into smaller sizes by horn sonication with corresponding time frames. In my first project, the cellular uptake characteristics of these graphene derivatives with similar polymer content, but different size and surface charges were investigated. It was found that large functionalized graphene sheets (1 μm) were preferable taken up via a phagocytic pathway, regardless of their surface charges. However, surface charge is a dominant factor for their small analogs (200 nm size). Small graphene sheets with positive charges mainly entered into the cells through clathrin-mediated endocytosis (CME), while this pathway did not play a significant role for the small ones with negative charge. Because of the surface charge, the negatively charged and positively charged graphene derivatives displayed size-independent and size-dependent uptake efficacy. Moreover, our results also revealed the cellular internalization of hPG-conjugated graphene sheets is negligible for all the sizes, which is attributed to the protein-resistant feature of hPG and low nonspecific interactions with biointerfaces.

In the next project, we prepared graphene sheets with similar polymer content, size (around 150 nm), but different functionalities and surface charges according to our established protocol of the first project. The hydrophobic anticancer drug, DOX, was loaded onto these graphene derivatives and a pH-sensitive dye was connected onto their surface and employed as an antenna to receive strong signals from the acidic cell compartments. It was found that these functionalized graphene sheets with different functionalities underwent the same cellular uptake and acidification process, while their intracellular release properties were fundamentally different. The protonation of DOX in acidic conditions decreased their hydrophobic and π-π stacking interaction with graphene backbone and facilitated its release from both sheets with different surface charges. However, protonated DOX was positively charged and exhibited attractive and repulsive

electrostatic interactions with negatively charged and positively charged hPG-conjugated graphene derivatives, respectively. While the release of DOX was accelerated by repulsive electrostatic force in the case of positive sheets, many of them were trapped on the surface of negative sheets via attractive electrostatic interactions. Therefore, the overall release rate and therapeutic effect was much higher in the first case. This study revealed that intracellular location and release features of the therapeutic agents are a function of their hydrophobic and electrostatic interactions with the graphene-based nanocarriers.

In the third project, a graphene-based delivery nanoplatforms was introduced to overcome the newly-emerging MDR in tumor cells. Triphenylphosphonium and 2,3-dimethylmaleic anhydride were conjugated onto the hPG-covered nanographene sheets to achieve mitochondria targeting and charge-convention properties. The average size of these functionalized nanographene sheets were around 75 nm with a narrow size-distribution, which was favorable for their accumulation in tumor site owning to the widely confirmed EPR effect. After internalization, these nanosheets targeted the mitochondria and finally disrupted them under laser irradiation, leading to the plunge of adenosine triphosphate (ATP) synthesis. Without enough "biological fuel," the P-gP lost its function and the MDR was successfully reversed. Both of the *in vitro* and *in vivo* antitumor results confirmed these functionalized graphene sheets could effectively surmount the troublesome MDR tumors and remarkably promote the synergic antitumor theranostic efficacy. Moreover, serious side effects caused by chemotherapy agents could also be avoided with these graphene-based nanocarriers.

During the doctoral studies, my work focused on the biological behavior of graphene derivatives and their potential application for antitumor therapy. Many promising results were obtained and several critical problems were addressed, including the cellular uptake properties, intracellular release features, and anti-MDR theranostic. These outcomes revealed that the biological behaviors of functionalized graphene sheets could be adjusted by their physiochemical characteristics and MDR reversal therapy could be achieved though the rational design of graphene-based nanoplatforms, which is of great significance for the future development of graphene-based nanomaterials for bioapplications.

5 Zusammenfassung und Ausblick

In dieser Arbeit wurden hPG-beschichtete Graphene synthetisiert und deren Fähigkeit zur zellulären Aufnahme, Wirkstofffreisetzung und anti-MDR-Fähigkeit untersucht und daraus einige signifikante Schlussfolgerungen gezogen. hPG wurde erfolgreich auf Graphen aufgebracht, welches zuvor über eine [2 + 1] -Cycloaddition mit Nitren funktionalisiert wurde. Die hPG-beschichteten Graphenfolien zeigten eine hohe Polymerdichte, kontrollierbare Größe, gute Wasserdispergierbarkeit, ausgezeichnete Biokompatibilität und können weiter funktionalisiert werden. Durch Aminierung und Sulfatierung wurden positiv geladene bzw. negativ geladene Graphenderivate erzeugt. Weiterhin konnten funktionalisierte Graphenschichten durch Ultraschallbehandlung durch Teilung zerkleinert werden. In meinem ersten Projekt wurden die zellulären Aufnahmeeigenschaften von Graphenderivaten mit ähnlichem Polymergehalt, aber unterschiedlicher Größe und Oberflächenladung untersucht. Es wurde festgestellt, dass große funktionalisierte Graphene (1 μm) bevorzugt über einen Phagozytoseweg aufgenommen werden, unabhängig von ihrer Oberflächenladung. Allerdings ist die Oberflächenladung ein dominanter Faktor für ihre kleinen Analoge (200 nm Größe). Kleine Graphene mit positiven Ladungen traten hauptsächlich durch Clathrin-vermittelte Endozytose (CME) in die Zellen ein, während dieser Weg für die kleinen mit negativen Ladungen keine bedeutende Rolle spielte. Aufgrund der Oberflächenladung zeigten die negativ geladenen und positiv geladenen Graphenderivate eine größenunabhängige und größenabhängige Aufnahmewirkung. Darüber hinaus haben unsere Ergebnisse auch gezeigt, dass die zelluläre Internalisierung von hPG-bedeckten Graphenen für alle Größen vernachlässigbar ist, was auf die proteinresistente Eigenschaft von hPG und der geringen unspezifischen Interaktion mit Biogrenzflächen zurückzuführen ist.

Im nächsten Projekt haben wir Graphene mit ähnlichem Polymergehalt, Größe (ca. 150 nm), aber unterschiedlichen Funktionalitäten und Oberflächenladungen nach unserem im ersten Projekt etablierten Protokoll hergestellt. Auf diese Graphenderivate wurde das hydrophobe Krebsmedikament DOX geladen und ein pH-empfindlicher Farbstoff auf deren Oberfläche aufgebracht. Es wurde festgestellt, dass die funktionalisierten Graphene mit unterschiedlichen Funktionalitäten einen gleichen zellulären Aufnahme- und Versauerungsprozess durchlaufen, während sich ihre intrazelluläre Freisetzung unterscheiden. Die Protonierung von DOX unter sauren Bedingungen verringerte ihre hydrophobe und π-π stacking Interaktion mit dem Graphen und erleichtert seine Freisetzung aus beiden Schichten mit unterschiedlichen Oberflächenladungen. Protoniertes

DOX war jedoch positiv geladen und zeigte attraktive und abstoßende elektrostatische Wechselwirkungen mit negativ geladenen bzw. positiv geladenen hPG-konjugierten Graphenderivaten. Während die Freisetzung von DOX bei positiven graphenen durch abstoßende elektrostatische Kräfte beschleunigt wurde, wurden viele von ihnen durch attraktive elektrostatische Wechselwirkungen auf der Oberfläche von negativen graphenen eingeschlossen. Dadurch war die Freisetzung und der therapeutische Effekt im ersten Fall viel höher. Die Studie ergab, dass die intrazellulären Lokalisierungs- und Freisetzungseigenschaften der Therapeutika eine Funktion ihrer hydrophoben und elektrostatischen Wechselwirkungen mit den graphenbasierten Nanocarriern sind.

Im Abschlussprojekt wurden graphenbasierte Nano-Transportplattformen vorgestellt, um das neu entstehende MDR-Puzzle zu überwinden. Triphenylphosphonium und 2,3-Dimethylmaleinsäureanhydrid wurden auf die hPG-bedeckten Nanographene konjugiert, um Mitochondrien gezielt und ladungskonventionell zu erreichen. Die durchschnittliche Größe dieser funktionalisierten graphene lag bei etwa 75 nm mit einer engen Größenverteilung, was für ihre Akkumulation in der Tumorstelle, die den weit verbreiteten EPR-Effekt besitzt, günstig war. Nach der Internalisierung zielen diese Nanoblätter auf die Mitochondrien und zerstörten sie schließlich unter Laserbestrahlung, was zum Abbruch der Adenosintriphosphat (ATP)-Synthese führte. Ohne genügend "biologischen Treibstoff" verlor der P-gP seine Funktion und der MDR wurde erfolgreich umgekehrt. Sowohl die in vitro- als auch die in vivo-Antitumorergebnisse bestätigten, dass diese funktionalisierten Graphene die MDR-Tumore effektiv überwinden und die synergistische antitumortherapeutische Wirksamkeit fördern könnten. Darüber hinaus könnten mit diesen graphenbasierten Nanocarriern auch schwerwiegende Nebenwirkungen durch Chemotherapeutika vermieden werden.

Während der 4-jährigen Promotion beschäftigte ich mich mit dem biologischen Verhalten von Graphenderivaten und ihrer möglichen Anwendung in der Antitumortherapie. Nach der langwierigen und anstrengenden Arbeit erhielten wir viele vielversprechende Ergebnisse und es wurden mehrere kritische Probleme angesprochen, einschließlich der zellulären Aufnahmeeigenschaften, der intrazellulären Freisetzungseigenschaften und der Anti-MDR-Theranostik. Diese Ergebnisse zeigten, dass das biologische Verhalten von funktionalisierten Graphenen durch ihre physikochemischen Eigenschaften angepasst werden kann und die MDR-Umkehrtherapie durch das Design von graphenbasierten Nanoplattformen erreicht werden kann, was für die zukünftige Entwicklung von graphenbasierten Nanomaterialien für Bioanwendungen von großer Bedeutung ist.

6 Abbreviations

GO	graphene oxide
rGO	reduced graphene oxide
CS	chitosan
PEG	polyethylene glycol
PVA	polyvinyl alcohol
PLL	poly-L-lysine
APTS	3-aminopropyltriethoxysilane
CNT	carbon nanotubes
SIPGP	self-initiated photografting and photopolymerization
GCS/GO	chitosan/GO complexes
MSC	mesenchymal stem cells
PCGO	protein-coated graphene nanosheets
CME	clathrin-mediated endocytosis
APN	aminopeptidase N
NIR	near-infrared
LDH	lactate dehydrogenase
ROS	reactive oxygen species
DOX	doxorubicin
DH	dihydroartemisinin
Tf	transferrin
PPa	pyropheophorbide-a
mAb	monoclonal antibody
HA	hyaluronic acid
PEI	polyethylenimine
RES	reticuloendothelial system
PTT	photothermal therapy
AuNRs	gold nanorods
GSH	glutathione
TNF	tumor necrosis factor
TRAIL	TNF-related, apoptosis-inducing ligand
GQDs	graphene quantum dots
SCNA	size-changeable GQDs nanoaircraft
RV	resveratrol
DHA	dihydroartemisinin
PDT	photodynamic therapy
Ce6	chlorin e6
Ru	ruthenium nitrosyl
TPP	triphenylphosphonium
CD44	cluster determinant 44
SP	spiropyran

CLSM	confocal laser scanning microscope
RGD	Arg-Gly-Asp peptide
ICG	indocyanine green
lipo-GNS	lipid bilayers-covered graphene nanosheets
DTX	docetaxel
PFH	gasified perfluorohexane
perylene-PCn	phosphorylcholine oligomer-grafted perylene
PSS	polystyrene sulfonate sodium salt
PVP	poly(vinylpyrrolidone)
CS	chitosan
DsiRNA	dicer-substrate small interfering RNA
GA	glycyrrhetinic acid
BSA	bovine serum albumin
HAp	hydroxyapatite
TfG	Tf-modified graphene
RFA	radiofrequency ablation
HCC	hepatocellular carcinoma
PTK7	protein tyrosine kinase 7 receptor
PA	photoacoustic
CT	computed tomography
SERS	surface-enhanced Raman scattering
MRI	magnetic resonance imaging
CAs	contrast agents
EPR	enhanced permeability and retention
RLN	regional lymph nodes
MS	mesoporous silica
hPG	hyperbranched polyglycerol
ROMBP	ring-opening multi-branching polymerization
FACS	fluorescence-activated cell sorting
FRET	förster resonance energy transfer
MDR	multidrug resistance
ABC	ATP-binding cassette
P-gP	P-glycoprotein
ATP	adenosine triphosphate

7 References

[1] Y. Chen, C. Tan, H. Zhang, L. Wang, *Chem. Soc. Rev.* **2015**, *44*, 2681.
[2] Z. Tu, G. Guday, M. Adeli, R. Haag, *Adv. Mater.* **2018**, *30,* 201706709.
[3] G. Reina, J. M. González-Domínguez, A. Criado, E. Vázquez, A. Bianco, M. Prato, *Chem. Soc. Rev.* **2017**, *46*, 4400.
[4] C. Cheng, S. Li, A. Thomas, N. A. Kotov, R. Haag, *Chem. Rev.* **2017**, *117*, 1826.
[5] P. Wick, A. E. Louw-Gaume, M. Kucki, H. F. Krug, K. Kostarelos, B. Fadeel, K. A. Dawson, A. Salvati, E. Vázquez, L. Ballerini, *Angew. Chemie Int. Ed.* **2014**, *53*, 7714.
[6] H. Zhao, R. Ding, X. Zhao, Y. Li, L. Qu, H. Pei, L. Yildirimer, Z. Wu, W. Zhang, *Drug Discov. Today* **2017**, *22*, 1302.
[7] W. Gong, Z. Hu, Y. Liang, Y. Wang, R. Zheng, J. Tan, Z. Lai, X. Li, J. Li, X. Lu, *J. Nanosci. Nanotechnol.* **2018**, *18*, 5155.
[8] R. K. Singh, R. Kumar, D. P. Singh, *Rsc Adv.* **2016**, *6*, 64993.
[9] S. Park, J. An, I. Jung, R. D. Piner, S. J. An, X. Li, A. Velamakanni, R. S. Ruoff, *Nano Lett.* **2009**, *9*, 1593.
[10] J. Zhang, H. Yang, G. Shen, P. Cheng, J. Zhang, S. Guo, *Chem. Commun.* **2010**, *46*, 1112.
[11] V. Georgakilas, M. Otyepka, A. B. Bourlinos, V. Chandra, N. Kim, K. C. Kemp, P. Hobza, R. Zboril, K. S. Kim, *Chem. Rev* **2012**, *112*, 6156.
[12] S. P. Lonkar, Y. S. Deshmukh, A. A. Abdala, *Nano Res.* **2015**, *8*, 1039.
[13] C. K. Chua, M. Pumera, *Chem. Soc. Rev.* **2013**, *42*, 3222.
[14] S. Mallakpour, A. Abdolmaleki, S. Borandeh, *Appl. Surf. Sci.* **2014**, *307*, 533.
[15] G. Xu, X. Chen, J. Hu, P. Yang, D. Yang, L. Wei, *Analyst* **2012**, *137*, 2757.
[16] H. Bao, Y. Pan, Y. Ping, N. G. Sahoo, T. Wu, L. Li, J. Li, L. H. Gan, *Small* **2011**, *7*, 1569.
[17] Z. Liu, J. T. Robinson, X. Sun, H. Dai, *J. Am. Chem. Soc.* **2008**, *130*, 10876.
[18] K. Yang, S. Zhang, G. Zhang, X. Sun, S.-T. Lee, Z. Liu, *Nano Lett.* **2010**, *10*, 3318.
[19] H. K. F. Cheng, N. G. Sahoo, Y. P. Tan, Y. Pan, H. Bao, L. Li, S. H. Chan, J. Zhao, *ACS Appl. Mater. Interfaces* **2012**, *4*, 2387.
[20] Y. Pan, H. Bao, N. G. Sahoo, T. Wu, L. Li, *Adv. Funct. Mater.* **2011**, *21*, 2754.
[21] C.-W. Lo, D. Zhu, H. Jiang, *Soft Matter* **2011**, *7*, 5604.
[22] C. Shan, H. Yang, D. Han, Q. Zhang, A. Ivaska, L. Niu, *Langmuir* **2009**, *25*, 12030.
[23] H. Yang, F. Li, C. Shan, D. Han, Q. Zhang, L. Niu, A. Ivaska, *J. Mater. Chem.* **2009**, *19*, 4632.
[24] J. Han, Y. Shen, W. Feng, *Nanoscale* **2016**, *8*, 14139.
[25] C. K. Chua, Z. Sofer, J. Luxa, M. Pumera, *Chem. Eur. J.* **2015**, *21*, 8090.
[26] H. Wang, Q. Zhang, X. Chu, T. Chen, J. Ge, R. Yu, *Angew. Chemie Int. Ed.* **2011**, *50*, 7065.
[27] C. K. Chua, M. Pumera, *ACS Nano* **2015**, *9*, 4193.
[28] A. Setaro, M. Adeli, M. Glaeske, D. Przyrembel, T. Bisswanger, G. Gordeev, F. Maschietto, A. Faghani, B. Paulus, M. Weinelt, *Nat. Commun.* **2017**, *8*.
[29] H. He, C. Gao, *Chem. Mater.* **2010**, *22*, 5054.
[30] L. Q. Xu, Y. K. Yee, K.-G. Neoh, E.-T. Kang, G. D. Fu, *Polymer (Guildf).* **2013**, *54*, 2264.
[31] D. Hong, K. Bae, D. Park, H. Kim, S. Hong, M. Kim, B. S. Lee, S. Ko, S. Jeon, X. Zheng, *Chem. Asian J.* **2015**, *10*, 568.
[32] A. Faghani, I. S. Donskyi, M. Fardin Gholami, B. Ziem, A. Lippitz, W. E. S. Unger, C. Böttcher, J. P. Rabe, R. Haag, M. Adeli, *Angew. Chemie Int. Ed.* **2017**, *56*, 2675.
[33] M. Quintana, K. Spyrou, M. Grzelczak, W. R. Browne, P. Rudolf, M. Prato, *ACS*

Nano **2010**, *4*, 3527.
[34] S. Zhao, H. Wang, L. Xin, J. Cui, Y. Yan, *Chem. Asian J.* **2015**, *10*, 1177.
[35] M. Steenackers, A. M. Gigler, N. Zhang, F. Deubel, M. Seifert, L. H. Hess, C. H. Y. X. Lim, K. P. Loh, J. A. Garrido, R. Jordan, *J. Am. Chem. Soc.* **2011**, *133*, 10490.
[36] L. H. Hess, A. Lyuleeva, B. M. Blaschke, M. Sachsenhauser, M. Seifert, J. A. Garrido, F. Deubel, *ACS Appl. Mater. Interfaces* **2014**, *6*, 9705.
[37] D. Han, P. Xiao, J. Gu, J. Chen, Z. Cai, J. Zhang, W. Wang, T. Chen, *RSC Adv.* **2014**, *4*, 22759.
[38] V. Georgakilas, J. N. Tiwari, K. C. Kemp, J. A. Perman, A. B. Bourlinos, K. S. Kim, R. Zboril, *Chem. Rev.* **2016**, *116*, 5464.
[39] D.-W. Lee, T. Kim, M. Lee, *Chem. Commun.* **2011**, *47*, 8259.
[40] P. Lin, Y. Cong, C. Sun, B. Zhang, *Nanoscale* **2016**, *8*, 2403.
[41] C. Sun, K. L. Walker, D. L. Wakefield, W. R. Dichtel, *Chem. Mater.* **2015**, *27*, 4499.
[42] Y. Liu, H. Zhong, Y. Qin, Y. Zhang, X. Liu, T. Zhang, *RSC Adv.* **2016**, *6*, 30184.
[43] D. Y. Lee, Z. Khatun, J.-H. Lee, Y. Lee, I. In, *Biomacromolecules* **2011**, *12*, 336.
[44] J. Liu, S. Guo, L. Han, T. Wang, W. Hong, Y. Liu, E. Wang, *J. Mater. Chem.* **2012**, *22*, 20634.
[45] A. Sahu, W. Il Choi, J. H. Lee, G. Tae, *Biomaterials* **2013**, *34*, 6239.
[46] Y. Liang, D. Wu, X. Feng, K. Müllen, *Adv. Mater.* **2009**, *21*, 1679.
[47] J. Li, N. Ren, J. Qiu, X. Mou, H. Liu, *Int. J. Nanomedicine* **2013**, *8*, 3415.
[48] W. Qi, W. Yuan, J. Yan, H. Wang, *J. Mater. Chem. B* **2014**, *2*, 5461.
[49] B. Zhang, P. Wei, Z. Zhou, T. Wei, *Adv. Drug Deliv. Rev.* **2016**, *105*, 145.
[50] M. Zhu, G. Nie, H. Meng, T. Xia, A. Nel, Y. Zhao, *Acc. Chem. Res.* **2012**, *46*, 622.
[51] S. Behzadi, V. Serpooshan, W. Tao, M. A. Hamaly, M. Y. Alkawareek, E. C. Dreaden, D. Brown, A. M. Alkilany, O. C. Farokhzad, M. Mahmoudi, *Chem. Soc. Rev.* **2017**.
[52] Q. Mu, G. Su, L. Li, B. O. Gilbertson, L. H. Yu, Q. Zhang, Y.-P. Sun, B. Yan, *ACS Appl. Mater. Interfaces* **2012**, *4*, 2259.
[53] J. Huang, C. Zong, H. Shen, M. Liu, B. Chen, B. Ren, Z. Zhang, *Small* **2012**, *8*, 2577.
[54] T. Mizuhara, K. Saha, D. F. Moyano, C. S. Kim, B. Yan, Y. Kim, V. M. Rotello, *Angew. Chemie Int. Ed.* **2015**, *54*, 6567.
[55] N. Luo, D. Ni, H. Yue, W. Wei, G. Ma, *ACS Appl. Mater. Interfaces* **2015**, *7*, 5239.
[56] S. Ye, P. Yang, K. Cheng, T. Zhou, Y. Wang, Z. Hou, Y. Jiang, L. Ren, *ACS Biomater. Sci. Eng.* **2016**, *2*, 722.
[57] J. Linares, M. C. Matesanz, M. Vila, M. J. Feito, G. Gonçalves, M. Vallet-Regí, P. A. A. P. Marques, M. T. Portolés, *ACS Appl. Mater. Interfaces* **2014**, *6*, 13697.
[58] F. Ding, F. Wu, Q. Tian, L. Guo, J. Wang, F. Xiao, Y. Yu, *RSC Adv.* **2016**, *6*, 68134.
[59] T. Zhou, X. Zhou, D. Xing, *Biomaterials* **2014**, *35*, 4185.
[60] S. M. Chowdhury, P. Manepalli, B. Sitharaman, *Acta Biomater.* **2014**, *10*, 4494.
[61] S. M. Chowdhury, C. Surhland, Z. Sanchez, P. Chaudhary, M. A. S. Kumar, S. Lee, L. A. Peña, M. Waring, B. Sitharaman, M. Naidu, *Nanomedicine Nanotechnology, Biol. Med.* **2015**, *11*, 109.
[62] Y.-W. Chen, Y.-L. Su, S.-H. Hu, S.-Y. Chen, *Adv. Drug Deliv. Rev.* **2016**.
[63] L. Feng, X. Yang, X. Shi, X. Tan, R. Peng, J. Wang, Z. Liu, *Small* **2013**, *9*, 1989.
[64] T. Hsieh, W. Huang, Y. Kang, C. Chu, W. Liao, Y. Chen, S. Chen, *Adv. Healthc. Mater.* **2016**, *5*, 3016.
[65] Y. Volkov, J. McIntyre, A. Prina-Mello, *2D Mater.* **2017**, *4*, 22001.
[66] Q. Zhang, Z. Wu, N. Li, Y. Pu, B. Wang, T. Zhang, J. Tao, *Mater. Sci. Eng. C* **2017**,

77, 1363.
[67] Y. Talukdar, J. T. Rashkow, G. Lalwani, S. Kanakia, B. Sitharaman, *Biomaterials* **2014**, *35*, 4863.
[68] L. M. Saeed, M. Mahmood, S. J. Pyrek, T. Fahmi, Y. Xu, T. Mustafa, Z. A. Nima, S. M. Bratton, D. Casciano, E. Dervishi, *J. Appl. Toxicol.* **2014**, *34*, 1188.
[69] T. Lammel, P. Boisseaux, M.-L. Fernández-Cruz, J. M. Navas, *Part. Fibre Toxicol.* **2013**, *10*, 27.
[70] J. Zhu, M. Xu, M. Gao, Z. Zhang, Y. Xu, T. Xia, S. Liu, *ACS Nano* **2017**, *11*, 2637.
[71] O. Akhavan, E. Ghaderi, A. Akhavan, *Biomaterials* **2012**, *33*, 8017.
[72] Y. Li, Q. Wu, Y. Zhao, Y. Bai, P. Chen, T. Xia, D. Wang, *ACS Nano* **2014**, *8*, 2100.
[73] J. Wu, R. Yang, L. Zhang, Z. Fan, S. Liu, *Toxicol. Mech. Methods* **2015**, *25*, 312.
[74] E. L. K. Chng, C. K. Chua, M. Pumera, *Nanoscale* **2014**, *6*, 10792.
[75] A. Sasidharan, L. S. Panchakarla, A. R. Sadanandan, A. Ashokan, P. Chandran, C. M. Girish, D. Menon, S. V Nair, C. N. R. Rao, M. Koyakutty, *Small* **2012**, *8*, 1251.
[76] K.-H. Liao, Y.-S. Lin, C. W. Macosko, C. L. Haynes, *ACS Appl. Mater. Interfaces* **2011**, *3*, 2607.
[77] W. Hu, C. Peng, M. Lv, X. Li, Y. Zhang, N. Chen, C. Fan, Q. Huang, *ACS Nano* **2011**, *5*, 3693.
[78] G. Duan, S. Kang, X. Tian, J. A. Garate, L. Zhao, C. Ge, R. Zhou, *Nanoscale* **2015**, *7*, 15214.
[79] M. Xu, J. Zhu, F. Wang, Y. Xiong, Y. Wu, Q. Wang, J. Weng, Z. Zhang, W. Chen, S. Liu, *ACS Nano* **2016**, *10*, 3267.
[80] H.-K. Na, M.-H. Kim, J. Lee, Y.-K. Kim, H. Jang, K. E. Lee, H. Park, W. Do Heo, H. Jeon, I. S. Choi, *Nanoscale* **2013**, *5*, 1669.
[81] J. Park, B. Kim, J. Han, J. Oh, S. Park, S. Ryu, S. Jung, J.-Y. Shin, B. S. Lee, B. H. Hong, *ACS Nano* **2015**, *9*, 4987.
[82] B. Wan, Z.-X. Wang, Q.-Y. Lv, P.-X. Dong, L.-X. Zhao, Y. Yang, L.-H. Guo, *Toxicol. Lett.* **2013**, *221*, 118.
[83] Y. Li, Z. Lu, Z. Li, G. Nie, Y. Fang, *J. Nanoparticle Res.* **2014**, *16*, 2384.
[84] J. Chen, H. Liu, C. Zhao, G. Qin, G. Xi, T. Li, X. Wang, T. Chen, *Biomaterials* **2014**, *35*, 4986.
[85] E. Song, W. Han, C. Li, D. Cheng, L. Li, L. Liu, G. Zhu, Y. Song, W. Tan, *ACS Appl. Mater. Interfaces* **2014**, *6*, 11882.
[86] Y. Chen, P. Xu, Z. Shu, M. Wu, L. Wang, S. Zhang, Y. Zheng, H. Chen, J. Wang, Y. Li, *Adv. Funct. Mater.* **2014**, *24*, 4386.
[87] T. Jiang, W. Sun, Q. Zhu, N. A. Burns, S. A. Khan, R. Mo, Z. Gu, *Adv. Mater.* **2015**, *27*, 1021.
[88] Y. Hu, D. Sun, J. Ding, L. Chen, X. Chen, *J. Mater. Chem. B* **2016**, *4*, 929.
[89] L. Li, W. Sun, J. Zhong, Q. Yang, X. Zhu, Z. Zhou, Z. Zhang, Y. Huang, *Adv. Funct. Mater.* **2015**, *25*, 4101.
[90] Y. Zeng, Z. Yang, S. Luo, H. Li, C. Liu, Y. Hao, J. Liu, W. Wang, R. Li, *RSC Adv.* **2015**, *5*, 57725.
[91] L. Liu, Y. Wei, S. Zhai, Q. Chen, D. Xing, *Biomaterials* **2015**, *62*, 35.
[92] H. Zhou, B. Zhang, J. Zheng, M. Yu, T. Zhou, K. Zhao, Y. Jia, X. Gao, C. Chen, T. Wei, *Biomaterials* **2014**, *35*, 1597.
[93] M. Jin, Z. Liu, W. Zhang, H. Dong, F. Zhou, J. Yu, X. Wang, Z. Guo, *Nano* **2015**, *10*, 1550121.
[94] Y. Wei, F. Zhou, D. Zhang, Q. Chen, D. Xing, *Nanoscale* **2016**, *8*, 3530.
[95] N. Chatterjee, H.-J. Eom, J. Choi, *Biomaterials* **2014**, *35*, 1109.
[96] M. C. Duch, G. R. S. Budinger, Y. T. Liang, S. Soberanes, D. Urich, S. E. Chiarella, L. A. Campochiaro, A. Gonzalez, N. S. Chandel, M. C. Hersam, *Nano Lett.* **2011**,

11, 5201.
[97] W. Zhang, C. Wang, Z. Li, Z. Lu, Y. Li, J. Yin, Y. Zhou, X. Gao, Y. Fang, G. Nie, *Adv. Mater.* **2012**, *24*, 5391.
[98] W. Zhang, L. Yan, M. Li, R. Zhao, X. Yang, T. Ji, Z. Gu, J.-J. Yin, X. Gao, G. Nie, *Toxicol. Lett.* **2015**, *237*, 61.
[99] S. Das, S. Singh, V. Singh, D. Joung, J. M. Dowding, D. Reid, J. Anderson, L. Zhai, S. I. Khondaker, W. T. Self, *Part. Part. Syst. Charact.* **2013**, *30*, 148.
[100] C. Wu, C. Wang, T. Han, X. Zhou, S. Guo, J. Zhang, *Adv. Healthc. Mater.* **2013**, *2*, 1613.
[101] Z. M. Markovic, L. M. Harhaji-Trajkovic, B. M. Todorovic-Markovic, D. P. Kepić, K. M. Arsikin, S. P. Jovanović, A. C. Pantovic, M. D. Dramićanin, V. S. Trajkovic, *Biomaterials* **2011**, *32*, 1121.
[102] Y. Li, Y. Liu, Y. Fu, T. Wei, L. Le Guyader, G. Gao, R.-S. Liu, Y.-Z. Chang, C. Chen, *Biomaterials* **2012**, *33*, 402.
[103] X. Hu, S. Ouyang, L. Mu, J. An, Q. Zhou, *Environ. Sci. Technol.* **2015**, *49*, 10825.
[104] S. C. Reshma, S. Syama, P. V Mohanan, *Colloids Surfaces B Biointerfaces* **2016**, *140*, 104.
[105] M.-C. Matesanz, M. Vila, M.-J. Feito, J. Linares, G. Gonçalves, M. Vallet-Regi, P.-A. A. P. Marques, M.-T. Portolés, *Biomaterials* **2013**, *34*, 1562.
[106] K. Wang, J. Ruan, *Wo, SW Guo DX Cui, Biocompat. graphene oxide, Nanoscale Res. Lett* **2011**, *6*, 1.
[107] C. Wang, C. Wu, X. Zhou, T. Han, X. Xin, J. Wu, J. Zhang, S. Guo, *Sci. Rep.* **2013**, *3*.
[108] G.-Y. Chen, C.-L. Meng, K.-C. Lin, H.-Y. Tuan, H.-J. Yang, C.-L. Chen, K.-C. Li, C.-S. Chiang, Y.-C. Hu, *Biomaterials* **2015**, *40*, 12.
[109] C. Ren, X. Hu, X. Li, Q. Zhou, *Biomaterials* **2016**, *93*, 83.
[110] A. L. Klibanov, K. Maruyama, V. P. Torchilin, L. Huang, *FEBS Lett.* **1990**, *268*, 235.
[111] K. Yang, L. Feng, H. Hong, W. Cai, Z. Liu, *Nat. Protoc.* **2013**, *8*, 2392.
[112] O. Akhavan, E. Ghaderi, *Small* **2013**, *9*, 3593.
[113] K. Yang, J. Wan, S. Zhang, B. Tian, Y. Zhang, Z. Liu, *Biomaterials* **2012**, *33*, 2206.
[114] L. Chen, X. Zhong, X. Yi, M. Huang, P. Ning, T. Liu, C. Ge, Z. Chai, Z. Liu, K. Yang, *Biomaterials* **2015**, *66*, 21.
[115] P. Rong, J. Wu, Z. Liu, X. Ma, L. Yu, K. Zhou, W. Zeng, W. Wang, *RSC Adv.* **2016**, *6*, 1894.
[116] S. Wang, Q. Zhang, X. F. Luo, J. Li, H. He, F. Yang, Y. Di, C. Jin, X. G. Jiang, S. Shen, *Biomaterials* **2014**, *35*, 9473.
[117] Y. Tao, E. Ju, J. Ren, X. Qu, *Biomaterials* **2014**, *35*, 9963.
[118] H. Zhang, H. Wu, J. Wang, Y. Yang, D. Wu, Y. Zhang, Y. Zhang, Z. Zhou, S. Yang, *Biomaterials* **2015**, *42*, 66.
[119] S. Gao, L. Zhang, G. Wang, K. Yang, M. Chen, R. Tian, Q. Ma, L. Zhu, *Biomaterials* **2016**, *79*, 36.
[120] X. Sun, Z. Liu, K. Welsher, J. T. Robinson, A. Goodwin, S. Zaric, H. Dai, *Nano Res.* **2008**, *1*, 203.
[121] H. Wen, C. Dong, H. Dong, A. Shen, W. Xia, X. Cai, Y. Song, X. Li, Y. Li, D. Shi, *Small* **2012**, *8*, 760.
[122] H. Chen, Z. Wang, S. Zong, P. Chen, D. Zhu, L. Wu, Y. Cui, *Nanoscale* **2015**, *7*, 15477.
[123] D. Yang, L. Feng, C. A. Dougherty, K. E. Luker, D. Chen, M. A. Cauble, M. M. B. Holl, G. D. Luker, B. D. Ross, Z. Liu, *Biomaterials* **2016**, *104*, 361.
[124] W. Zhang, Z. Guo, D. Huang, Z. Liu, X. Guo, H. Zhong, *Biomaterials* **2011**, *32*,

8555.
[125] L. Feng, K. Li, X. Shi, M. Gao, J. Liu, Z. Liu, *Adv. Healthc. Mater.* **2014**, *3*, 1261.
[126] Y. Su, T. Yu, W. Chiang, H. Chiu, C. Chang, C. Chiang, S. Hu, *Adv. Funct. Mater.* **2017**, *27*.
[127] X. Ma, H. Tao, K. Yang, L. Feng, L. Cheng, X. Shi, Y. Li, L. Guo, Z. Liu, *Nano Res.* **2012**, *5*, 199.
[128] Y. Wang, R. Huang, G. Liang, Z. Zhang, P. Zhang, S. Yu, J. Kong, *Small* **2014**, *10*, 109.
[129] F. Wang, Q. Sun, B. Feng, Z. Xu, J. Zhang, J. Xu, L. Lu, H. Yu, M. Wang, Y. Li, *Adv. Healthc. Mater.* **2016**, *5*, 2227.
[130] R. K. Thapa, J. H. Byeon, S. K. Ku, C. S. Yong, J. O. Kim, *NPG Asia Mater.* **2017**, *9*, e416.
[131] L. Hai, D. He, X. He, K. Wang, X. Yang, J. Liu, H. Cheng, X. Huang, J. Shangguan, *J. Mater. Chem. B* **2017**, *5*, 5783.
[132] J. Li, Z. Lyv, Y. Li, H. Liu, J. Wang, W. Zhan, H. Chen, H. Chen, X. Li, *Biomaterials* **2015**, *51*, 12.
[133] C. Zhang, T. Lu, J. Tao, G. Wan, H. Zhao, *RSC Adv.* **2016**, *6*, 15460.
[134] Y. Pang, Z. Mai, B. Wang, L. Wang, L. Wu, X. Wang, T. Chen, *Oncotarget* **2017**, *8*, 93800.
[135] Y. Zhao, M. Huan, M. Liu, Y. Cheng, Y. Sun, H. Cui, D. Liu, Q. Mei, S. Zhou, *Sci. Rep.* **2016**, *6*, 35267.
[136] D. E. Dolmans, D. Fukumura, R. K. Jain, *Nat. Rev. cancer* **2003**, *3*, 380.
[137] P. Kalluru, R. Vankayala, C.-S. Chiang, K. C. Hwang, *Biomaterials* **2016**, *95*, 1.
[138] B. Tian, C. Wang, S. Zhang, L. Feng, Z. Liu, *ACS Nano* **2011**, *5*, 7000.
[139] Y. Li, Z. Wu, D. Du, H. Dong, D. Shi, Y. Li, *RSC Adv.* **2016**, *6*, 6516.
[140] J. Cao, H. An, X. Huang, G. Fu, R. Zhuang, L. Zhu, J. Xie, F. Zhang, *Nanoscale* **2016**, *8*, 10152.
[141] W. Miao, G. Shim, S. Lee, S. Lee, Y. S. Choe, Y.-K. Oh, *Biomaterials* **2013**, *34*, 3402.
[142] C. Wu, D. Li, L. Wang, X. Guan, Y. Tian, H. Yang, S. Li, Y. Liu, *Acta Biomater.* **2017**, *53*, 631.
[143] X. Yan, G. Niu, J. Lin, A. J. Jin, H. Hu, Y. Tang, Y. Zhang, A. Wu, J. Lu, S. Zhang, *Biomaterials* **2015**, *42*, 94.
[144] Y. Cao, H. Dong, Z. Yang, X. Zhong, Y. Chen, W. Dai, X. Zhang, *ACS Appl. Mater. Interfaces* **2016**, *9*, 159.
[145] D.-Y. Zhang, Y. Zheng, C.-P. Tan, J.-H. Sun, W. Zhang, L.-N. Ji, Z.-W. Mao, *ACS Appl. Mater. Interfaces* **2017**, *9*, 6761.
[146] Y.-H. Li, M. Guo, S.-W. Shi, Q.-L. Zhang, S.-P. Yang, J.-G. Liu, *J. Mater. Chem. B* **2017**, *5*, 7831.
[147] M. Guo, H.-J. Xiang, Y. Wang, Q.-L. Zhang, L. An, S.-P. Yang, Y. Ma, Y. Wang, J.-G. Liu, *Chem. Commun.* **2017**, *53*, 3253.
[148] L. Y. Qiu, Y. H. Bae, *Biomaterials* **2007**, *28*, 4132.
[149] H. Wang, X. Wang, *Rsc Adv.* **2015**, *5*, 75380.
[150] B. Du, J. Liu, G. Ding, X. Han, D. Li, E. Wang, J. Wang, *Nano Res.* **2017**, *10*, 2280.
[151] H. Chen, Z. Wang, S. Zong, L. Wu, P. Chen, D. Zhu, C. Wang, S. Xu, Y. Cui, *ACS Appl. Mater. Interfaces* **2014**, *6*, 17526.
[152] C. Wang, X. Wang, T. Lu, F. Liu, B. Guo, N. Wen, Y. Du, H. Lin, J. Tang, L. Zhang, *RSC Adv.* **2016**, *6*, 22461.
[153] B. Xie, J. Yi, J. Peng, X. Zhang, L. Lei, D. Zhao, Z. Lei, H. Nie, *J. Mater. Sci. Technol.* **2017**, *33*, 807.
[154] K. Y. Choi, H. Chung, K. H. Min, H. Y. Yoon, K. Kim, J. H. Park, I. C. Kwon, S.

Y. Jeong, *Biomaterials* **2010**, *31*, 106.
[155] S. H. Kim, J. E. Lee, S. M. Sharker, J. H. Jeong, I. In, S. Y. Park, *Biomacromolecules* **2015**, *16*, 3519.
[156] A.-A. Nahain, J.-E. Lee, J. H. Jeong, S. Y. Park, *Biomacromolecules* **2013**, *14*, 4082.
[157] T. Yin, J. Liu, Z. Zhao, Y. Zhao, L. Dong, M. Yang, J. Zhou, M. Huo, *Adv. Funct. Mater.* **2017**.
[158] Y. Guo, H. Xu, Y. Li, F. Wu, Y. Li, Y. Bao, X. Yan, Z. Huang, P. Xu, *J. Biomater. Appl.* **2017**, *32*, 54.
[159] L. Shao, R. Zhang, J. Lu, C. Zhao, X. Deng, Y. Wu, *ACS Appl. Mater. Interfaces* **2017**, *9*, 1226.
[160] Y. Yang, Y. Wang, W. Xu, X. Zhang, Y. Shang, A. Xie, Y. Shen, *Eur. J. Inorg. Chem.* **2017**, *2017*, 2236.
[161] P. N. Joshi, S. Agawane, M. C. Athalye, V. Jadhav, D. Sarkar, R. Prakash, *Mater. Sci. Eng. C* **2017**, *78*, 1203.
[162] W. Miao, G. Shim, G. Kim, S. Lee, H.-J. Lee, Y. B. Kim, Y. Byun, Y.-K. Oh, *J. Control. Release* **2015**, *211*, 28.
[163] H. Y. Kim, F. Li, J. Y. Park, D. Kim, J. H. Park, H. S. Han, J. W. Byun, Y.-S. Lee, J. M. Jeong, K. Char, *Biomaterials* **2017**, *121*, 144.
[164] Y.-L. Su, K.-T. Chen, Y.-C. Sheu, S.-Y. Sung, R.-S. Hsu, C.-S. Chiang, S.-H. Hu, *ACS Nano* **2016**, *10*, 9420.
[165] Q. Wu, M. Chu, Y. Shao, F. Wo, D. Shi, *Carbon N. Y.* **2016**, *108*, 21.
[166] L. Guo, H. Shi, H. Wu, Y. Zhang, X. Wang, D. Wu, L. An, S. Yang, *Carbon N. Y.* **2016**, *107*, 87.
[167] C. Zhou, H. Wu, M. Wang, C. Huang, D. Yang, N. Jia, *Mater. Sci. Eng. C* **2017**, *78*, 817.
[168] B. Sun, J. Wu, S. Cui, H. Zhu, W. An, Q. Fu, C. Shao, A. Yao, B. Chen, D. Shi, *Nano Res.* **2017**, *10*, 37.
[169] N. Tyagi, N. F. Attia, K. E. Geckeler, *J. Colloid Interface Sci.* **2017**, *498*, 364.
[170] C. Dai, S. Zhang, Z. Liu, R. Wu, Y. Chen, *ACS Nano* **2017**, *11*, 9467.
[171] Y. Zhang, H. Zhang, Y. Wang, H. Wu, B. Zeng, Y. Zhang, Q. Tian, S. Yang, *J. Mater. Chem. B* **2017**, *5*, 1846.
[172] M. M. Kemp, R. J. Linhardt, *Wiley Interdiscip. Rev. Nanomedicine Nanobiotechnology* **2010**, *2*, 77.
[173] G. Shim, J.-Y. Kim, J. Han, S. W. Chung, S. Lee, Y. Byun, Y.-K. Oh, *J. Control. Release* **2014**, *189*, 80.
[174] B. Zhang, X. Yang, Y. Wang, G. Zhai, *Mater. Sci. Eng. C* **2017**, *75*, 198.
[175] N. Yan, X. Chen, *Nature* **2015**, *524*, 155.
[176] H. Katas, M. Amin, M. C. Iqbal, N. Moideen, L. Y. Ng, M. Baharudin, P. A. Adhwa, *J. Nanomater.* **2017**, *2017*.
[177] C. Zhang, Z. Liu, Y. Zheng, Y. Geng, C. Han, Y. Shi, H. Sun, C. Zhang, Y. Chen, L. Zhang, *Small* **2018**, *14*.
[178] G. Chang, Y. Wang, B. Gong, Y. Xiao, Y. Chen, S. Wang, S. Li, F. Huang, Y. Shen, A. Xie, *ACS Appl. Mater. Interfaces* **2015**, *7*, 11246.
[179] B. Zhang, Y. Yan, Q. Shen, D. Ma, L. Huang, X. Cai, S. Tan, *Mater. Sci. Eng. C* **2017**, *79*, 185.
[180] S. F. Kiew, Y. T. Ho, L. V. Kiew, J. C. Y. Kah, H. B. Lee, T. Imae, L. Y. Chung, *Int. J. Pharm.* **2017**, *534*, 297.
[181] N. Mauro, C. Scialabba, G. Cavallaro, M. Licciardi, G. Giammona, *Biomacromolecules* **2015**, *16*, 2766.
[182] Z. Sheng, L. Song, J. Zheng, D. Hu, M. He, M. Zheng, G. Gao, P. Gong, P. Zhang,

Y. Ma, *Biomaterials* **2013**, *34*, 5236.
[183] P.-X. Lai, C.-W. Chen, S.-C. Wei, T.-Y. Lin, H.-J. Jian, I. P.-J. Lai, J.-Y. Mao, P.-H. Hsu, H.-J. Lin, W.-S. Tzou, *Biomaterials* **2016**, *109*, 12.
[184] G. Battogtokh, Y. T. Ko, *J. Control. Release* **2016**, *234*, 10.
[185] Y. A. Cheon, J. H. Bae, B. G. Chung, *Langmuir* **2016**, *32*, 2731.
[186] N. Ma, J. Liu, W. He, Z. Li, Y. Luan, Y. Song, S. Garg, *J. Colloid Interface Sci.* **2017**, *490*, 598.
[187] G. Bharath, B. S. Latha, E. H. Alsharaeh, P. Prakash, N. Ponpandian, *Anal. Methods* **2017**, *9*, 240.
[188] G. Liu, H. Shen, J. Mao, L. Zhang, Z. Jiang, T. Sun, Q. Lan, Z. Zhang, *ACS Appl. Mater. Interfaces* **2013**, *5*, 6909.
[189] D. Bijukumar, C. M. Girish, A. Sasidharan, S. Nair, M. Koyakutty, *ACS Biomater. Sci. Eng.* **2015**, *1*, 1211.
[190] Q. Yu, B. Zhang, J. Li, M. Li, *Chem. Commun.* **2017**, *53*, 11433.
[191] S. Hu, R. Fang, Y. Chen, B. Liao, I. Chen, S. Chen, *Adv. Funct. Mater.* **2014**, *24*, 4144.
[192] M.-G. Kim, J. Y. Park, W. Miao, J. Lee, Y.-K. Oh, *Biomaterials* **2015**, *48*, 129.
[193] R. Mo, T. Jiang, W. Sun, Z. Gu, *Biomaterials* **2015**, *50*, 67.
[194] L. Yang, Y.-T. Tseng, G. Suo, L. Chen, J. Yu, W.-J. Chiu, C.-C. Huang, C.-H. Lin, *ACS Appl. Mater. Interfaces* **2015**, *7*, 5097.
[195] S. Kang, J. Lee, S. Ryu, Y. Kwon, K.-H. Kim, D. H. Jeong, S. R. Paik, B.-S. Kim, *Chem. Mater.* **2017**, *29*, 3461.
[196] Y. Chen, T. Liu, P. Chen, P. Chang, S. Chen, *Small* **2016**, *12*, 1458.
[197] J. Song, X. Yang, O. Jacobson, L. Lin, P. Huang, G. Niu, Q. Ma, X. Chen, *ACS Nano* **2015**, *9*, 9199.
[198] X. Wang, Q. Han, N. Yu, J. Li, L. Yang, R. Yang, C. Wang, *J. Mater. Chem. B* **2015**, *3*, 4036.
[199] H. Chen, Z. Liu, S. Li, C. Su, X. Qiu, H. Zhong, Z. Guo, *Theranostics* **2016**, *6*, 1096.
[200] S. E. Day, M. I. Kettunen, F. A. Gallagher, D.-E. Hu, M. Lerche, J. Wolber, K. Golman, J. H. Ardenkjaer-Larsen, K. M. Brindle, *Nat. Med.* **2007**, *13*, 1382.
[201] Y.-X. J. Wang, *Quant. Imaging Med. Surg.* **2011**, *1*, 35.
[202] C. Xu, S. Shi, L. Feng, F. Chen, S. A. Graves, E. B. Ehlerding, S. Goel, H. Sun, C. G. England, R. J. Nickles, *Nanoscale* **2016**, *8*, 12683.
[203] K. Yang, L. Hu, X. Ma, S. Ye, L. Cheng, X. Shi, C. Li, Y. Li, Z. Liu, *Adv. Mater.* **2012**, *24*, 1868.
[204] R. Justin, K. Tao, S. Román, D. Chen, Y. Xu, X. Geng, I. M. Ross, R. T. Grant, A. Pearson, G. Zhou, *Carbon N. Y.* **2016**, *97*, 54.
[205] J. Wen, K. Yang, F. Liu, H. Li, Y. Xu, S. Sun, *Chem. Soc. Rev.* **2017**, *46*, 6024.
[206] A. Pourjavadi, Z. M. Tehrani, S. Jokar, *Polymer (Guildf).* **2015**, *76*, 52.
[207] Y. Chen, P. Chen, S. Hu, I. Chen, S. Chen, *Adv. Funct. Mater.* **2014**, *24*, 451.
[208] W. Jiang, F. Mo, X. Jin, L. Chen, L. J. Xu, L. Guo, F. Fu, *Adv. Mater. Interfaces* **2017**, *4*.
[209] M. Calderón, M. A. Quadir, S. K. Sharma, R. Haag, *Adv. Mater.* **2010**, *22*, 190.
[210] S. Abbina, S. Vappala, P. Kumar, E. M. J. Siren, C. C. La, U. Abbasi, D. E. Brooks, J. N. Kizhakkedathu, *J. Mater. Chem. B* **2017**, *5*, 9249.
[211] L. Hirsch, R. J. Stafford, J. A. Bankson, S. R. Sershen, B. Rivera, R. E. Price, J. D. Hazle, N. J. Halas, J. L. West, *Proc. Natl. Acad. Sci.* **2003**, *100*, 13549.
[212] Z. Chen, T. Shi, L. Zhang, P. Zhu, M. Deng, C. Huang, T. Hu, L. Jiang, J. Li, *Cancer Lett.* **2016**, *370*, 153.
[213] M. Bar-Zeev, Y. D. Livney, Y. G. Assaraf, *Drug Resist. Updat.* **2017**.

[214] A. G. Assanhou, W. Li, L. Zhang, L. Xue, L. Kong, H. Sun, R. Mo, C. Zhang, *Biomaterials* **2015**, *73*, 284.
[215] S. Chen, Q. Lei, W.-X. Qiu, L.-H. Liu, D.-W. Zheng, J.-X. Fan, L. Rong, Y.-X. Sun, X.-Z. Zhang, *Biomaterials* **2017**, *117*, 92.

8 Appendix

8.1 Publications and Conference Contributions

Publications

First author

1. Z. Tu, G. Guday, C., M. Adeli, R. Haag, Multivalent interactions between 2D nanomaterials and biointerfaces, *Adv. Mater.* **2018**, just accepted.

2. Z. Tu, V. Wycisk, C. Cheng, W. Chen, M. Adeli, R. Haag, Functionalized graphene sheets for intracellular controlled release of therapeutic Agents, *Nanoscale* **2017**, *9*, 18931.

3. Z. Tu, K. Achazi, A. Schulz, R. Mülhaupt, S. Thierbach, E. Rühl, M. Adeli, and R. Haag, Combination of surface charge and size controls the cellular uptake of functionalized graphene Sheets, *Adv. Funct. Mater.* **2017**, *27*, 1701837.

4. D. Zhong, Z. Tu, X. Zhang, Y. Li, Z. Gu, Bioreducible peptide-dendrimeric nanogels with abundant expanded voids for efficient drug entrapment and delivery, *Biomacromolecules*, **2017**, *18*, 3498. (co-first author)

5. Z. Tu, Y. Jian, D. Zhong, B. He, Z. Gu, Self-assembly of amphiphilic tripeptides into nanoparticles for drug delivery, *Protein & Peptide Letters*, **2014**, *21*, 194.

Submitted and in preparation:

6. Z. Tu, H. Qiao, Y. Yan, G. Guday, Y. Li, M. Adeli, W. Chen, R. Haag, Graphene-based nanoplatforms for hyperthermia surmounting of multiple-drug resistance, *Angew. Chem. Int. Ed.* **2018**, submitted.

7. Z. Tu, H. Qiao, Z. Zhu, G. Guday, C. P. R. Hackenberger, M. Adeli, W. Chen, R. Haag, Nuclear-Targeted Drug Delivery Nanoplatforms of cyclic TAT Peptide-Conjugated Graphene Nanosheets, in preparation.

Co-author

8. L. Gao, M. Li, S. Ehrmann, Z.Tu, N. Ma, R. Haag, Zwitterionic pillar[5]arene forming positively charged nanoaggregates with high activity against planktonic bacteria and biofilms, *Angew. Chem. Int. Ed.* **2018**, submitted.

9. M. Li, L. Gao, C. Schlaich, J. Zhang, I. S. Donskyi, G. Yu, W. Li, Z. Tu, J. Rolff, T. Schwerdtle, N. Ma, and R. Haag, Construction of functional coatings with durable and

broad-spectrum antibacterial potential based on mussel-inspired dendritic polyglycerol and in situ-formed copper nanoparticles, *ACS Appl. Mater. Interfaces*, **2017**, *9*, 35411.
10. E. Mohammadifar, F. Zabihi, Z. Tu, S. Hedtrich, A. Nemati, M. Adeli, and R. Haag, One-pot and gram-scale synthesis of biodegradable polyglycerol at ambient conditions; nanocarriers for intradermal drug delivery, *Polym. Chem.*, **2017**, *8*, 7375.
11. A. Bodaghi, M. Adeli, A. Dadkhahtehrani, Z. Tu, Synthesis of polyglycerol-citric acid nanoparticles as biocompatible vectors for biomedical applications, *J. Mol. Liq.*, **2017**, *242*, 53.
12. Z. Beiranvand, A. Kakanejadifard, I. S. Donskyi, A. Faghani, Z. Tu, A. Lippitz, P. Sasanpour, F. Maschietto, B. Paulus, W. E. S. Unger, R. Haag and M. Adeli, Functionalization of fullerene at room temperature: toward new carbon vectors with improved physicochemical properties, *RSC Adv.,* **2016**, *6*, 112771.
13. W. Chen, Y. Hou, Z. Tu, L. Gao, and R. Haag, pH-Degradable PVA-based nanogels via photo-crosslinking of thermo-preinduced nanoaggregates for controlled drug delivery, *J. Controlled Release*, **2016**, *259*, 160.
14. X Xu, Y Jian, Y Li, X Zhang, Z Tu, Z Gu, Bio-inspired supramolecular hybrid dendrimers self-assembled from low-generation peptide dendrons for highly efficient gene delivery and biological tracking, *ACS Nano*, **2014**, *8*, 9255.

Poster Presentations

Z. Tu, K. Achaiz, A. Schulz, M. Adeli, R. Haag
Cellular uptake mechanism of polymer-coated graphene derivatives; how size and charge matter
International Symposium 2016 “Functional Biointerfaces,” Berlin, Germany, 2016

Z. Tu, M. Adeli, R. Haag
Combination of surface charge and size controls the cellular uptake of functionalized graphene sheets
The 3rd Edition of the European Graphene Forum 2017 Conference and Exhibition, Paris, France, 2017

8.2 Curriculum Vitae

The CV is not included for privacy reasons.